# Preliminary Design Study of a
# Quiet, High-Flow Fan (QHF) Stage

C. L. Walker, L. S. Kisner, R. A. Delaney,

A. A. Beguhn, and D. E. Frye

Detroit Diesel Allison Division of

General Motors Corporation

prepared for

**NATIONAL AERONAUTICS AND SPACE ADMINISTRATION**

| 1 Report No. NASA CR-134780 | 2. Government Accession No. | 3. Recipient's Catalog No. |
|---|---|---|
| 4 Title and Subtitle PRELIMINARY DESIGN STUDY OF A QUIET, HIGH-FLOW FAN (QHF) STAGE | | 5. Report Date 15 October 1974 |
| | | 6. Performing Organization Code |
| 7. Author(s) C. L. Walker, L. S. Kisner, R. A. Delaney, A. A. Beguhn, and D. E. Frye | | 8. Performing Organization Report No. EDR 8317 |
| | | 10. Work Unit No. |
| 9. Performing Organization Name and Address Detroit Diesel Allison Division General Motors Corporation Indianapolis, Indiana 46206 | | 11. Contract or Grant No. NAS3-18521 |
| | | 13. Type of Report and Period Covered |
| 12. Sponsoring Agency Name and Address National Aeronautics and Space Administration Washington, D.C. 20546 | | |
| | | 14. Sponsoring Agency Code |

15. Supplementary Notes

Project Manager, James G. Lucas, V/STOL and Noise Division, NASA Lewis Research Center, Cleveland, Ohio

16. Abstract

Concepts selected to reduce fan generated noise in the QHF (Quiet, High-Flow) fan are near-sonic flow at the fan inlet to reduce upstream propagated noise and the use of long-chord vanes to reduce downstream noise. The near-sonic condition at the rotor inlet plane is achieved by designing for high specific mass flow and by maintaining the high flow at reduced power by variable stators and variable fan exhaust nozzle. The long-chord vanes reduce response to unsteady flow.

The purpose of this study was to provide the preliminary design of a 508 mm (20 inch) fan to be built and tested at NASA Lewis to demonstrate these concepts for reducing fan source noise.

The acoustic design showed that long-chord stators would significantly reduce fan source noise and that other stator design parameters have no appreciable effect on noise for the spacing and chord length of the QHF design.

Four rig flow paths studied in the aerodynamic preliminary design are discussed. The final two were acoustically satisfactory and the selected configuration had satisfactory loading distributions and surge margin predictions.

Noise contours for 100 EPNdB levels for a 79379 kg (175,000 lb) aircraft powered with untreated QHF fan engines had areas much smaller than for aircraft with conventional fan engines. Noise prediction results indicate that a QHF powered aircraft would be under FAR Part 36 levels without any acoustic treatment.

| 17. Key Words (Suggested by Author(s)) Noise Fan Stage High Flow | 18. Distribution Statement Unclassified - unlimited |
|---|---|

| 19 Security Classif. (of this report) Unclassified | 20. Security Classif. (of this page) Unclassified | 21 No. of Pages 75 | 22. Price* $4.25 |
|---|---|---|---|

NASA-C-168 (Rev. 6-71)

# TABLE OF CONTENTS

# LIST OF FIGURES

# LIST OF FIGURES (CONTINUED)

iv

## LIST OF FIGURES (CONTINUED)

## LIST OF FIGURES (CONTINUED)

# LIST OF TABLES

# PRELIMINARY DESIGN STUDY
## OF A
## QUIET, HIGH-F!OW FAN (QHF) STAGE

By C. L. Walker, L. S. Kisner, R. A. Delaney, A. A. Beguhn, D. E. Frye
DETROIT DIESEL ALLISON DIVISION OF GENERAL MOTORS CORPORATION

## SUMMARY

Concepts selected to reduce fan generated noise in the QHF (Quiet, High-Flow)
fan are near-sonic flow at the fan inlet to reduce upstream propagated noise
and the use of long-chord vanes to reduce downstream noise. The near-sonic
condition at the rotor inlet plane is achieved by designing for high specific
mass flow and by maintaining the high flow at reduced power by variable
geometry--variable angle tandem stators and a variable fan exhaust nozzle.
The long-chord vanes reduce their response to unsteady flow phenomena.

The purpose of the study reported herein was to perform an acoustic design
along with preliminary aerodynamic and mechanical designs to assure that a
508 mm (20 inch) rig could be built and tested at NASA Lewis to demonstrate
these concepts for reducing fan source noise.

The acoustic design showed that long-chord stators would significantly reduce
fan source noise. In fact, the analysis indicates that other stator design
parameters have no appreciable effect on noise for the spacing and chord
length of the QHF design.

The aerodynamic preliminary design resulted from iterations between acoustic
and aerodynamic characteristics related to hub loading (D factor) and ap-
proach power vane Mach number. Four rig flow paths are discussed. The final
two were acoustically satisfactory and the selected configuration had
satisfactory loading distributions and surge margin predictions.

The mechanical preliminary design indicates no serious interface problems,
and--based on similar rotor operation at DDA--no insurmountable final design
mechanical problems.

Noise contours provide a method of describing the area of annoyance in the
vicinities of airports. Contours for 100 EPNdB levels for the 79379 kg
(175,000 lb.) aircraft powered with untreated QHF fan engines had areas much
smaller than for aircraft with conventional fan engines, and the QHF fan
engine 100 EPNdB contours would be contained within many airport boundaries.
Noise prediction results indicate that a QHF powered aircraft would be under
FAR Part 36 levels without any acoustic treatment.

# INTRODUCTION

This report describes preliminary aerodynamic and mechanical designs and a detailed acoustic analysis of a single-flow-path, inlet-guide-vaneless fan stage subsequently referred to as the QHF (Quiet, High-Flow) fan. Future advanced turbofan powered transport aircraft, both CTOL and STOL, are expected to require extensive noise treatment in the fan inlet and exit ducts to meet environmental noise requirements during take-off and approach. For several reasons it is desirable to minimize internal duct treatment. One method of reducing noise propagating forward from the fan stage is to use a sonic or near-sonic inlet to attenuate forward propagating noise. Advocates of this method have usually proposed a restriction in the inlet followed by a diffuser to the fan inlet with some sort of variable geometry to permit a near-sonic condition to be maintained at both take-off and approach power settings. The concept being developed under this program is to design the fan to have a high inlet specific flow which will result in a near-sonic flow condition at the fan-face to reduce forward propagating fan noise at design mass flow without a diffuser upstream of the fan. In exchange for variable geometry in the engine inlet required for conventional sonic inlets, this design will require a variable fan stage outlet guide vane and a large-area-change fan nozzle to permit achieving approach thrust at design fan mass flow. To reduce fan source exit noise at these high mass flow conditions, the QHF (Quiet, High Flow) fan will use long-chord exit vanes which have been theoretically shown to reduce both discrete frequency and broadband noise by reducing the vane response to blade wakes and turbulent eddies. The fan has a rotor tip diameter of 508 millimeters (20 inches) and is designed to operate in the NASA Lewis Research Center aerodynamic performance facility, W-8, and fan noise facility, W-2, as shown in Figure 1.

The preliminary aerodynamic and mechanical designs provided the information necessary for a complete and thorough acoustic analysis of the concept of a constant high-specific-flow rotor combined with long-chord, double-row stators (constant inlet flow for all noise-rating conditions). The preliminary mechanical design is sufficiently detailed to assure that mechanical feasibility of the configuration and blading can be obtained during final design.

The detailed acoustic analysis of the concept, developed concurrently with the aerodynamic and mechanical design, was used in conjunction with them to optimize the fan from the acoustic standpoint. Upon completion of the preliminary aerodynamic and mechanical designs, a thorough and detailed acoustic analysis of the selected fan design was performed. Finally, a calculation was made of the distributed and maximum take-off and approach perceived noise at two specified altitudes. These results are compared with similar information for existing fans of the same general aerodynamic characteristics.

There are several advantages which should accompany the adoption of the QHF concepts in a turbofan engine. The QHF inlet will be shorter and lighter and should also be less subject to distortion at the fan face because of the absence of diffusion in the inlet duct. This should also mean that the engine needs less stall margin. The complexity introduced by the variable outlet guide vanes and fan exit nozzle is offset by the lack of a requirement for variable geometry in the inlet duct and very rapid response from approach to take-off thrust. This latter advantage accrues from the engine rotor being at full speed during approach. Whether the engine would be lighter than a conventional engine is undoubtedly more dependent on other details than whether the higher specific mass flow fan stage benefit is outweighed by the penalty of the longer outlet guide vanes.
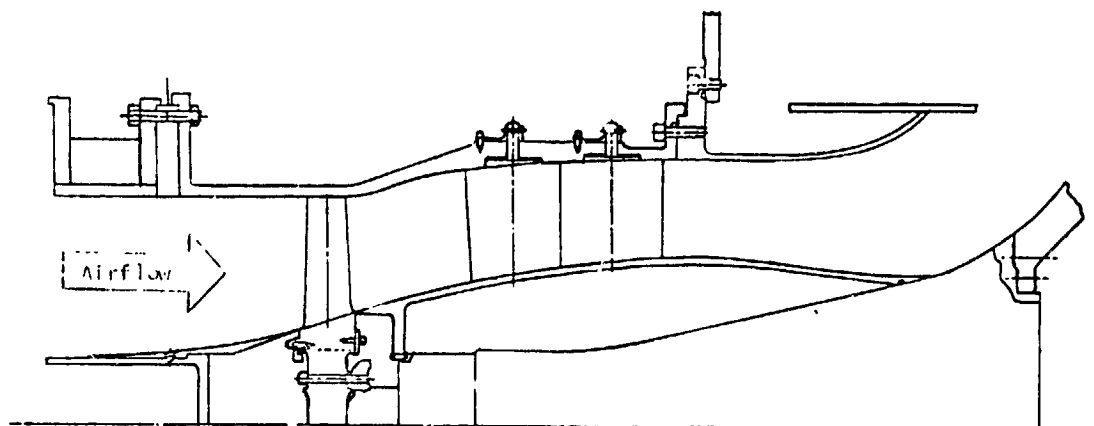
2

QHF Fan installed in W-8, aerodynamic performance facility



Fan Inlet Noise Position

Airflow

Airflow

Fan Exit Noise Position
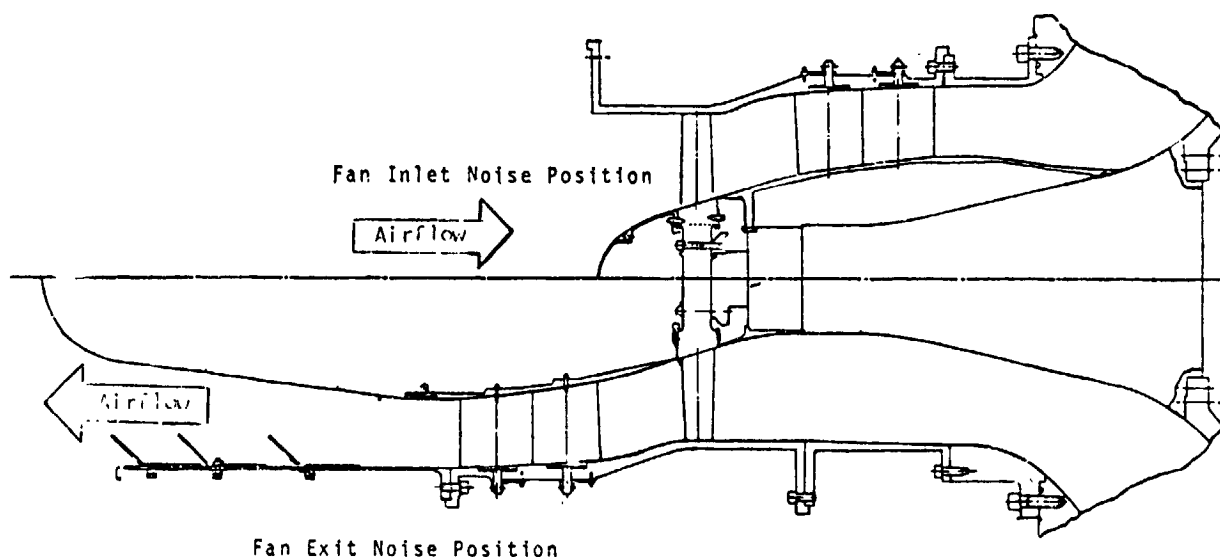
QHF Fan installed in W-2, noise facility

Figure 1.  QHF Fan installed in NASA Lewis Facilities

# ACOUSTIC DESIGN

## DESIGN TOOLS

The key element in predicting fan noise is the unsteady response of the blade rows to disturbances in the flow. For the IGV-less fan, the rotor-stator interaction is the primary source of discrete noise, and thus the stator response to rotor wakes plays the major role in determining fan discrete noise levels. This study employed two response models: a compressible extension of Kemp-Sears[1] developed by Osborne[2] and an incompressible combined gust response model using the Sears-Horlock[3] theory for cambered airfoils developed by Naumann and Yeh[4]. Both models were used to calculate rotor-stator interaction noise and the Naumann and Yeh model allowed the consideration of the effects of incidence and camber.

Broadband noise can also be related to the unsteady response of the blade rows. This was accomplished by using the compressible response theory and a model for the turbulence spectrum. The turbulence spectrum was considered to be a superposition of sinusoidal gusts at all frequencies. The fluctuating force was computed at each streamline location across the span in a strip theory model. The total sound pressure level was obtained by assuming an array of incoherent sources such that the mean squared sound pressures add linearly. The broadband noise model includes the effects of important parameters such as turbulence intensity and nondimensional ratio of length scale to stator spacing suggested by Mani[5].

A theoretical noise prediction program based upon the considerations discussed above was used to analyze the effects of the geometric flow path, blade shapes, and aerodynamic flow variables upon discrete and broadband noise generation. An acoustic design procedure was thus developed that can be factored into the aerodynamic design function. The chart in Figure 2 illustrates this capability. This system provided the theoretical background for parametric studies and analysis of final designs.
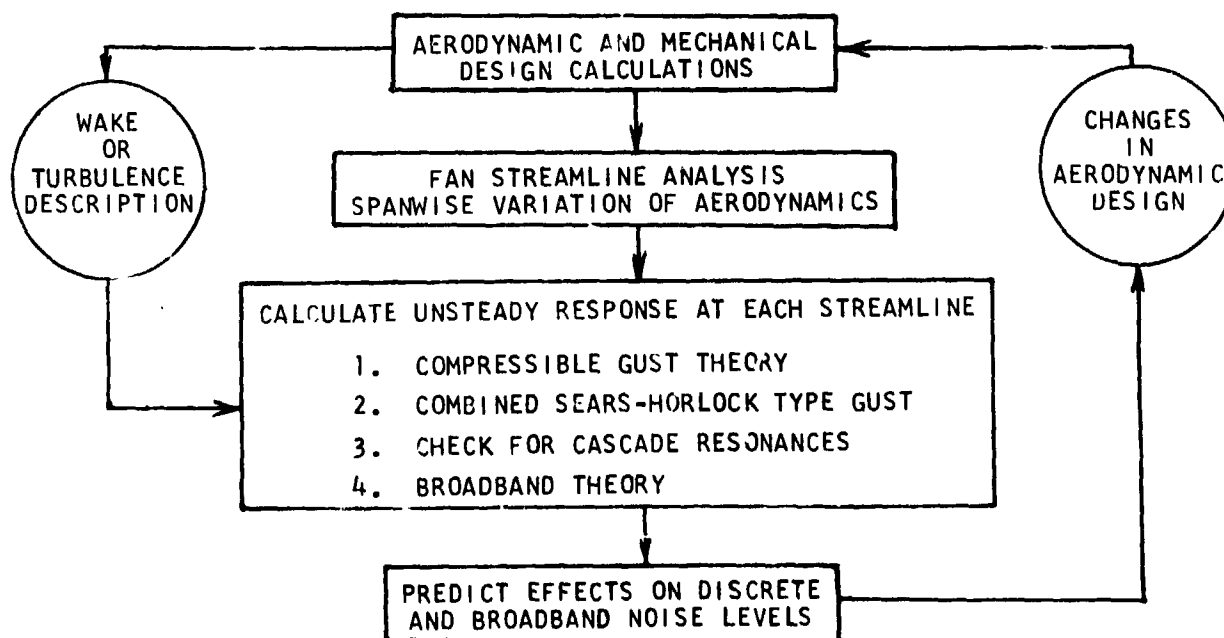


Figure 2. Aero/Acoustic Design Interaction

In addition to the theoretical calculations, absolute noise predictions were made in accordance with semi-empirical techniques developed at DDA[6] representing multiple regression best fit of published noise data as a function of the important fan and jet aerodynamic parameters. A summary of the acoustic design tools is shown in Table 1.

| TABLE 1. ACOUSTIC DESIGN TOOLS | |
|---|---|
| RESPONSE THEORY | REFERENCES |
| COMPRESSIBLE EXTENSION OF SEARS THEORY | SEARS/OSBORNE[1,2] |
| COMBINED EFFECTS OF TRANSVERSE AND PARALLEL GUSTS INCLUDING SMALL CAMBER | NAUMANN/YEH[3,4] |
| BROADBAND RESPONSE THEORY | MANI[5] DDA |
| NOISE THEORY | |
| GENERATION/PROPAGATION/RADIATION | DDA |
| EMPIRICAL NOISE PREDICTION | |
| BEST FIT OF PUBLISHED FAN DATA | DDA[6] |

ACOUSTIC PHILOSOPHY

Forward Radiated Noise

It has been demonstrated that a near-sonic inlet design is effective in reducing forward radiated noise. The results of DDA model testing are shown in Figure 3 along with NASA data and a theoretical curve. The theoretical curve was deduced from the DDA noise prediction equations to be

$$20 \log \left( \frac{1}{1-M^2} \right)$$

assuming a uniform flow condition at the throat ahead of the fan face of Mach number M. This curve appears to represent the ideal attainable suppression of noise due to the partial sonic block.

A modification of this concept is an integral part of the QHF fan design to obtain substantial (~12 dB) reduction over conventional designs. This concept uses high specific flow to significantly suppress the forward radiated noise due to discrete frequency blade row interaction, broadband phenomena, and multiple pure tones. Results of DDA model testing and full scale fan data show that the noise levels of high speed fans actually decrease as the tip Mach number is increased to values beyond about 1.4. The results of narrow band analysis of a DDA model fan illustrate this noise reduction in Figure 4. The QHF fan will operate at an even higher Mach number of 1.8 and thus substantial reduction in all noise mechanisms radiating out the inlet to the far field is predicted. The fan design to accomplish

5
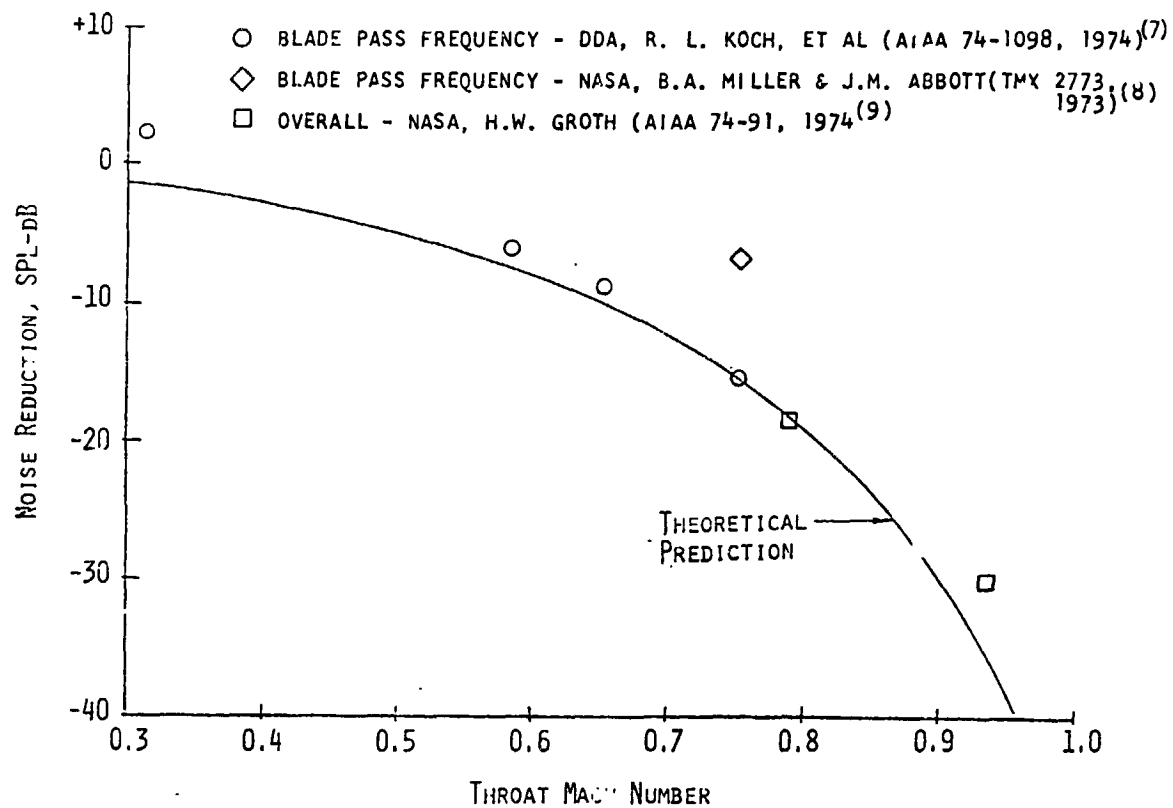
FIGURE 3. NEAR-SONIC INLET NOISE REDUCTION
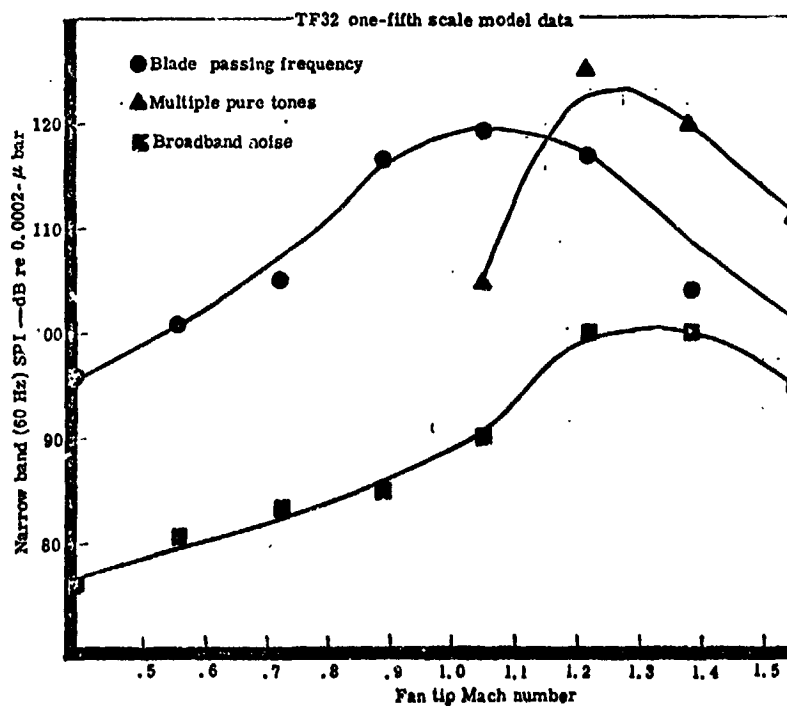


FIGURE 4. EFFECT OF HIGH SPEED ON FAN NOISE
GENERATION MECHANISMS

6

the required high flow is determined solely by aerodynamic considerations. Because the rotor design could not therefore be changed, parametric evaluation of rotor noise was not considered.

## Stator Noise

Because of the large attenuation of forward noise by the rotor inlet condition, the problem of acoustic design became one of reducing the rearward radiated discrete and broadband noise due to the unsteady response of stator vanes to periodic and random excitations. The fundamental concept employed in this design is the use of fewer, long chord vanes of conventional solidity. This concept has been studied experimentally at DDA. Figure 5 shows a noise reduction of 7-8 dB using 10 long-chord vanes incorporating acoustic treatment on the surfaces rather than 64 conventional vanes. By calculating the maximum attenuation from Rice's theory[10] for the suppression treatment used and the airfoil response from Sears' theory[2] it was found that most of the noise reduction observed from long chord vanes was due to the lower response of the vanes to high reduced frequency fluctuations. This reduction was observed for broadband noise that was dominant over discrete tones and established a basis for analyzing broadband noise in terms of unsteady blade response. Broadband mechanisms that can be reduced by long-chord vanes are:

- turbulence-blade row interaction
- broadband wake modulation
- stator vortex shedding

It was concluded that in addition to the expected reduction in discrete noise, broadband noise could be reduced with long-chord vanes.
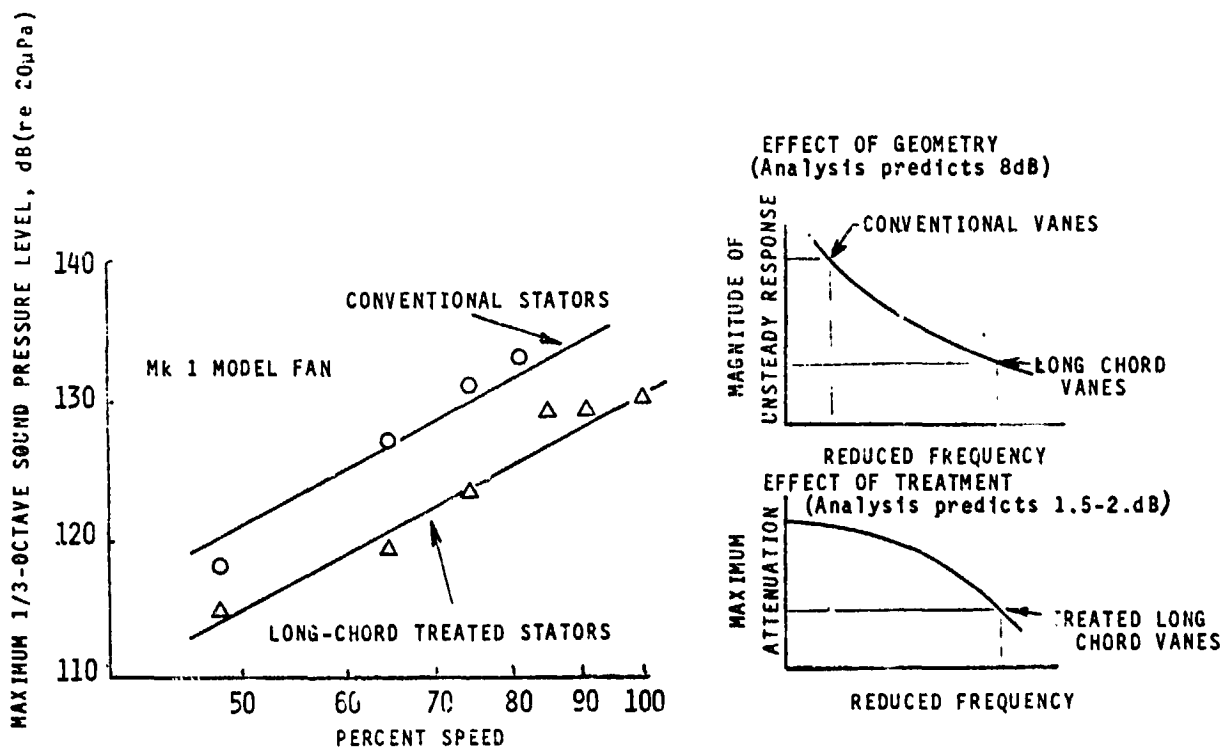


FIGURE 5. EVALUATION OF TREATED LONG CHORD VANES--TREATMENT VS. GEOMETRY

7

## TAKEOFF NOISE PARAMETERS

The acoustic design studies involved detailed parametric evaluation of the effects of aerodynamic design parameters on noise generation. The parameters studied were number of stator vanes, rotor loss coefficient, rotor exit absolute angle, stator camber, stator incidence angle, blade-vane interaction angle, and stator setting angle. Each parameter was varied + 20% about the initial design value uniformly from hub to tip. For convenience the mean streamline value of the parameter is given. Detailed aerodynamic and geometric parameters are defined in Figure 6. Calculation of stator response for all parameters was done with both the compressible Sears and Naumann and Yeh combined gust response models where possible. These results were used to predict changes in both forward and rearward radiated discrete far field noise levels (maximum SPL and PWL).

$\alpha$ = Stator Absolute Inlet Angle
$\beta$ = Rotor Relative Exit Angle
$i$ = Incidence Angle
$\gamma°$ = Setting Angle
$\beta + \alpha$= Interaction Angle
$C$ = True Chord
$\phi/2$ = Camber Half-Angle
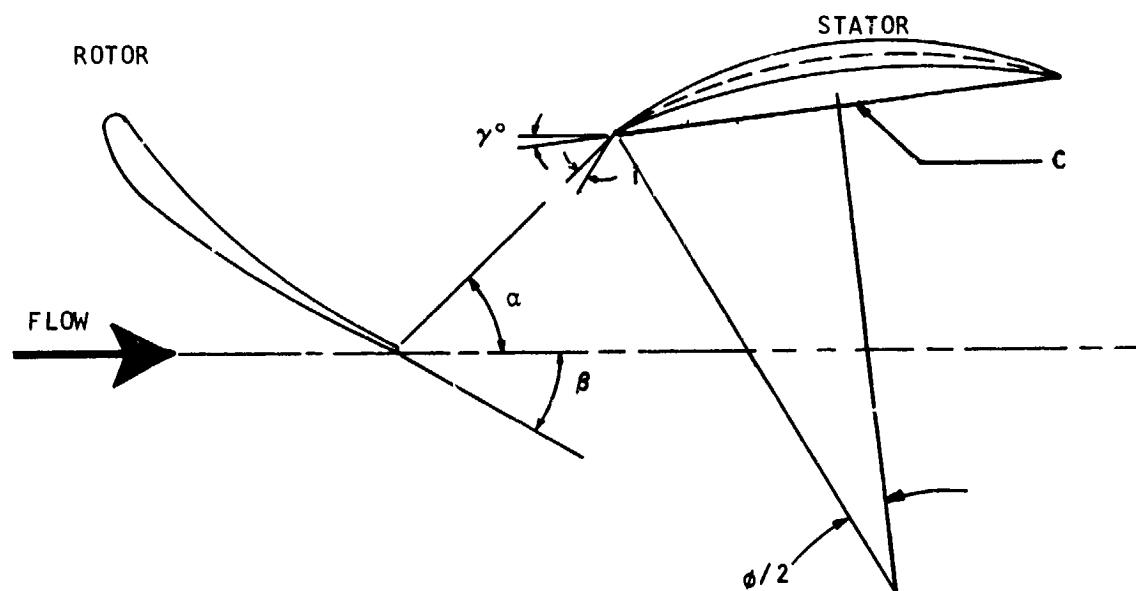


FIGURE 6. DETAILED AERODYNAMIC PARAMETERS

8

Each figure to be presented in the parametric study contains a plot of the maximum sound pressure level at a constant radius and the total blade passing tone sound power level. When assessing the effect of the design variable on the noise, the sound pressure level reflects changes in radiated directivity that depend upon the propagating modal patterns, whereas the sound power represents physically the total modal discrete energy. This explains the smoother shapes of the sound power curves.

Discrete Noise Radiation Parametrics

Number of Stator Vanes. For a given rotor aerodynamic design and stator solidity, interaction noise was computed for a range of stator vane numbers, 10-16, and stator chord, 130-200 mm (5.1 - 7.9 in.). The fluctuating stator response to incoming gusts was used to compute sound power and sound pressure levels generated by rotor stator interactions. Both the compressible Sears and Naumann-Yeh response models exhibited the same trends. The results shown in Figures 7-10 point to the advantage of fewer vanes of longer chord to maintain the same solidity. It was recommended that the aerodynamic design incorporate the minimum possible number of vanes, in this case 10.
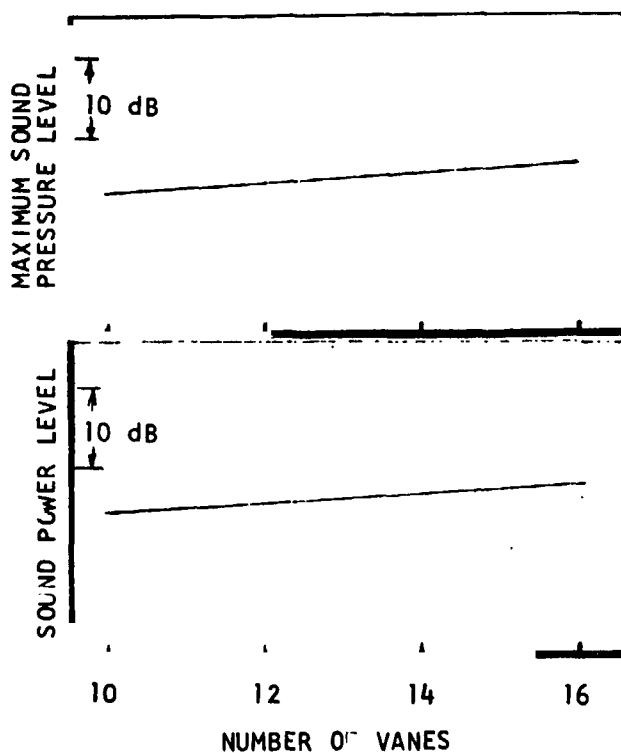


FIGURE 7. EFFECT OF VANE NUMBER ON UPSTREAM PROPAGATED DISCRETE NOISE. SEARS COMPRESSIBLE RESPONSE MODEL
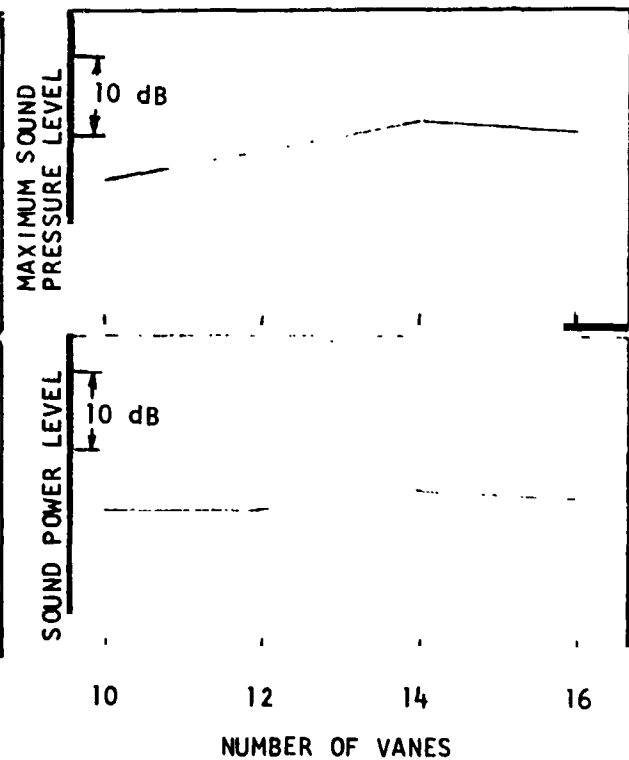
FIGURE 8. EFFECT OF VANE NUMBER ON UPSTREAM PROPAGATED DISCRETE NOISE. NAUMANN-YEH RESPONSE MODEL

9
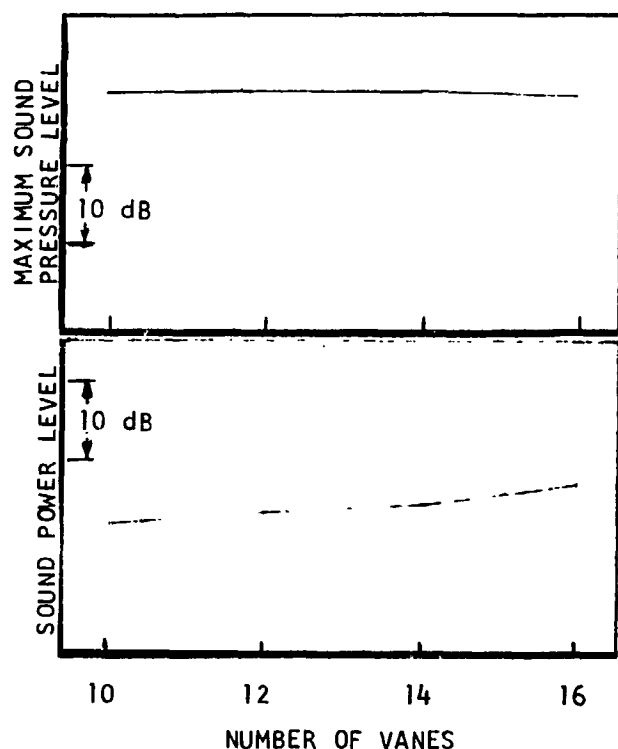
FIGURE 9.  EFFECT OF VANE NUMBER ON
DOWNSTREAM PROPAGATED
DISCRETE NOISE.  SEARS
COMPRESSIBLE RESPONSE
MODEL
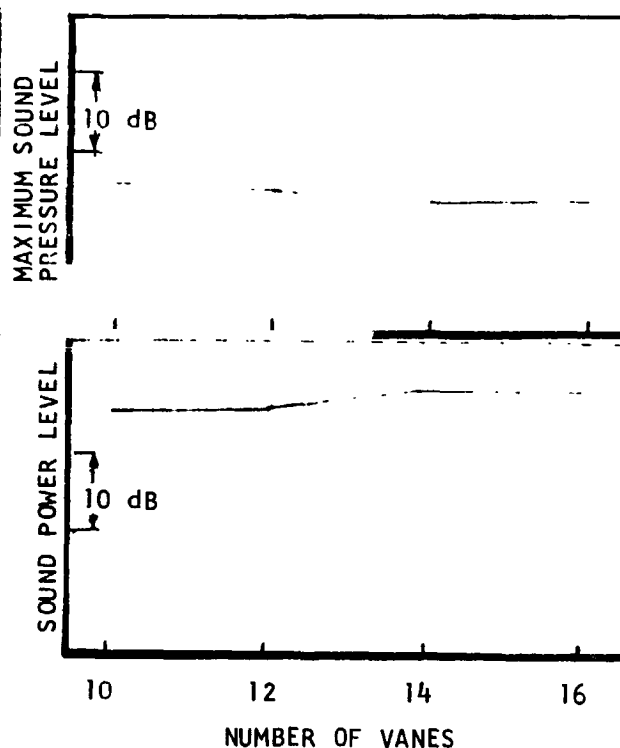
FIGURE 10.  EFFECT OF VANE NUMBER ON
DOWNSTREAM PROPAGATED
DISCRETE NOISE.  NAUMANN-
YEH RESPONSE MODEL

Rotor Exit Relative Flow Angle.  The rotor exit relative flow angle was varied
± 5 degrees from the design value.  The results are shown in Figures 11-12,
indicating a reduction in noise with increasing exit angle.  This is due
primarily to the increase in distance of wake travel resulting in reduced
wake strength.  This could be interpreted as an increase in effective rotor
stator spacing.

Stator Camber.  The Naumann-Yeh model was used to vary the camber angle ± 5
degrees with the resultant noise predicted in Figures 13-14.  Noise increases
with increasing camber for a given chord, possibly due to an increase in
turning across the vane.

Interaction Angle.  The interaction angle is defined as the sum of rotor
relative exit angle and stator absolute inlet angle (see Figure 6).  Maximum
wake interaction should occur at 90° with a $\sin(\beta + \alpha)$ variation that is
relatively flat over a ± 5° range.  This explains the relatively flat noise
level curves shown in Figures 15-16.

Incidence Angle.  A ± 5° variation in stator incidence angle produced only
a slight increase in noise as incidence is increased as shown in Figures
17-18.  This could be due to the effects of high reduced frequency.

10
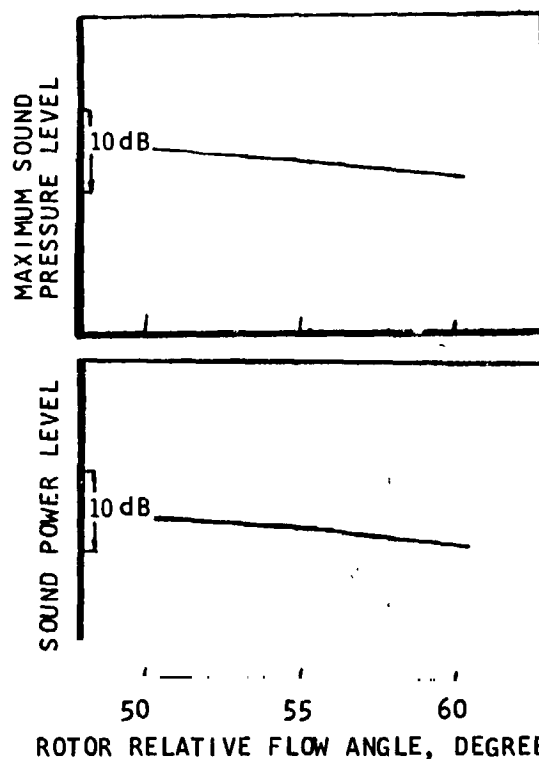
FIGURE 11.  EFFECT OF ROTOR EXIT AIR
ANGLE ON UPSTREAM PROPA-
GATED NOISE.  SEARS COM-
PRESSIBLE RESPONSE MODEL
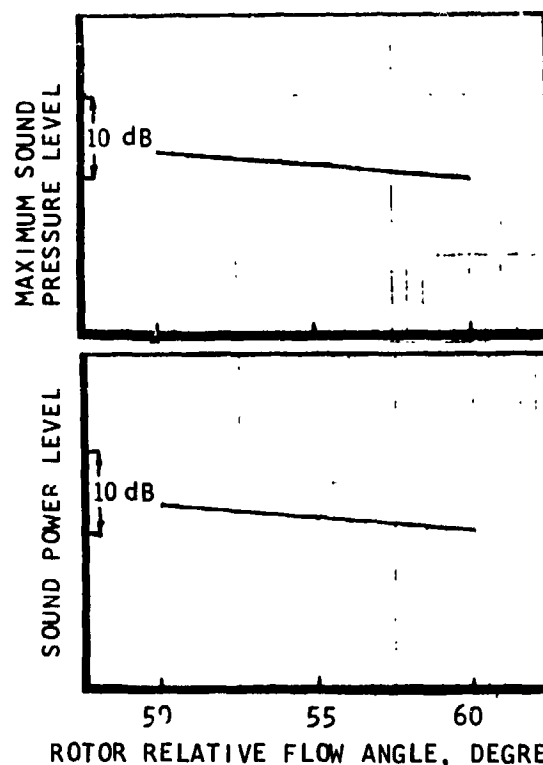
FIGURE 12.  EFFECT OF ROTOR EXIT AIR
ANGLE ON DOWNSTREAM PRO-
PAGATED NOISE.  SEARS COM-
PRESSIBLE RESPONSE MODEL
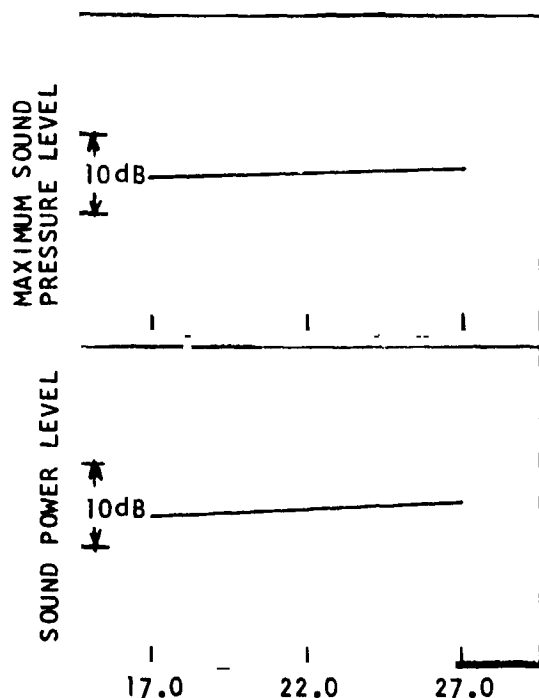
FIGURE 13.  EFFECT OF CAMBER ON UP-
STREAM PROPAGATED NOISE.
NAUMANN-YEH RESPONSE MODEL
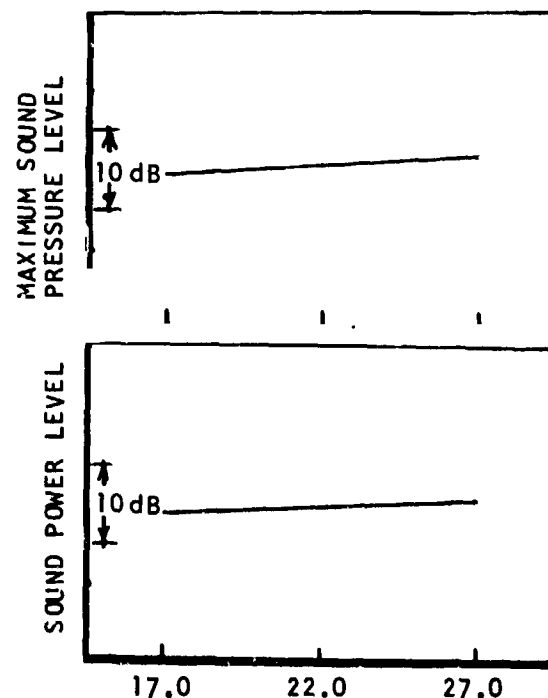
FIGURE 14.  EFFECT OF CAMBER ON DOWN-
STREAM PROPAGATED NOISE.
NAUMANN-YEH RESPONSE MODEL

11

MEANLINE INTERACTION ANGLE, DEGREES
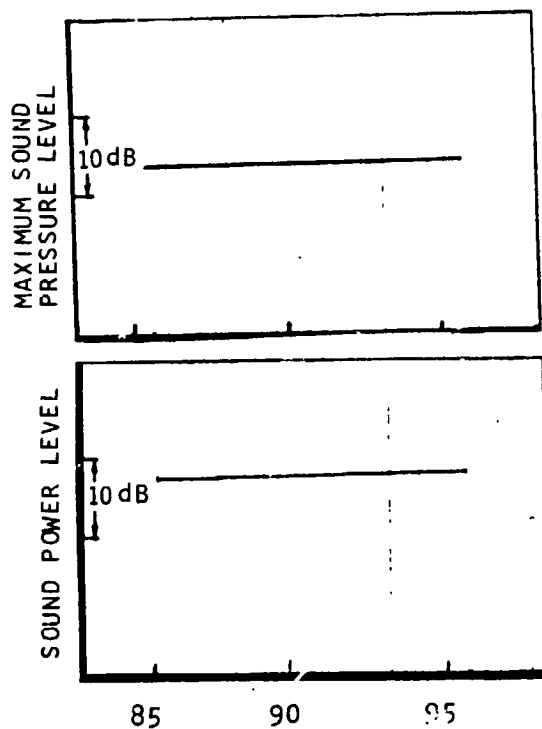
FIGURE 15.    EFFECT OF INTERACTION
             ANGLE ON UPSTREAM PROPA-
             GATED NOISE.   SEARS COM-
             PRESSIBLE MODEL



MEANLINE INTERACTION ANGLE, DEGREES
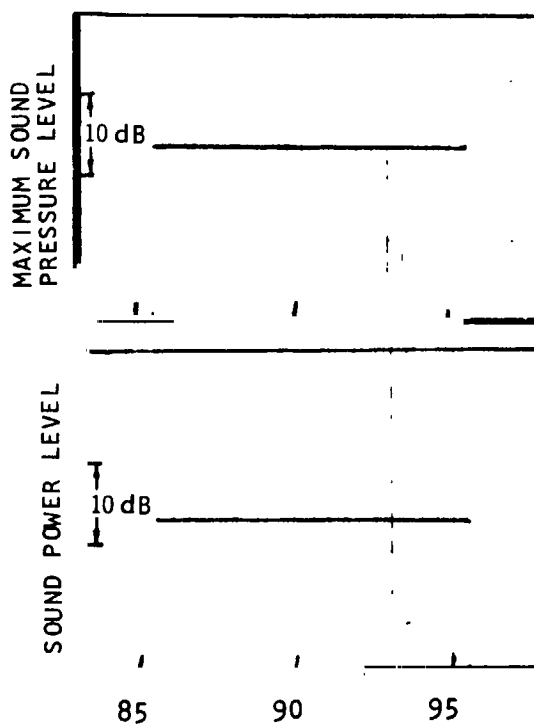
FIGURE 16.    EFFECT OF INTERACTION
             ANGLE ON DOWNSTREAM PRO-
             PAGATED NOISE.   SEARS
             COMPRESSIBLE MODEL



MEANLINE INCIDENCE ANGLE, DEGREES
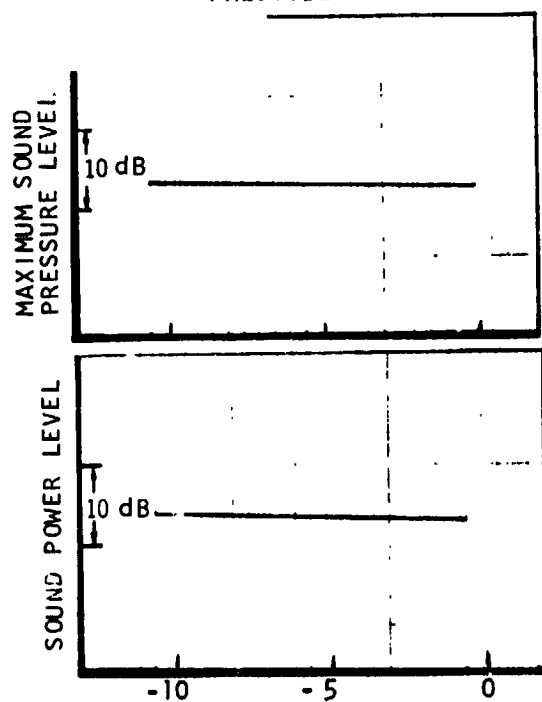
FIGURE 17.    EFFECT OF INCIDENCE ANGLE
             ON UPSTREAM PROPAGATED
             NOISE.   NAUMANN-YEH
             RESPONSE MODEL



MEANLINE INCIDENCE ANGLE, DEGREES
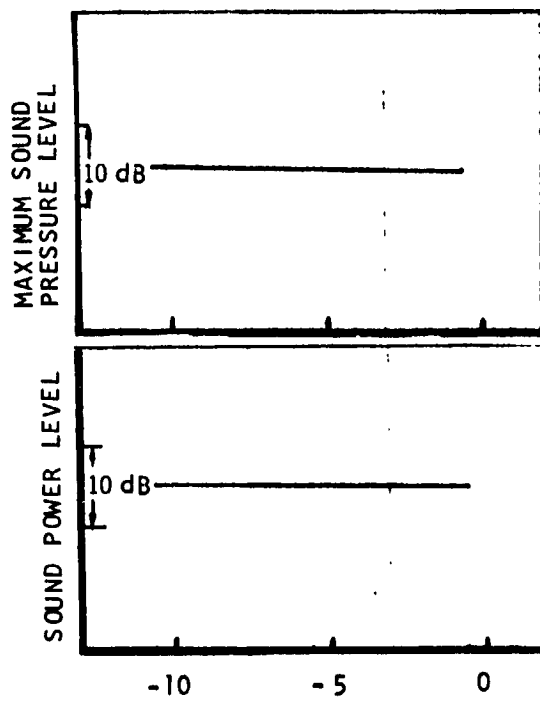
FIGURE 18.    EFFECT OF INCIDENCE ANGLE
             ON DOWNSTREAM PROPAGATED
             NOISE.   NAUMANN-YEH
             RESPONSE MODEL

12

Pressure Loss Coefficient. The loss coefficient was related to an effective drag coefficient that enters into the wake model. Figures 19 and 20 show that the noise does not change significantly with reduced losses until a very low value of loss is assumed.
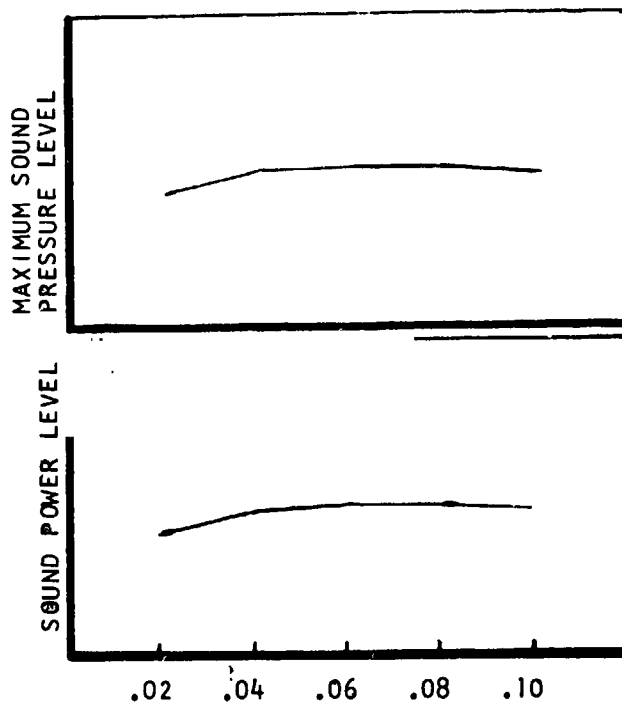


FIGURE 19. EFFECT OF TOTAL PRESSURE LOSS COEFFICIENT ON DOWN-STREAM PROPAGATED NOISE. SEARS COMPRESSIBLE RESPONSE MODEL
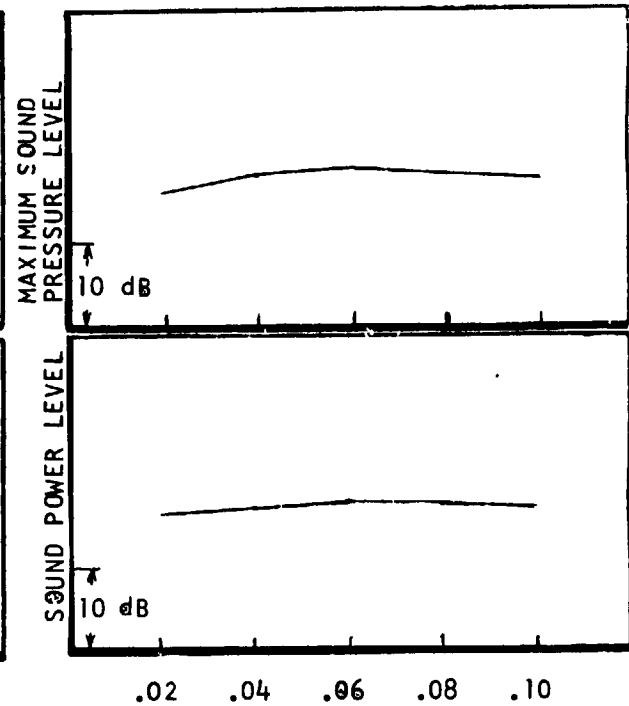
FIGURE 20. EFFECT OF TOTAL PRESSURE LOSS COEFFICIENT ON UP-STREAM PROPAGATED NOISE. SEARS COMPRESSIBLE RESPONSE MODEL

Broadband Noise

A model for estimating the effects of airfoil design parameters on broad-band noise generation was developed. Results from the broadband noise predicted spectra and directivity are shown in Figures 21 and 22. The basic assumption for this broadband noise calculation is that the origin of turbulence impinging upon the stator is the turbulent wakes of the rotor. An upper limit to the turbulence scale should be the wake width at the stator inlet. Using the conventional Silverstein NACA wake model, the wake width was calculated as a function of rotor solidity, $\sigma_r$, drag coefficient, $C_D^r$, and nondimensional distance of wake travel/rotor chord, $X_r/C_r$, according to the equation

$$ Y = 0.96 \ C_r (C_D^r \ X_r'/C_r)^{\frac{1}{2}} $$

The resultant scale of turbulence divided by stator spacing is approximately 0.4, representing an upper bound for the QHF fan. However, the turbulence in the wakes is assumed to be composed of a distribution of

13

TURBULENCE SCALE/STATOR SPACING
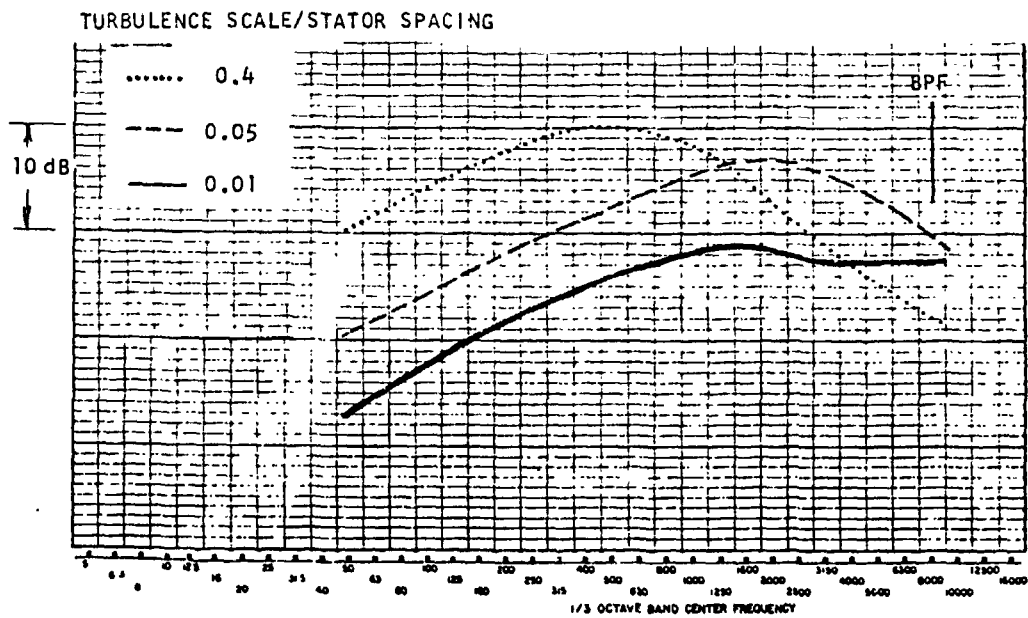


FIGURE 21.  BROADBAND FREQUENCY SPECTRA



Upstream Propagated Noise

Downstream Propagated Noise

DIRECTIVITY ANGLE - DEGREES FROM AXIS
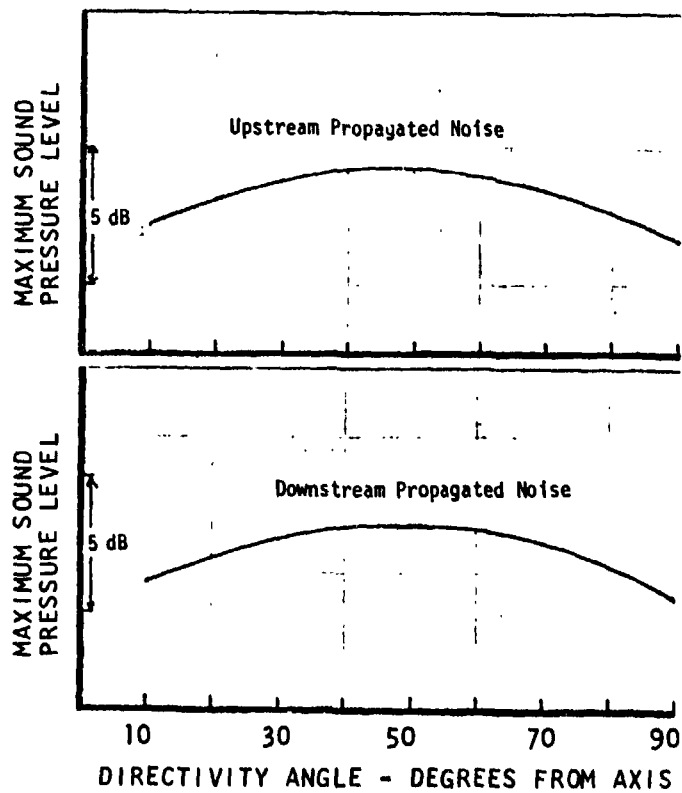
FIGURE 22.  MAXIMUM 1/3 OCTAVE BROADBAND
NOISE DIRECTIVITY AT 1250 Hz

14

eddies smaller than the wake width. A scale of 0.05 appears to yield representative broadband spectra for modern fans. This implies a turbulence correlation length of one-eighth of the wake width.

It was found that most detailed aerodynamic design parameters did not significantly effect the predicted broadband noise levels. The only exception is the effect of the number of stator vanes, and these results are presented in the Final Acoustic Design section.


## APPROACH NOISE STUDIES

At the approach power setting, the QHF is designed to achieve design point airflow and tip speed. The noise reduction features of high specific flow for forward noise attenuation and high reduced frequencies for reduced stator noise should be maintained.

To maintain high specific flow while preventing choking at the stator, a variable tandem stator design was employed. The approach geometry is shown in Figure 23. Aerodynamic analysis for first stator reset angles of -25°,



——————— VANE SETTING AT TAKEOFF

———————— VANE SETTING AT APPROACH

RESET ANGLE=25-35°

FORWARD VANE ROW

REAR VANE ROW
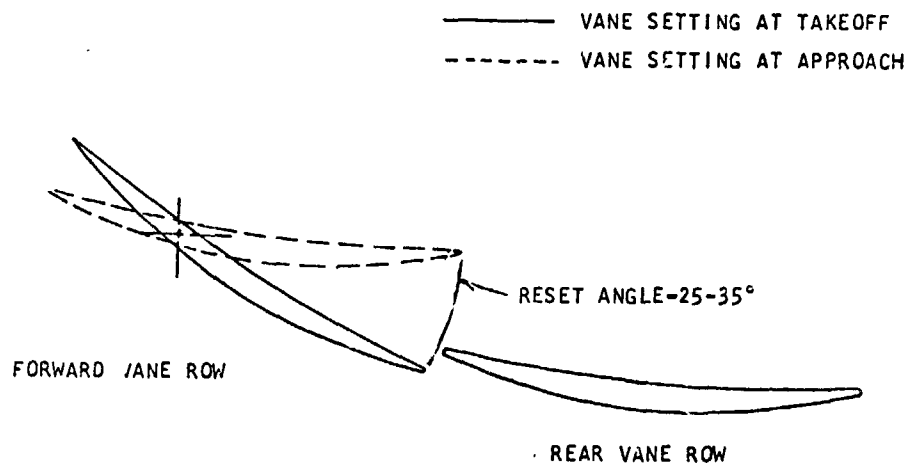
FIGURE 23. VANE GEOMETRY FOR TAKEOFF AND APPROACH POWER

-30°, and -35° were used as inputs for noise predictions based upon the Naumann-Yeh combined gust response model and the DDA theoretical noise prediction program. The acoustic disadvantage of the approach condition is that there are now two shorter chord stator rows responding to the rotor wakes. It was assumed that the maximum noise at approach would occur with each rotor-stator interaction computed and added acoustically, thus neglecting any shielding of the second stator row. Each stator row interaction was computed in terms of changes in rotor relative exit flow angle, stator incidence angle, stator setting angles, and stator camber. The results for downstream noise as a function of stator setting angle are shown in Figure 24. The advantage of increasing the first stator chord was explored and results are shown in Figure 25, i.e. an almost insignificant change in noise due to increasing first stator chord. The results of the approach noise studies are summarized in the following conclusions:

    1.  Approach noise increases slightly as the reset angle is increased

    2.  Stator 1 is the dominant noise source at approach
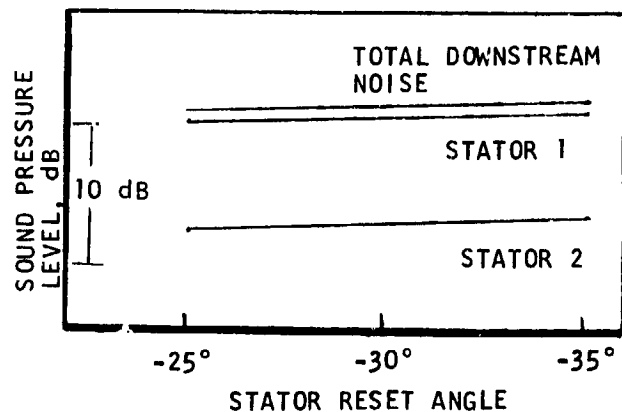
FIGURE 24. EFFECT OF STATOR RESET ANGLE
ON APPROACH NOISE
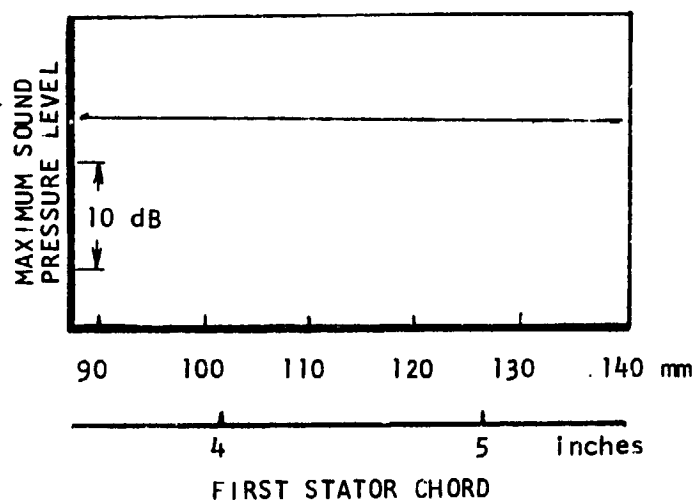


FIGURE 25. EFFECT OF FIRST STATOR CHORD
ON DOWNSTREAM APPROACH NOISE

## FINAL ACOUSTIC DESIGN

Continuous feedback between aerodynamic design and acoustic design was main-
tained throughout this program. As the final design evolved through this
interaction, final acoustic calculations were made for the best two aero-
dynamic designs. The two main objectives of the final acoustic design were
to establish quantitative noise reduction benefits of the QHF fan, and to
determine the acoustic superiority of the final design.

Noise Reduction Benefits of the QHF Fan

The high specific flow is an attractive concept for significantly reducing
forward radiated discrete, broadband, and multiple pure tone noise. Al-
though absolute knowledge of the noise reduction benefits will not be known

16

until the actual testing at NASA, an expected forward noise reduction of at least 12 dB is predicted based upon near sonic inlet and high speed fan data and simplified theoretical considerations (see Figures 3 and 4). The rearward radiated noise reduction benefits are attained through long chord stators which reduce discrete and broadband noise due to fluctuating forces on the vanes. The effect of vane number on discrete noise is shown in Figure 26. In these predictions the solidity is maintained and the vane chord increased as the number of vanes is reduced. The number of vanes is also the most important parameter in reducing broadband noise as shown in Figure 27.
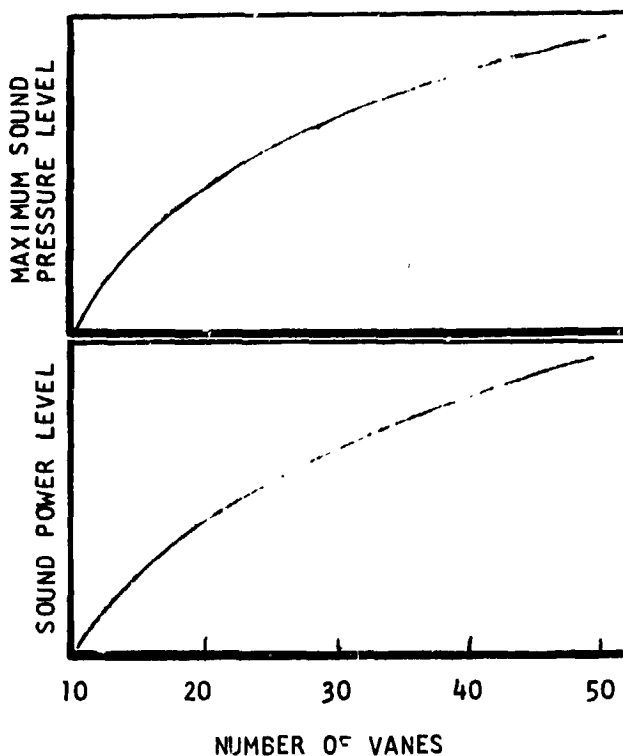


FIGURE 26.   EFFECT OF VANE NUMBER ON
             DOWNSTREAM DISCRETE
             NOISE
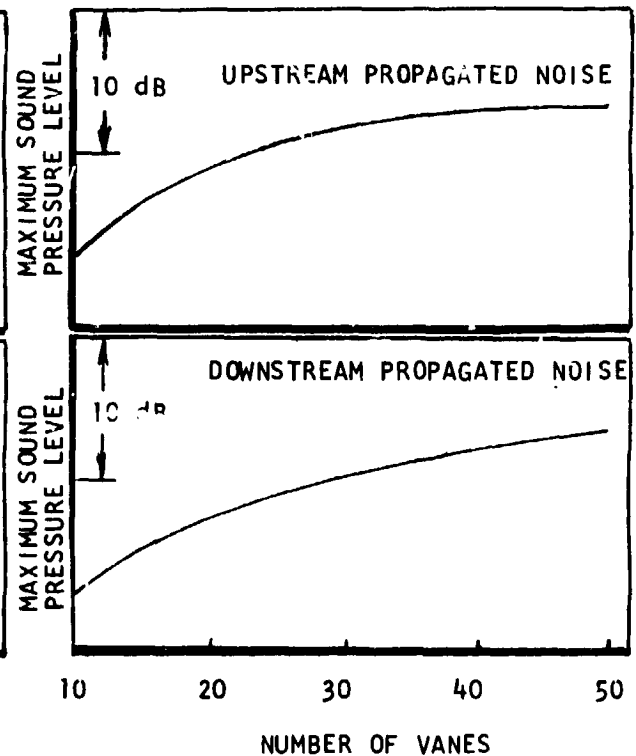
FIGURE 27.   EFFECT OF VANE NUMBER
             ON BROADBAND NOISE

17

The effect of vane number on broadband noise spectra is shown in Figures 28 and 29. The correlation length is held constant as the vane number is varied. The nondimensional SCALE, defined as the ratio of turbulence scale to stator spacing, appears in the noise model and is proportional to the number of vanes. The value of SCALE = .05 was matched to the 50 vane and 10 vane case in Figures 28 and 29, respectively. The advantage of fewer, long chord vanes is clearly seen and a 12-13 dB reduction in rearward radiated stator noise is expected for the QHF fan.

Acoustic Comparison of Final Designs

Acoustic analysis of the final aerodynamic design configurations (defined in Aerodynamic Design Section), was performed to determine acoustic superiority and to provide guidance for the final aerodynamic design. The results are based upon both theoretical noise prediction and empirical correlation of noise from existing fans. The maximum blade passing tone and broadband 1/3 octave SPL at 30.5 m (100 ft.) radius are compared for takeoff and approach power in Table 2. The results are scaled to full size 9072 kg (20,000 lb) thrust class and bypass ratio of 6. Configuration 3 is somewhat better acoustically than configuration 4. Therefore, from both aerodynamic and acoustic standpoint, configuration 3 was selected.

## ACOUSTIC DESIGN SUMMARY

The results of the acoustic design studies can be summarized in terms of a series of guidelines for the aerodynamicist to follow for the development of a quiet, high speed fan:

- Maintain high specific flow through fan
- Increase rotor relative exit angle
- Minimize the number of stator vanes
- Increase stator chord
- Reduce stator camber

Changes in other geometric and aerodynamic parameters produced insignificant changes in noise generation and radiation.

| | TABLE 2. SOUND PRESSURE LEVEL COMPARISONS OF QHF CONFIGURATIONS, dB re 2 x 10$^{-5}$ PASCAL | | | | |
|---|---|---|---|---|---|
| | Maximum Value at 30.5 Meters (100 Ft.) BPF = Blade Passage Frequency BB = Maximum 1/3 Octave Excluding BPF | | | | |
| | CONFIGURATION 3 | | CONFIGURATION 4 | |
| | TAKEOFF | APPROACH | TAKEOFF | APPROACH |
| FRONT BPF | 98 | 94 | 102 | 93 |
| FRONT BB | 92 | 82 | 85 | 82 |
| REAR BPF | 91 | 77 | 88 | 84 |
| REAR BB | 103 | 84 | 111 | 84 |
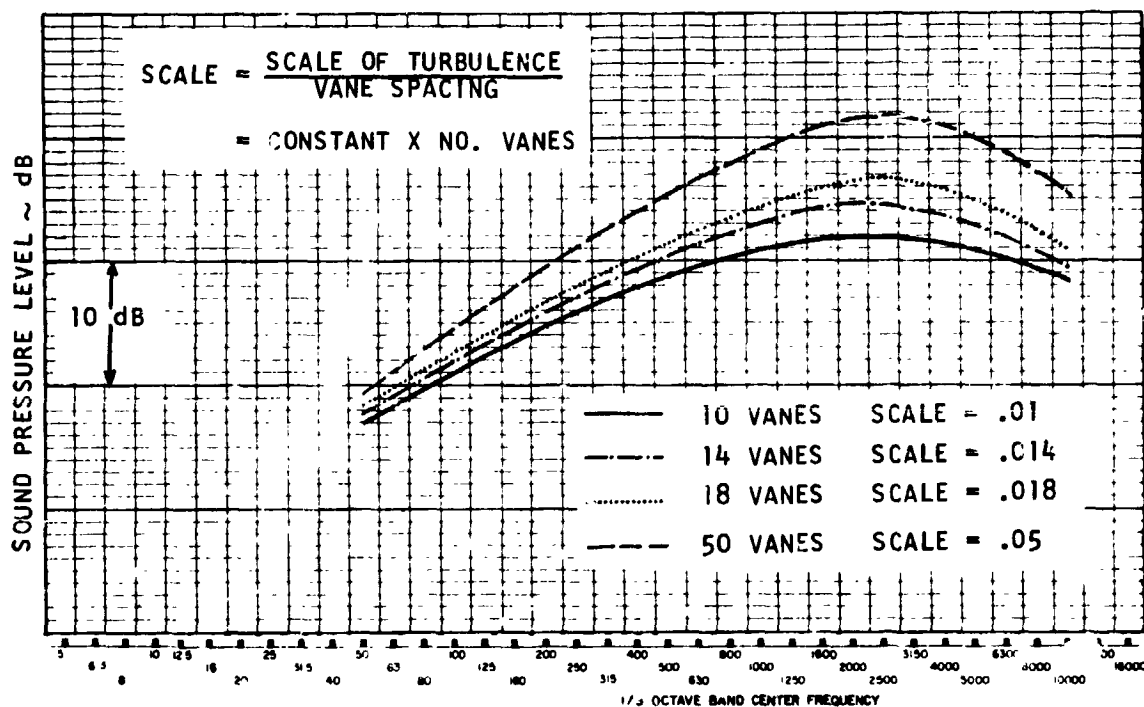
FIGURE 28.   EFFECT OF VANE NUMBER ON DOWNSTREAM BROADBAND SPECTRA--
             CONFIGURATION 3. SMALL SCALE TURBULENCE
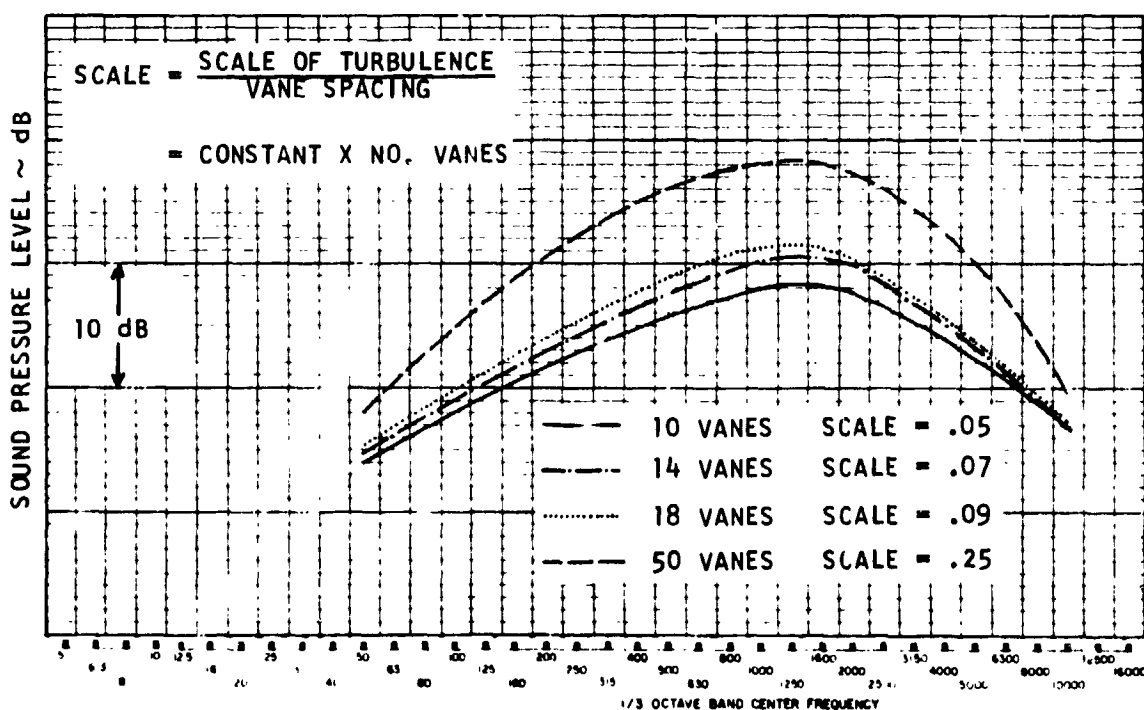


FIGURE 29.   EFFECT OF VANE NUMBER ON DOWNSTREAM BROADBAND SPECTRA--
             CONFIGURATION 3. LARGE SCALE TURBULENCE

# AERODYNAMIC DESIGN

## DESIGN CONSTRAINTS

Design parameters for the QHF fan are:

| | |
|---|---|
| Stage pressure ratio | 1.65 |
| Corrected airflow per unit frontal area - kg/sec m$^2$ (lbm/sec-ft$^2$) | 219.71 (45) |
| Rotor corrected tip speed - m/sec (ft/sec) | 548.64 (1800) |
| Rotor inlet hub-tip ratio | 0.426 |
| Rotor blade aspect ratio | 1.715 |
| Fan efficiency | 84% |

The QHF fan has a 508 mm (20 in.) tip diameter which corresponds to a 0.337 linear scale of the size required to produce the same thrust as the GMA 100/1 fan, a conventional DDA 1.65 pressure ratio fan used to compare QHF performance. The tip speed of 548.64 m/sec (1800 ft/sec) was chosen to keep the rotor and stator loading levels within acceptable limits. Design point corrected airflow and speed for the rig are 36.56 kg/sec (80.6 lb/sec) and 20,626 RPM, respectively.

A relatively low value of rotor blade aspect ratio (1.715) was selected to eliminate the need for part-span shrouds. With the high inlet specific flow, part-span shroud blockage would be sufficient to increase the effective flow per unit area to a point very near choke at the rotor inlet.

To ensure the near-sonic block capability of the high inlet specific flow, the flow path walls are contoured to give an essentially flat inlet velocity profile. Rotor inlet Mach number distributions are shown in Figure 30. The average value of inlet axial Mach number is 0.725.
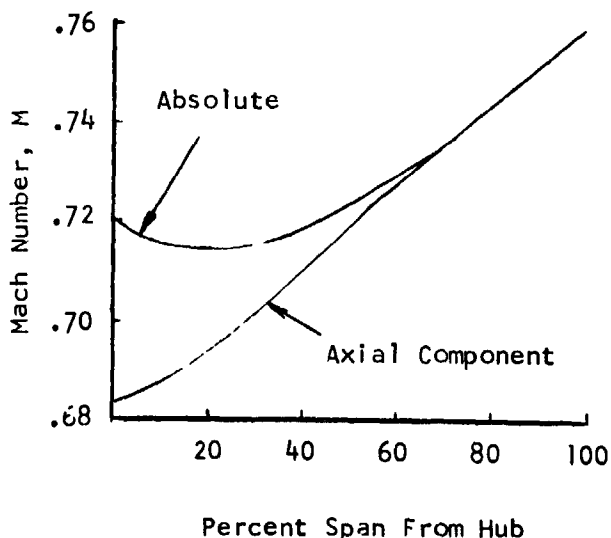


FIGURE 30. ROTOR INLET MACH NUMBER DISTRIBUTIONS

The high fan-face-inlet absolute Mach number combined with the high tip speed yield supersonic inlet relative Mach numbers over the entire span with a tip value of 1.83. The rotor exit relative Mach numbers are supersonic over the upper 40% of the span.

The number of rotor and stator airfoils are 24 and 10, respectively. The number of rotor airfoils was fixed by performance and structural considerations while the number of vanes was set by acoustic constraints.

The preliminary design point analysis of the QHF fan was performed using the DDA developed Axial Compressor Design Calculation which obtains a solution to the continuity, energy, and full radial equilibrium equations for an axisymetric flow field. The equations account for streamline curvature and radial gradients of total enthalpy and entropy. This calculation procedure predicts the aerodynamic solution of the flow process along streamlines at interblade row stations.

## ENGINE OPERATION

The QHF fan operation is explained in terms of the typical 1.65 pressure ratio fan map shown in Figure 31. Typical fan operation is along line B-A-C in Figure 31, where points B, A and C represent the approach, takeoff and maximum-cruise operating points, respectively. In this case, thrust modulation is accompanied by changes in both airflow and rotor speed. For the QHF fan, however, a minimum airflow equal to the takeoff value must be achieved at the approach thrust level to maintain the near sonic acoustic block at the rotor face. This condition can be achieved through the addition of a variable area fan exhaust nozzle and variable fan stator. The QHF approach operating point at takeoff airflow and at the same thrust level as the approach condition for the typical fan is shown on the map in Figure 31 as point B'. This condition is reached from takeoff by increasing the secondary nozzle area 96% for an approach thrust of 30% of takeoff.
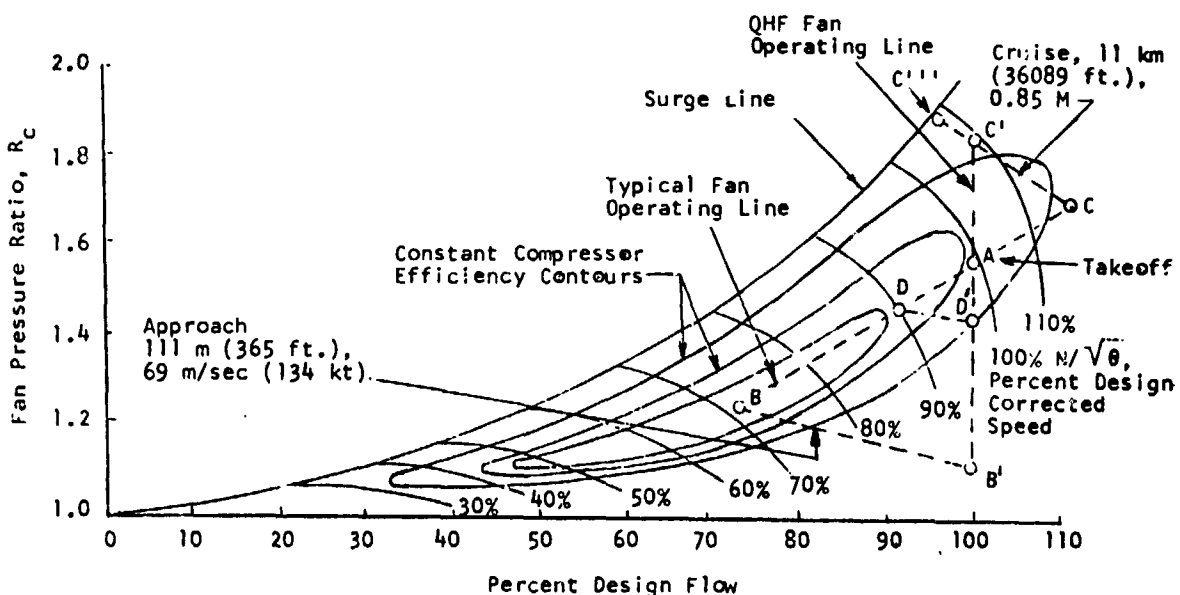


FIGURE 31. TYPICAL 1.65 PRESSURE RATIO FAN MAP

The maximum-cruise point for the QHF fan corresponding to 100% design air-flow is shown in Figure 31 as point C' and lies along the constant maximum cruise thrust line through point C. An 18% reduction in secondary nozzle area is required to reach point C' from point A. Since quiet operation is not important during maximum cruise operation, the maximum cruise operating point could be chosen to lie anywhere along the maximum cruise thrust line C-C'''. However, the surge margin for maximum cruise operating points with airflow less than the 100% design flow value is considered marginal. Also the amount of airflow in excess of the design point value which can be achieved is limited due to the high specific inlet flow at the design point. The actual value of limiting corrected airflow should be determined during rig tests.

Maximum-Cruise Surge Margin

The data from two similar fan rigs with design tip speeds of 549 m/sec (1800 ft/sec) and 625 m/sec (2050 ft/sec) have been used to construct the high speed fan map for the QHF fan shown in Figure 32. Rotor performance
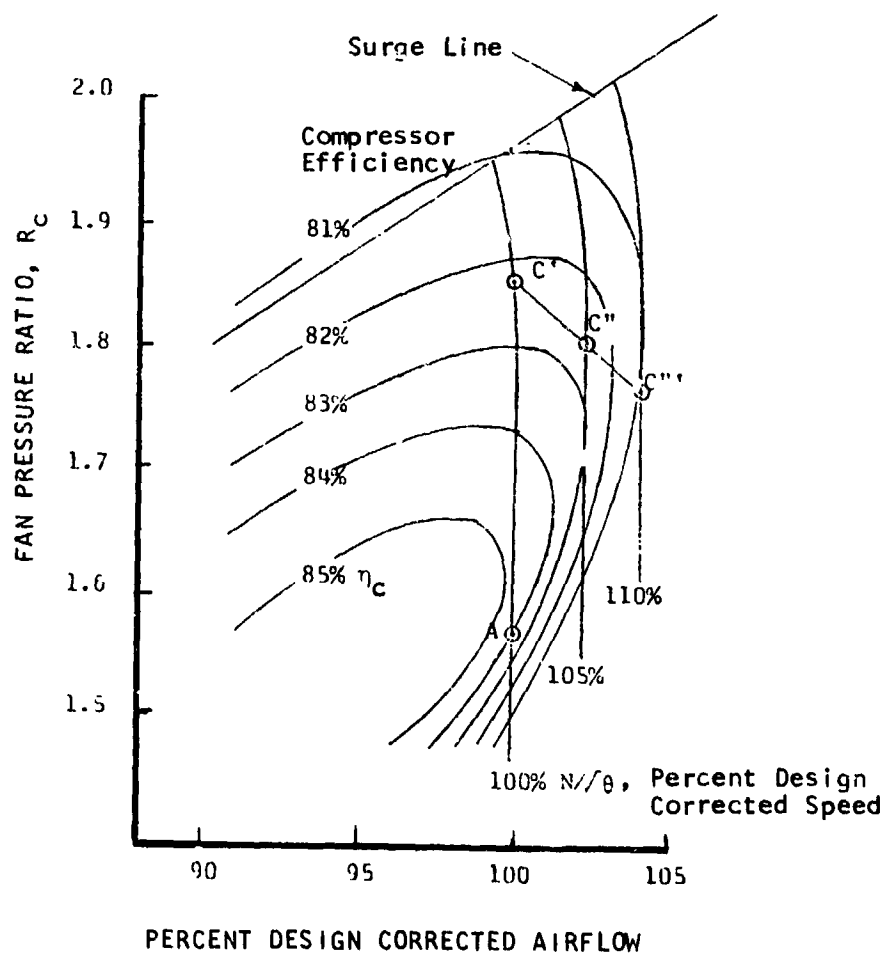


FIGURE 32. QHF ESTIMATED HIGH SPEED PERFORMANCE MAP

22

at 100% of design corrected speed is the 549 m/sec fan measured first rotor performance and the stator performance is analytically projected from 625 m/sec fan stage stator performance. The line labeled "Surge Line" is a straight line through the steady state 549 m/sec fan data points nearest to the surge line at 90% and 100% of design corrected speed. This estimate of the surge line is conservative since:

- o Steady state data points could have been taken at a higher first stage pressure ratio at both 90% and 100% of design corrected speed, and

- o The second stage of the 549 m/sec fan was most likely responsible for surge at 90% and 100% of design corrected speed

The performance at 105% and 110% of design corrected speed is obtained by analytically projecting the performance of the 625 m/sec fan stage. Airflow as a function of speed is obtained by holding rotor incidence constant, e.g., a 5% speed increase results in a 5% increase in axial velocity at fan rotor inlet which is equivalent to an airflow increase of about 2.1%. At 110% of design corrected speed, the efficiency is equal to that demonstrated by the 625 m/sec stage at its design speed.

The point C' in Figure 32 located at 100% of design corrected speed and an $R_c$ equal to 1.83, is the same operating point as C' in Figure 31 and was chosen as the maximum-cruise thrust condition. The same value of thrust can be obtained at points C' ' and C' ' ' located at 105% and 110% of design corrected speed, respectively. The surge margin* at these three points is:

| Point | Surge Margin |
|-------|--------------|
| C' | 7.7% |
| C' ' | 10.5% |
| C' ' ' | 13.5% |

Since there is minimal inlet distortion in the QHF fan, an 8% surge margin is considered adequate at the maximum-cruise thrust condition.

---

*Surge Margin is defined:

$$\text{Surge Margin} = \left[ \left. \frac{\left( \dfrac{R_c}{W \frac{\sqrt{\theta}}{\delta}} \right)_{S.L.}}{\left( \dfrac{R_c}{W \frac{\sqrt{\theta}}{\delta}} \right)_{O.P.}} \right|_{\frac{N}{\sqrt{\theta}} = \text{Constant}} - 1.0 \right] \times 100$$

where:     $R_c$ = fan pressure ratio

$W \dfrac{\sqrt{\theta}}{\delta}$ = corrected airflow

$\dfrac{N}{\sqrt{\theta}}$ = corrected speed

S.L. = surge line

O.P. = operating point

Approach Thrust Level. Typical approach thrust levels of approximately 30 percent for CTOL and 70 percent for STOL have been selected as representative numbers for this study. The 30 percent thrust point represents the lower range of the thrust requirements of typical CTOL transports. The actual thrust requirements depend upon the type of aircraft and the gross weight during approach; however these requirement normally fall in the range of 30 to 50 percent (Reference 11, page 467). Recent industry studies have indicated that for STOL application 70 percent thrust is representative. Again depending upon the lift system used, the aircraft, the gross weight, and the field length, this number can vary between 50 and 70 percent. The selection of the higher value for STOL and the lower value for CTOL thus brackets the complete range.

Operating conditions shown by B-B' and D-D' in Figure 31 are those representing low altitude approach, during which noise control is desired. B-B' is obtained at approximately 30 percent thrust level, with conventional mechanical flaps. As such, B-B' represents the lowest expected thrust level during approach.

For STOL aircraft using augmented flaps for achievement of high lift, the landing approach condition is represented by D-D' on the figure, which occurs at approximately 70% thrust level. At this condition, the secondary nozzle flow area need be increased only about 20%.

The approach and maximum-cruise operating points are identified as critical areas to the QHF aerodynamic concept. At the approach point, the noise reduction potential of the QHF fan rests on the ability to achieve the design point airflow, while at the maximum-cruise operating point, the engine performance could be seriously limited by insufficient surge margin. The QHF fan design, therefore, must consider the aerodynamic performance at these operating points in addition to design point operation at takeoff power.

The QHF fan can certainly be evaluated over this entire operating range in the Lewis performance facility, W-8, and during aft noise testing in the noise facility, W-2. A study of the losses expected in the exhaust collector of W-2 indicate that forward noise measurements may be possible only down to a pressure ratio of about 1.25, corresponding to 45% of maximum thrust. This is as low an approach thrust as many aircraft would require and should demonstrate that forward noise of the QHF fan is independent of downstream conditions as long as the rotor is operating at its design flow conditions.

## RIG FLOW PATH CONFIGURATIONS

A series of four rig flow path configurations were studied during the
QHF preliminary design. Various geometric and aerodynamic parameters for
these configurations are presented in Table 3 where the numberical designa-
tions indicate the chronological order of investigation. Configurations
1, 2 and 4 have essentially the same rotor which was designed for zero
radial total pressure gradient downstream of the stage, while configura-
tion 3 rotor was designed for a 5% positive hub-to-tip total pressure
gradient at the rotor exit. In order to decrease rotor-stator interaction
noise, the stator leading edge was located two rotor chords from the
rotor trailing edge in all configurations. Configuration 1 stator row
consists of a single row of 7 inch chord vanes. To avoid choking the
stator row at the approach condition, the single stator row of configuration
1 was replaced in configurations 2, 3 and 4 with a tandem row with the
first vane resetable. Also, in configurations 3 and 4, the overall stator
chord length was increased from 178 mm (7 inches) to 229 mm (9 inches) to
reduce the response of the stator to rotor wakes and hence reduce aft-
radiated noise. In configurations 2, 3 and 4 the stator chord and camber
were equally divided between the first and second stators.

TABLE 3.   RIG FLOW PATH CONFIGURATIONS

|  | CONFIGURATION | | | |
| --- | --- | --- | --- | --- |
|  | 1 | 2 | 3 | 4 |
| Stator Exit Tip Radius mm, (in.) | 2⌐⌐ (10) | 279.4 (11) | 298.45 (11.75) | 298.45 (11.75) |
| Rotor Total Pressure Gradient | Uniform | Uniform | 5% | Uniform |
| Stator Exit Mach Number (Takeoff) | 0.50 | 0.40 | 0.40 | 0.35 |
| Stator Hub D Factor (Takeoff) | 0.54 | 0.55 | 0.60 | 0.60 |
| Stator Hub Inlet Mach Number (Approach) | 1.0 | 0.95 | 0.82 | 0.90 |

Configuration 1. Configuration 1 flowpath, shown schematically in Figure 33 has a constant tip diameter of 508 mm (20 in.) throughout the stage. The stator hub exit radius was fixed at 146 mm (5.75 in.) for a stator exit Mach number of 0.52 at takeoff. Radial distributions of rotor and stator diffusion factors, shown in Figure 34, indicate moderate loading. The rotor inlet is supersonic across the entire span as indicated in Figure 35 where relative Mach numbers are plotted versus percent span. Moderately high stator inlet Mach numbers at takeoff are shown in Figure 36. Substantially higher stator hub inlet Mach numbers would exist at the approach condition. An off-design calculation at the approach condition yields a stator exit Mach number of 0.92 which is sufficiently high to choke the entire annulus. For this reason, configuration 1 flowpath was discarded early in the preliminary design.
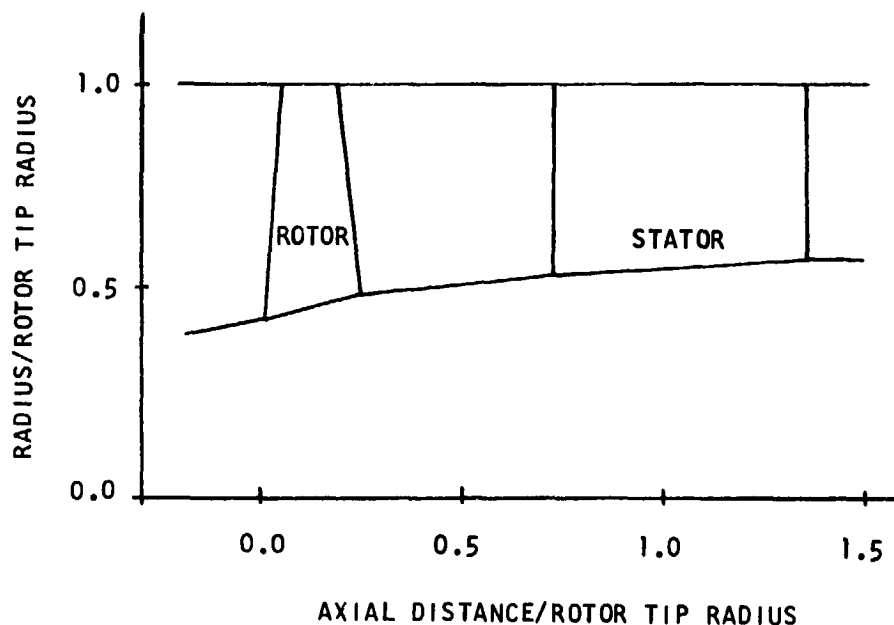


FIGURE 33. SCHEMATIC OF CONFIGURATION 1 RIG FLOW PATH

26
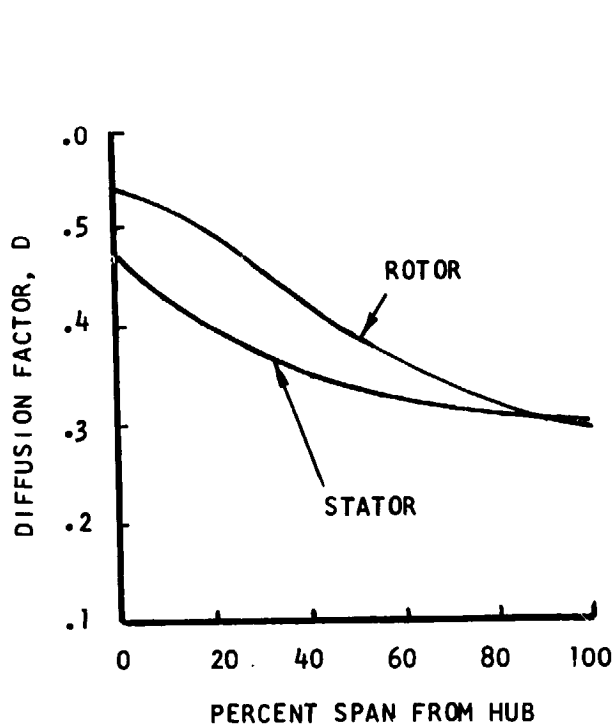
FIGURE 34. BLADE ROW DIFFUSION FACTOR
DISTRIBUTIONS AT TAKEOFF--
CONFIGURATION 1 RIG FLOW
PATH
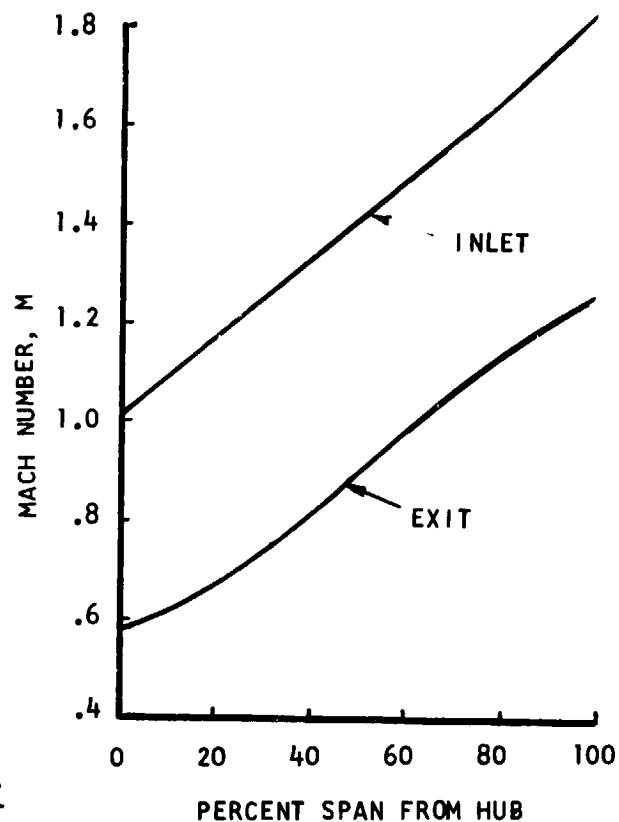


FIGURE 35. ROTOR INLET AND EXIT
RELATIVE MACH NUMBER
DISTRIBUTIONS AT TAKEOFF--
CONFIGURATION 1 RIG FLOW
PATH
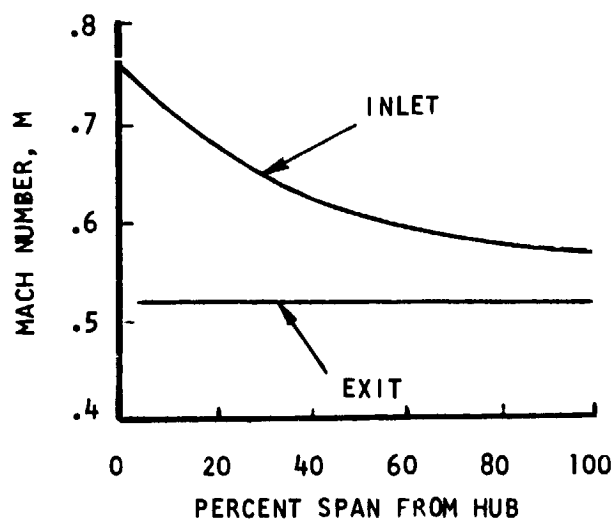


FIGURE 36. STATOR INLET AND EXIT MACH NUMBER
DISTRIBUTIONS AT TAKEOFF--
CONFIGURATION 1 RIG FLOW PATH

27

Configuration 2. In configuration 2, shown in Figure 37, the exit annulus area was opened up to avoid choking the annulus at approach. Also, to eliminate excessive stator hub loading at takeoff, the stator was moved radially outward (stator exit tip radius = 27.94 cm (11 in.). Radial distributions of stator Mach numbers and diffusion factors are presented in Figures 38 and 39, respectively. The lower level of stator exit Mach number (0.41) for this design is accompanied by higher stator loading; however, the maximum loading level at the stator hub (D = 0.56) is considered acceptable. Stator inlet Mach numbers have been reduced substantially due to both increased annulus area and radial displacement of the stator.
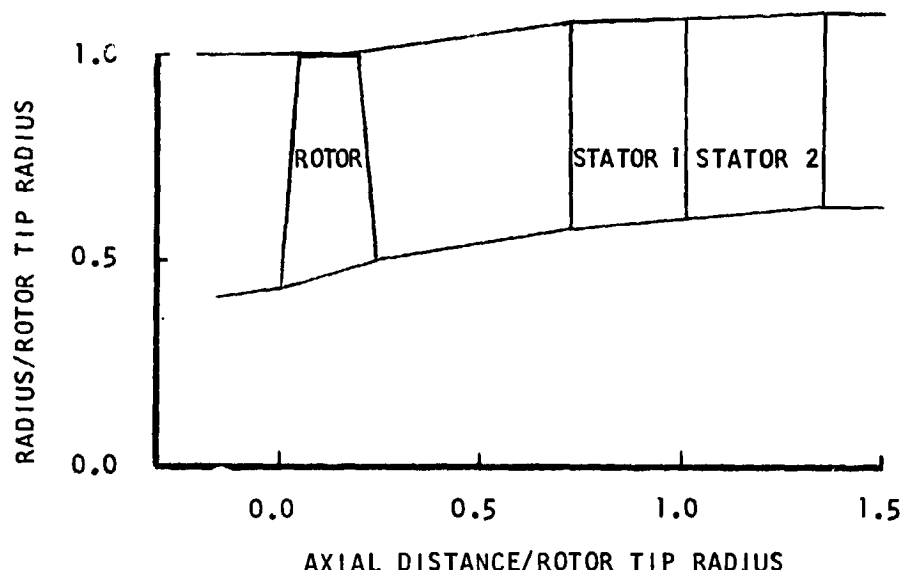


FIGURE 37. SCHEMATIC OF CONFIGURATION 2 RIG FLOW PATH
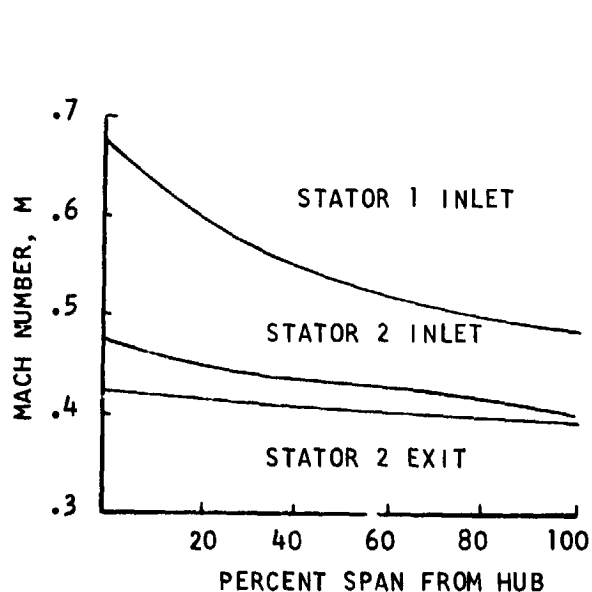


FIGURE 38. STATOR INLET AND EXIT MACH NUMBER DISTRIBUTIONS AT TAKEOFF-- CONFIGURATION 2 RIG FLOW PATH
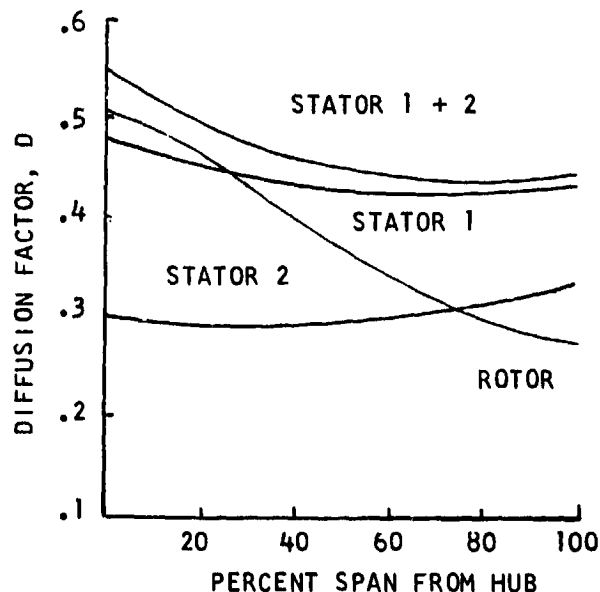
FIGURE 39. ROTOR AND STATOR DIFFUSION FACTOR DISTRIBUTIONS AT TAKEOFF-- CONFIGURATION 2 RIG FLOW PATH

28

As noted previously, configurations 2-4 incorporated tandem vanes. The combined diffusion factor for the tandem vanes was used as a limiting loading parameter in this investigation. Although a small increase in performance has been demonstrated with tandem vanes[12], essentially no increase in operating range has been achieved. The failure of tandem vanes to increase operating range results because, contrary to theoretical calculations, the rear airfoil loading does not remain constant as incidence angle changes. Another contributing factor is thought to be the endwall boundary layers which are not regenerated in passing through the region between the vanes.

A detailed off-design analysis was made to determine the performance of configuration 2 at approach. In the numerical solution for the approach point flow conditions the total pressure distribution at the rotor exit must be known. For this purpose, the assumption was made that the rotor exit flow angle distribution is independent of rotor pressure ratio at a particular rotor speed. The rationale for this assumption is apparent from Figures 40 and 41 where radial distributions of measured rotor exit total pressure and relative flow angle downstream of the GMA 100 fan rotor are plotted for stage pressure ratios of 1.70 and 1.46 at design speed. The data shown in Figure 41 indicates essentially no change in the rotor exit relative flow angle distribution with pressure ratio.
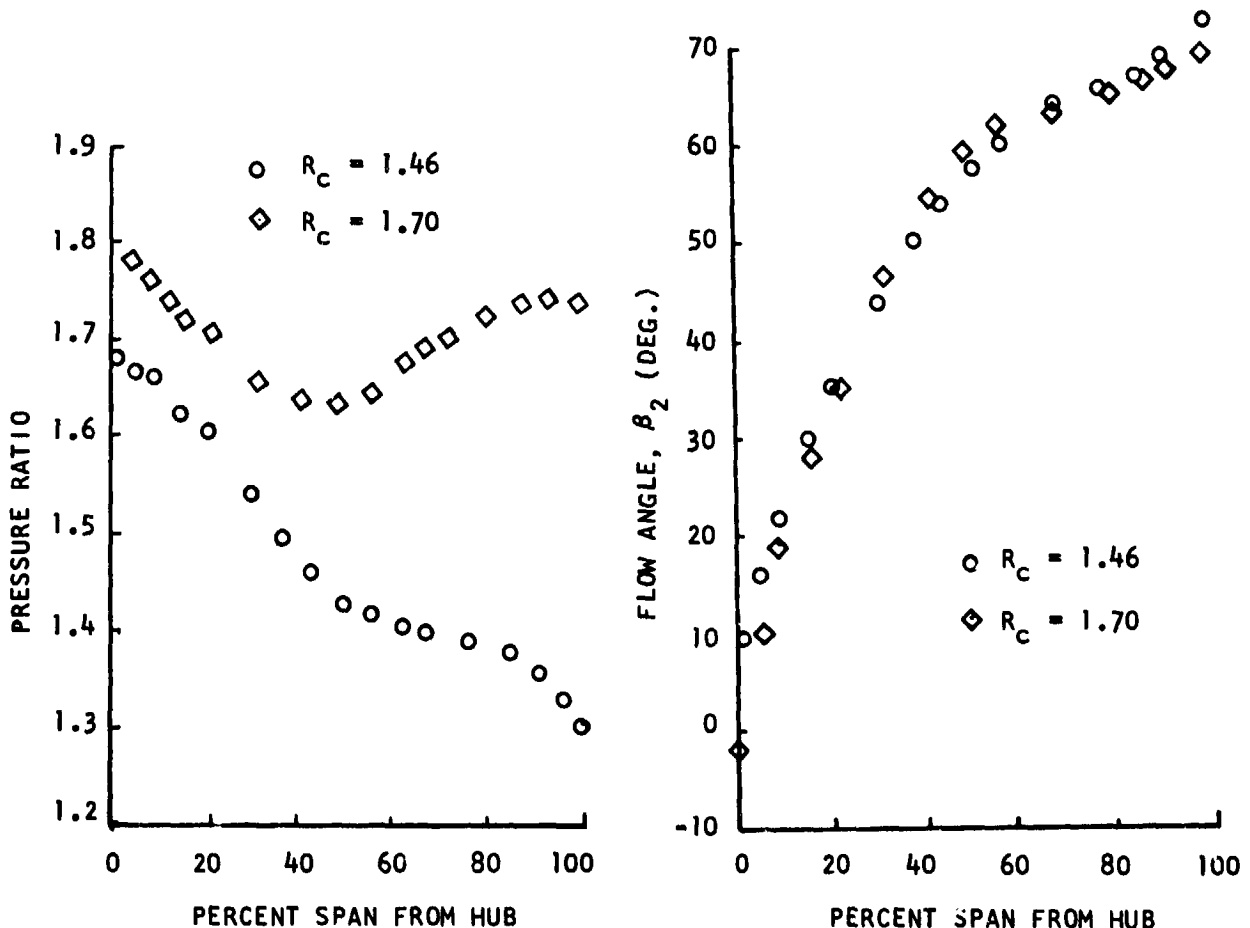


FIGURE 40. GMA 100 ROTOR PRESSURE RATIO DISTRIBUTIONS AT DESIGN SPEED FOR STAGE PRESSURE RATIOS OF 1.70 AND 1.46

FIGURE 41. GMA 100 ROTOR EXIT RELATIVE FLOW ANGLE DISTRIBUTIONS AT DESIGN SPEED FOR STAGE PRESSURE RATIOS OF 1.70 AND 1.46

29

In calculating the approach point flow conditions, an iterative procedure was used wherein an estimate of the rotor exit total pressure distribution was made and the computed rotor exit relative flow angle distribution was compared with the design point flow angle distribution. Subsequently, the estimate of total pressure distribution was revised to yield better agreement between the design point and computed flow angle distributions.

This iterative numerical solution procedure is depicted in Figures 42 and 43 where three total pressure distributions and the corresponding relative flow angle distributions are shown for the approach point stage pressure ratio of 1.15. The last solution corresponding to pressure distribution 3 yields good agreement between the design point and computed relative flow angle distributions and is taken as the approach point solution.
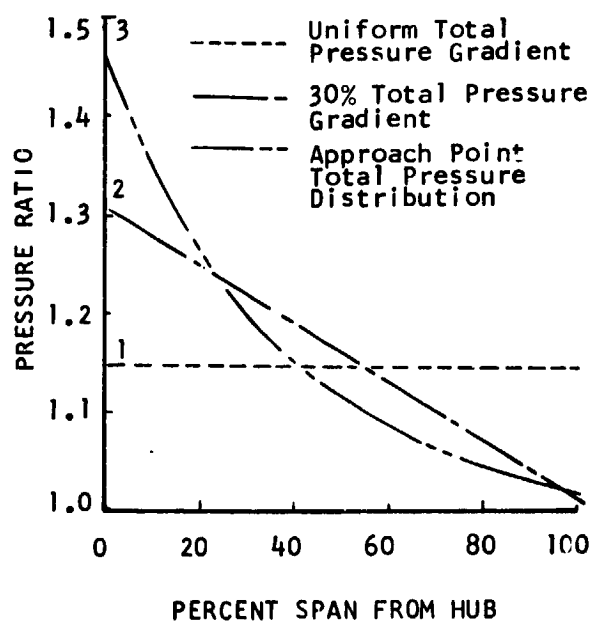


FIGURE 42. ROTOR EXIT TOTAL PRESSURE RATIO DISTRIBUTIONS WITH STAGE PRESSURE RATIO OF 1.15-- CONFIGURATION 2 RIG FLOW PATH
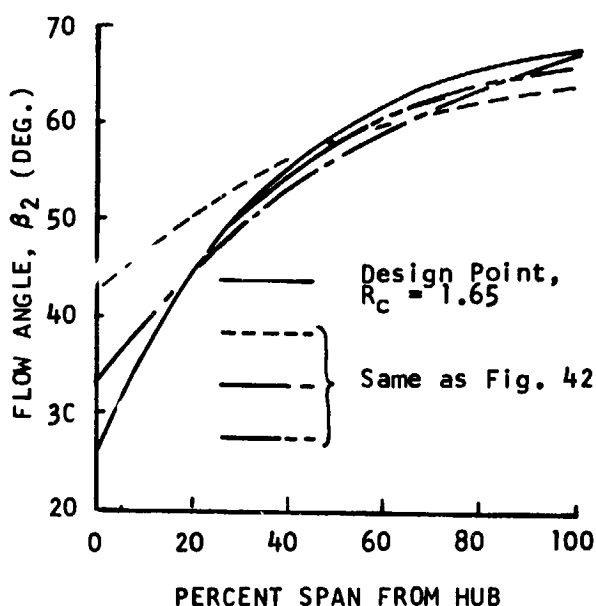
FIGURE 43. ROTOR EXIT RELATIVE FLOW ANGLE DISTRIBUTIONS FOR VARIOUS ROTOR EXIT TOTAL PRESSURE DISTRIBUTIONS WITH STAGE PRESSURE RATIO OF 1.15-- CONFIGURATION 2 RIG FLOW PATH

30

In all off-design calculations it was assumed that the rotor total pressure
loss distribution was the same as at the design point. Cascade data shows
that the total pressure loss coefficient is essentially independent of
static pressure ratio for the QHF operating range.

Configuration 2 stator inlet Mach number distribution at approach is shown
in Figure 44. The stator inlet hub Mach number was considered sufficiently
high to choke the hub. However, the steep inlet Mach number gradient
suggested that the high Mach number at the hub might be avoided by designing
for a positive hub-to-tip total pressure gradient downstream of the rotor
at takeoff.
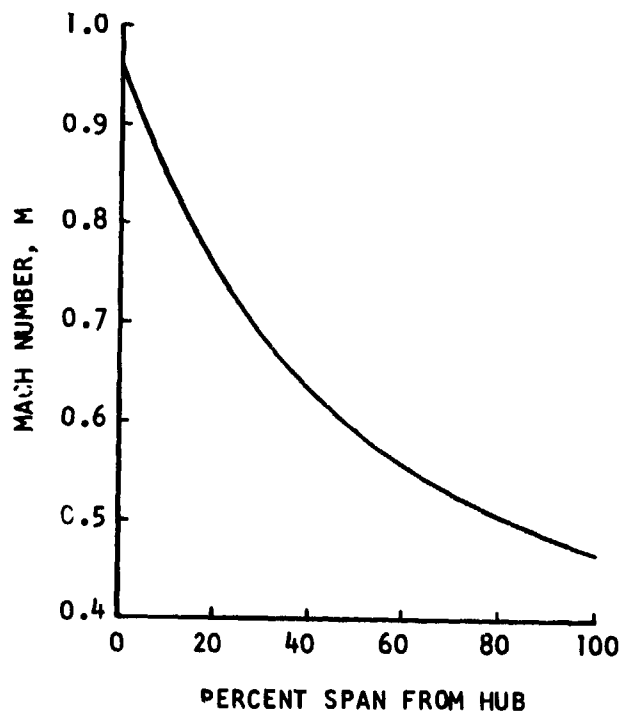


FIGURE 44. STATOR INLET MACH NUMBER DISTRIBUTION AT
APPROACH-- CONFIGURATION 2 RIG FLOW PATH

Configuration 3. Configuration 3 flowpath, shown in Figure 45, was designed for a positive 5% hub-to-tip total pressure gradient at the rotor exit. In this case, rotor relative Mach number and diffusion factor distributions differ only slightly from the previous designs. As predicted, the total pressure gradient decreased the stator hub Mach number at approach; however, the stator hub loading at takeoff increased sufficiently so that the stator had to be moved further out radially--stator exit tip radius = 29.85 cm (11.75 in.). Stator inlet and exit Mach number distributions and diffusion factor distributions are presented in Figures 46 and 47, respectively. A substantial reduction in stator inlet hub Mach number is shown over the previous design, while the stator hub loading increased slightly.

A concern in this design was the annulus wall boundary layer behavior between the rotor and stator due to the large adverse pressure gradient. Skin friction coefficients obtained from a Mellor-Herring turbulent boundary layer calculation for both inner and outer annulus walls are presented in Figure 48. Using the criterion $C_f = 0$ for separated flow, these results indicate no boundary layer separation.

Approach point flow conditions for configuration 3 flowpath were determined in the same manner as outlined above for configuration 2. Stator inlet and exit Mach number distributions at approach are presented in Figure 49. As shown, the maximum stator inlet Mach number occurs at the hub and, as predicted, its value (0.83) is much lower than that for configuration 2.
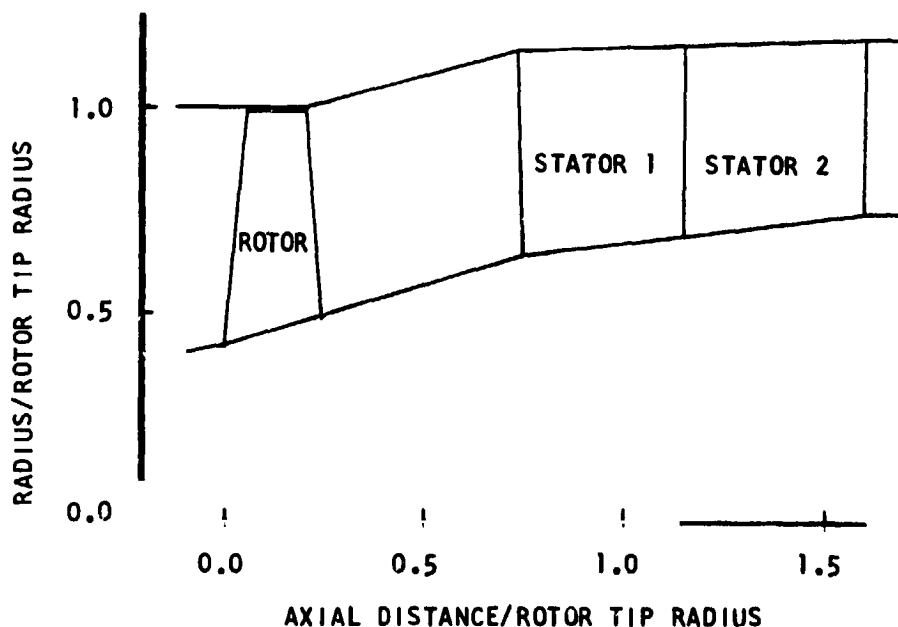


FIGURE 45.   SCHEMATIC OF CONFIGURATION 3 RIG FLOW PATH

32
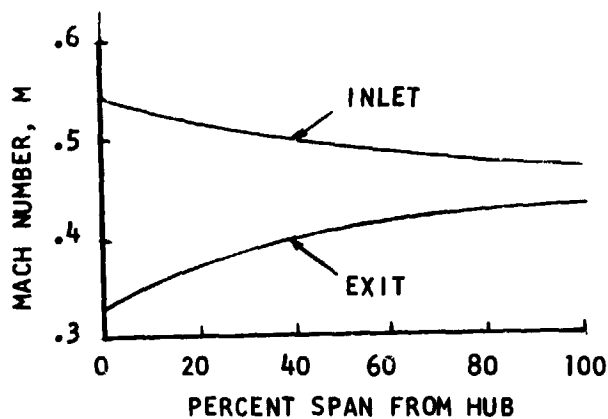
FIGURE 46.  STATOR INLET AND EXIT
MACH NUMBER DISTRIBUTIONS
AT TAKEOFF-- CONFIGURATION
3 RIG FLOW PATH
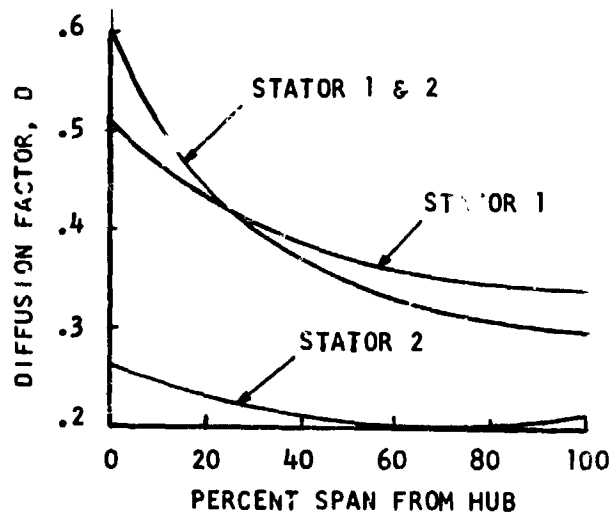


FIGURE 47.  STATOR DIFFUSION FACTOR
DISTRIBUTIONS AT TAKEOFF--
CONFIGURATION 3 RIG FLOW
PATH
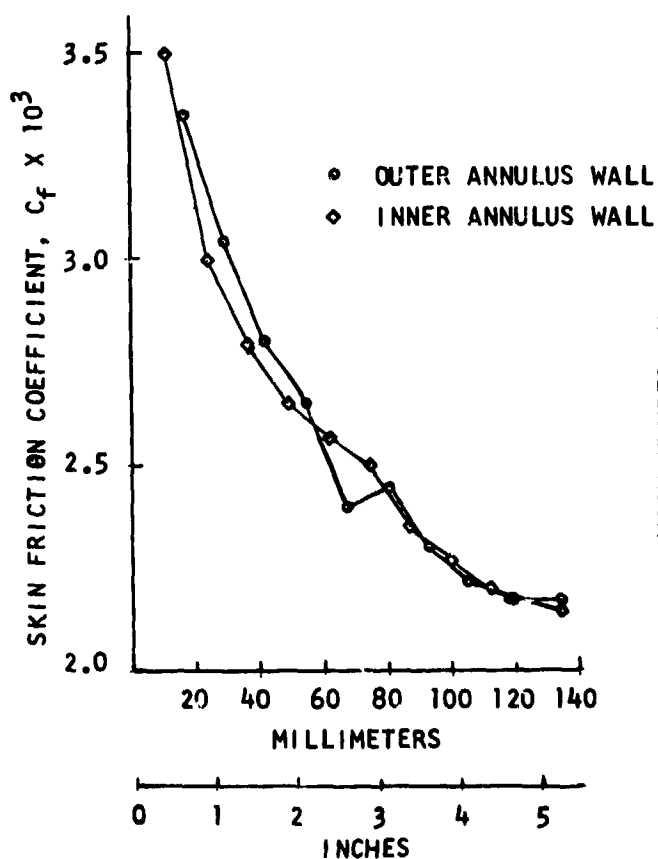


AXIAL DISTANCE FROM ROTOR TRAILING EDGE

FIGURE 48.  SKIN FRICTION COEFFICIENTS
FOR INNER AND OUTER ANNULUS
WALLS BETWEEN ROTOR AND
STATOR AT TAKEOFF-- CON-
FIGURATION 3 RIG FLOW PATH
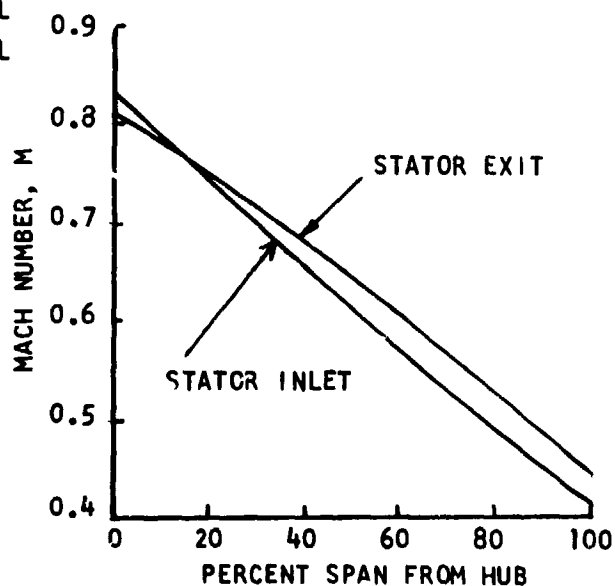


FIGURE 49.  STATOR INLET AND EXIT MACH
NUMBER DISTRIBUTIONS AT
APPROACH-- CONFIGURATION 3
RIG FLOW PATH

33

The approach point flow conditions in the stators are further illustrated in Figure 50 for varying first stator reset angle (negative reset angles are in the direction of increasing blade passage area). The ordinate for these curves, $(A/A*)_{min}$, is the ratio of the minimum blade passage area, $A_{min}$, to the critical throat area, $A*$, as determined by the Kantrowitz starging criterion ($A*$ is the choking area with a normal shock at the passage inlet). In addition, the critical throat area calculation accounts for profile total pressure loss, streamtube contraction and nonaxial streamlines. Values of $(A/A*)_{min}$ less tha.. 1.0 imply the blade passage is choked. As shown in Figure 50 the stator hub is choked in both the first and second stator for all values of first stator reset angle. However, the radial distribution of $(A/A*)_{min}$, shown in Figure 51 for -20° reset angle indicates that only a small portion of the blade row 's choked. According to Figure 50, -20° reset appears to be a near optimum reset angle in that it yields the smallest portion of the blade passage area which is choked.
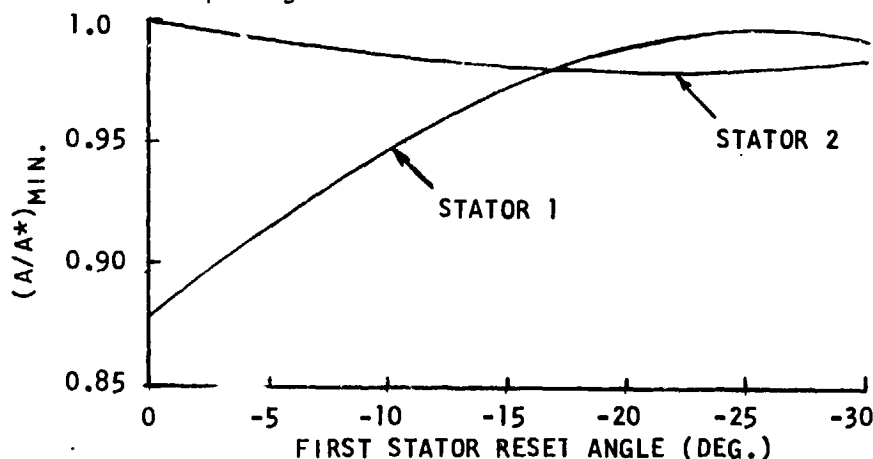


FIGURE 50. STATOR HUB MINIMUM PASSAGE A/A* VERSUS FIRST STATOR RESET ANGLE AT APPROACH-- CONFIGURATION 3 RIG FLOW PATH
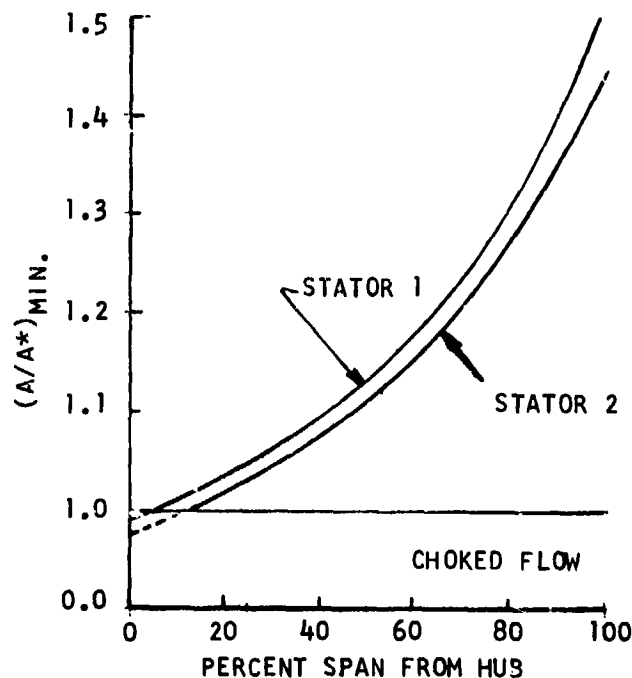


FIGURE 51. STATOR MINIMUM PASSAGE A/A* DISTRIBUTION OF APPROACH FOR -20 DEG. FIRST STATOR RESET ANGLE-- CONFIGURATION 3 RIG FLOW PATH

34

Another consideration in the preliminary design was the maximum local stator blade surface Mach number at the approach condition. While high locally supersonic Mach numbers are objectionable from a performance standpoint, they also provide a noise generation mechanism which should be avoided. Since the stator hub represents the most severe condition in this regard, a blade-to-blade flow analysis was made on the hub stream surface with -20° reset on the first stator. The hub stream tube contained 10% of the full passage flow. When choked flow is encountered in the numerical solution the flow is reduced to the point of incipient choke, indicating a radial re-distribution of the flow, and a solution is made at the reduced flow. The blade surface Mach number distribution, shown in Figure 52 was made at 98% of the predicted hub-stream tube flow. The maximum blade surface Mach number shown is approximately 1.2 which is considered within performance and acoustic limits.
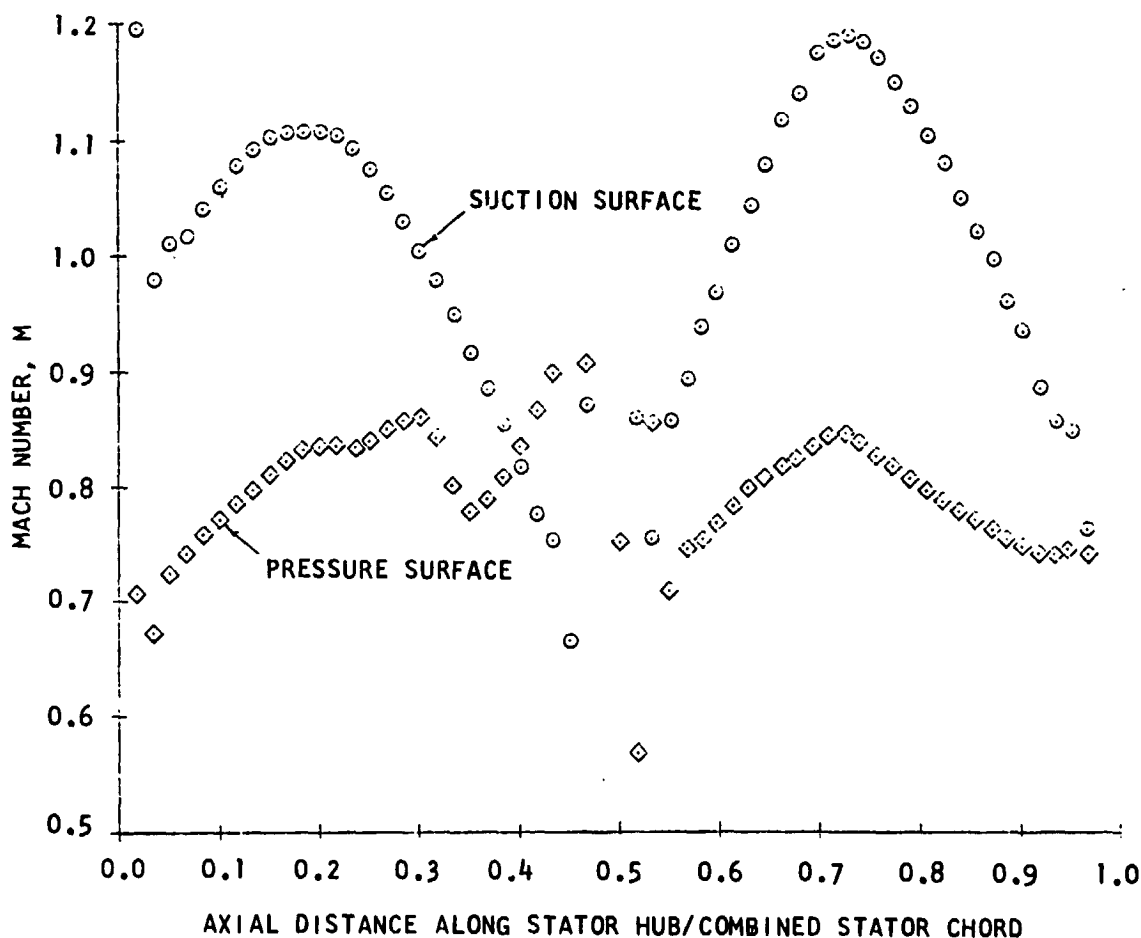


FIGURE 52.    STATOR HUB BLADE SURFACE MACH NUMBER DISTRIBUTION AT
             APPROACH FOR -20 DEG. FIRST STATOR RESET--
             CONFIGURATION 3 RIG FLOW PATH

35

A detailed off-design calculation was made at the maximum cruise point(pressure ratio=1.83) to ensure sufficient surge margin. A concern at this operating point was the stator row blade loading distribution. Again, it was assumed that the radial distribution of rotor exit relative flow at maximum cruise was the same as that at the design point. The same iterative numerical solution procedure outlined above for determination of the approach point flow conditions was used at maximum cruise. The radial distribution of the combined stator diffusion factors at maximum cruise, presented in Figure 53, shows an unacceptable level of blade loading at the stator hub indicating that the hub would pr~'.sbly be stalled. It should be noted that these results are for the rig configuration in which the full rotor flow passes through the stator. In the engine configuration (see Engine Flow Path Section), the core flow does not pass through the stator and the stator hub loading is substantially reduced.
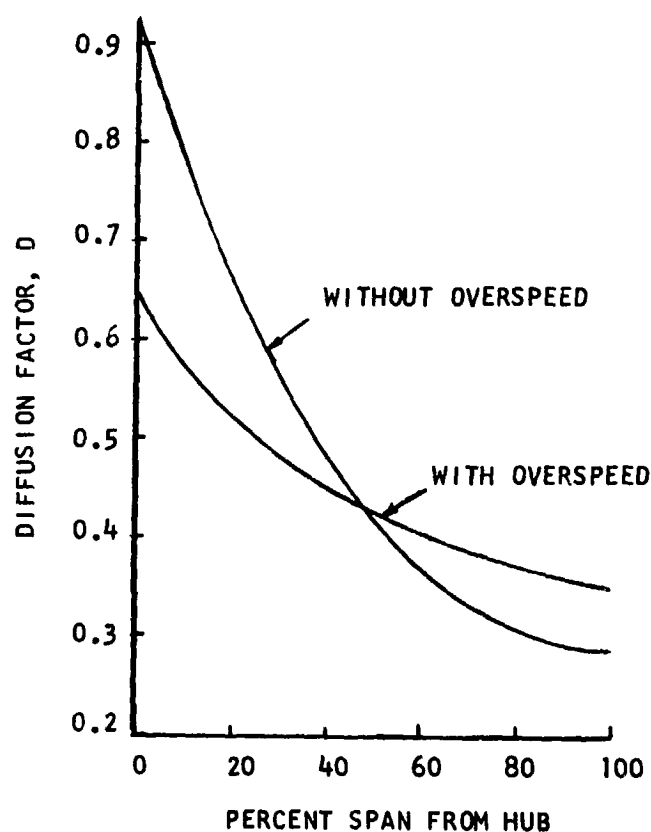


FIGURE 53. COMBINED STATOR DIFFUSION FACTOR
DISTRIBUTION AT MAXIMUM CRUISE--
CCNFIGURATION 3 RIG FLOW PATH

36

In order to demonstrate the engine operation at maximum cruise with the rig, the maximum cruise operating point could be shifted from point C in Figure 32 along the constant thrust line C'-C'' to a point of increased flow. A typical operating point would be at 103% design point flow and 1.80 stage pressure ratio. In the numerical solution for the flow conditions at this operating point it was assumed that the rotor exit relative flow angle distribution was the same as that at the design point. Also, the rotor tip speed, 591 m/sec (1939 ft/sec), was determined by assuming no change in rotor inlet relative flow angle. Combined stator diffusion factors for this condition, plotted in Figure 53 show a substantial reduction in stator hub loading (D = 0.65) and indicate that sufficient surge margin can be achieved at this operating point.

Configuration 4. The fourth and last flow path configuration considered in the preliminary design is shown in Figure 54. This configuration represents an alternate attempt at reducing the stator hub inlet Mach number at approach by increasing the annulus area through the stator thus decreasing the mean Mach number level through the stator. In this case, the stator exit tip radius was held at 298.5 mm (11.75 in.) and the hub radius was decreased to 144.8 mm (5.7 in.) to give 0.35 stator exit Mach number at takeoff. Also, the 5% rotor exit total pressure gradient was eliminated in favor of uniform stage pressure ratio. Stator diffusion factors and Mach
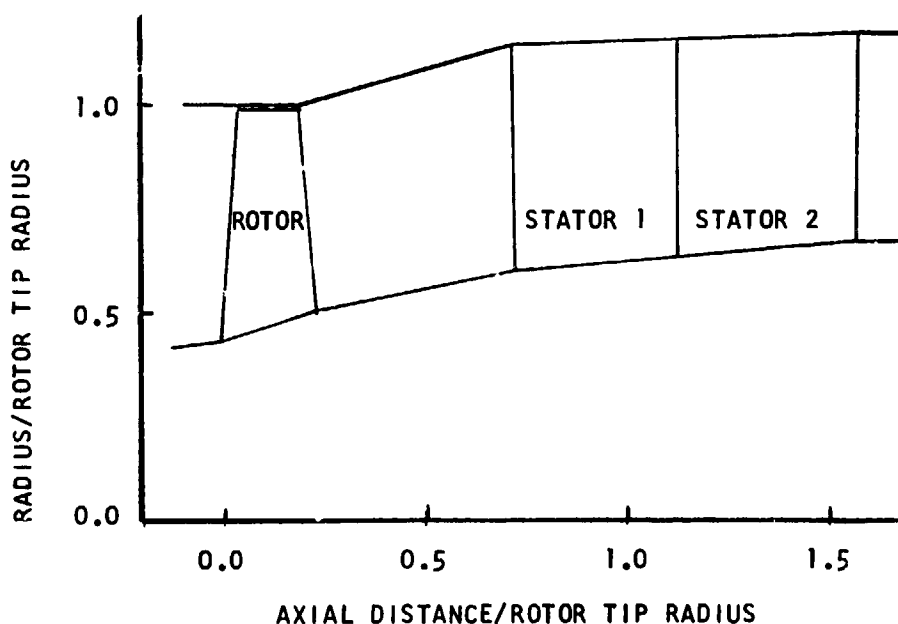


FIGURE 54. SCHEMATIC OF CONFIGURATION 4 RIG FLOW PATH

37

numbers at takeoff are plotted in Figures 55 and 56, respectively. Comparison of these results with those for configuration 3 shows that while the stator hub diffusion factor is about the same in both configurations, the mean loading level is substantially higher in configuration 4. Also, although the mean stator inlet Mach number level is lower in configuration 4, the stator hub value is considerably greater. Therefore, it is reasonable to conclude that the stator hub inlet Mach number at approach would be higher in configuration 4. This conclusion is substantiated in Figure 57, where stator inlet and exit Mach numbers at approach are sufficiently high that a large portion of the blade passage would be choked. Therefore configuration 4 was eliminated from further consideration.



PERCENT SPAN FROM HUB
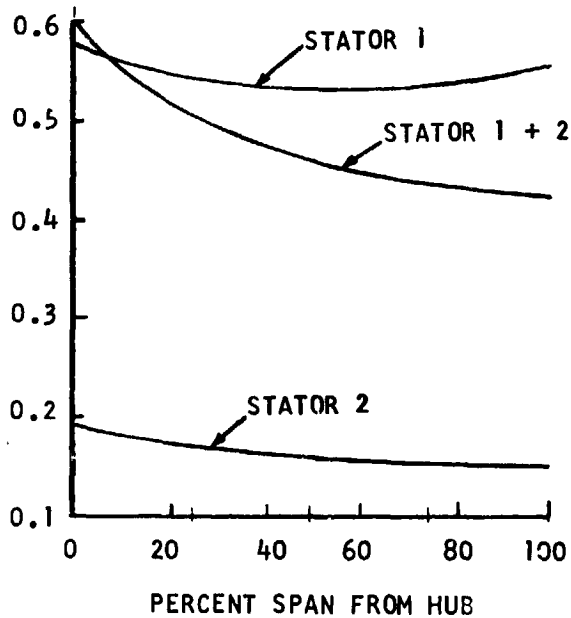
FIGURE 55.  STATOR DIFFUSION FACTOR DISTRIBUTIONS AT TAKEOFF-- CONFIGURATION 4 RIG FLOW PATH



PERCENT SPAN FROM HUB
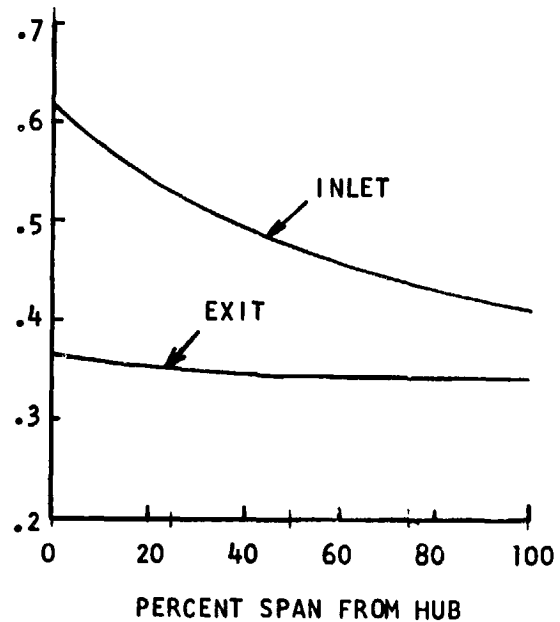
FIGURE 56.  STATOR INLET AND EXIT MACH NUMBER DISTRIBUTIONS AT TAKEOFF-- CONFIGURATION 4 RIG FLOW PATH
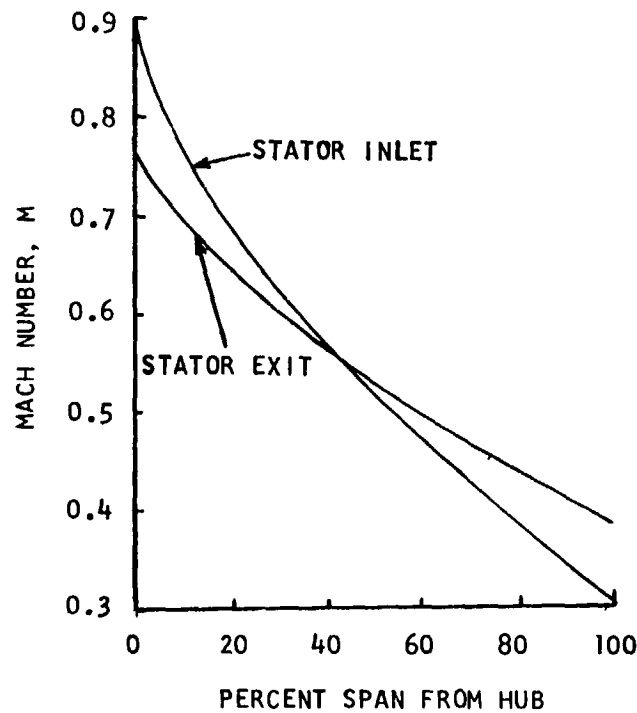
FIGURE 57.   STATOR INLET AND EXIT MACH NUMBER
            DISTRIBUTIONS AT APPROACH--
            CONFIGURATION 4 RIG FLOW PATH


Selection of Final Rig Flow Path.   Configuration 3 was chosen as the final
design for the QHF rig flow path.   Of the four flow paths considered,
configuration 3 represents the best aerodynamic design and demonstrates
the best off-design performance at the approach and maximum cruise operating
points.   Furthermore, the acoustic design analysis indicated no signi-
ficant difference between configurations 3 and 4, which represented the
best acoustic designs.

## ENGINE FLOW PATH

An engine flow path and the rig flow path (configuration 3) are shown overlaid in Figure 58. Both flow paths are drawn to the same scale for comparison purposes. The engine flow path shown is a 0.337 linear scale of the size required to produce the same thrust as the GMA 100/1 fan and was obtained from configuration 3 rig flowpath by diverting 1/7 of the rotor flow through the core engine and tracing the streamline which splits the core engine and bypass flow to determine the hub contour of the bypass duct. Detailed design and off-design analyses were made to determine the engine configuration performance at takeoff, approach and maximum cruise operating points. Comparisons of these results with those for configuration 3 rig flowpath follow.
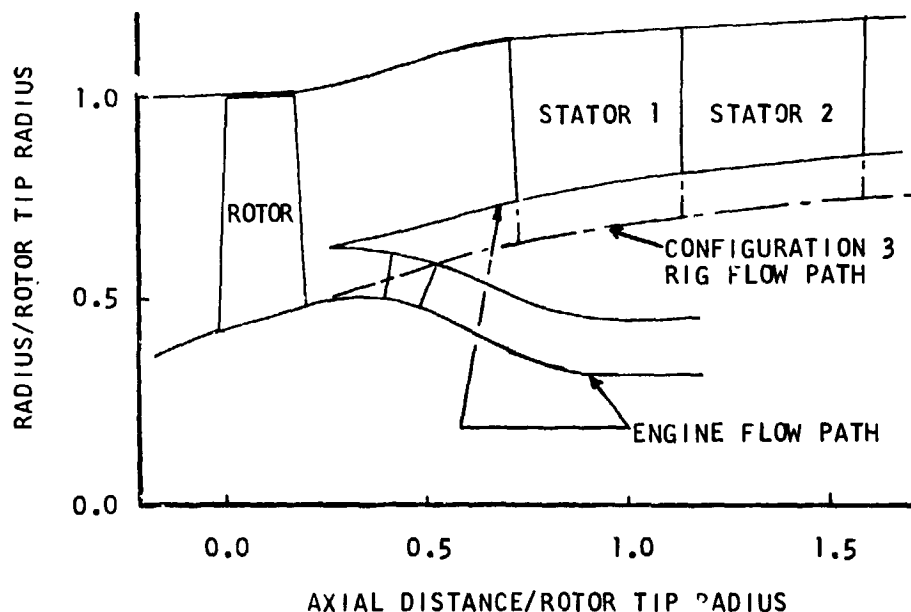
FIGURE 58. SCHEMATIC OF ENGINE AND CONFIGURATION 3 RIG FLOW PATHS

Radial distributions of the bypass stator diffusion factors and inlet Mach numbers at takeoff are presented in Figures 59 and 60, respectively. A substantial reduction in stator hub loading is indicated in Figure 59 for the engine flowpath over the results for configuration 3 rig flowpath shown in Figure 47. However, little difference in stator inlet Mach number is shown between the two flowpaths, Figures 46 and 60.

40
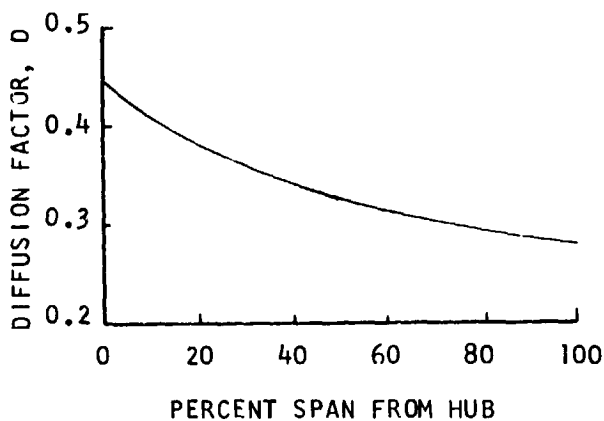
FIGURE 59. STATOR DIFFUSION FACTOR
DISTRIBUTION AT TAKEOFF--
ENGINE FLOW PATH
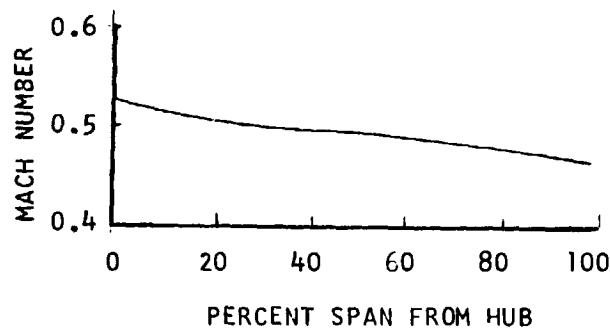
FIGURE 60. STATOR INLET MACH NUMBER
DISTRIBUTION AT TAKEOFF--
ENGINE FLOW PATH

At approach, the stator hub Mach number in the engine configuration (M = 0.725) is much lower than in the rig flowpath (M = 0.825), as shown in Figures 49 and 61. At -20° reset on the first stator, both stators were unchoked over the entire span.

At maximum cruise, the engine stator hub loading (D = 0.70) was substantially lower than in the rig configuration (D = 0.92), as shown in Figures 62 and 53, respectively. However, the stator hub diffusion factor was still marginal with respect to stalling the stator hub. Thus, an off-design analysis was made at the maximum cruise thrust with the operating point shifted to 103% design speed and 1.80 stage pressure ratio, as outlined for the rig configuration in the previous section. In this case, the stator hub loading (Figure 62) was well within loading limits indicating sufficient surge margin is available.
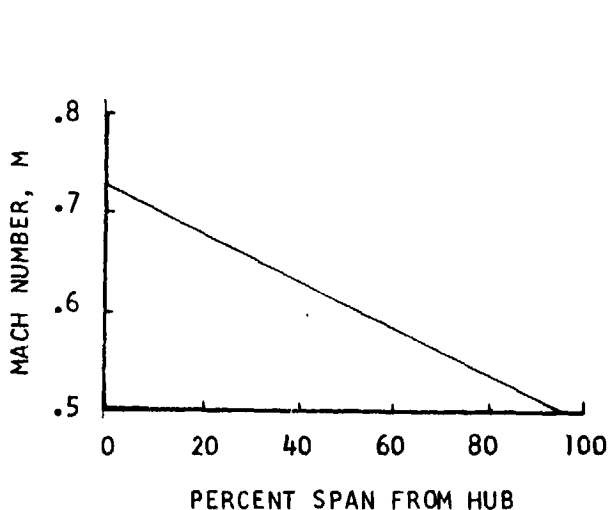


FIGURE 61. STATOR INLET MACH NUMBER
DISTRIBUTION AT APPROACH--
ENGINE FLOW PATH
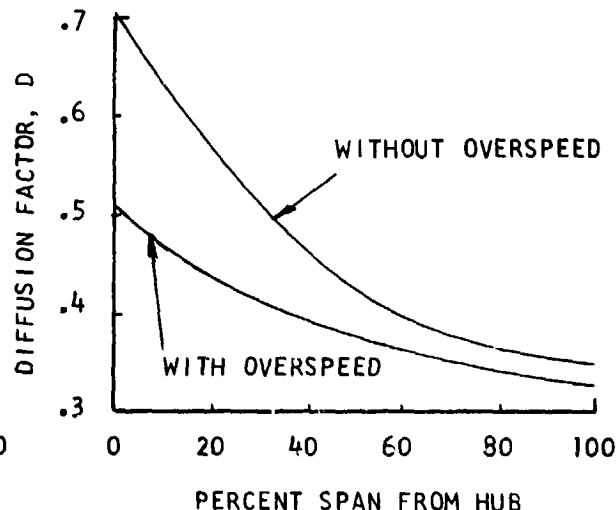
FIGURE 62. STATOR DIFFUSION FACTOR
DISTRIBUTIONS AT MAXIMUM
CRUISE--ENGINE FLOW PATH

41

## AIRFOIL DESIGN

The objectives which have to be satisfied to achieve a good rotor design are low total pressure loss and structural integrity. Due to the high outer span relative Mach numbers, low shock losses are difficult to achieve with conventional multiple arc (MCA) airfoils. For this purpose, a new blade type was developed for the Advanced Fan/Compressor Program and used in the high tip speed (HTS) fan first rotor (RI). This blade type incorporates internal shock control and is referred to as the SCS airfoil.

The upper 40% of the QHF rotor is wholly supersonic and was designed using SCS airfoil sections while the lower 60% of the rotor has subsonic relative exit velocities and was designed with MCA sections.

From both the aerodynamic and structural aspects, the QHF rotor was designed to be similar to the HTS first stage rotor. Figure 63 shows a plot of the QHF solidity versus percent span. Hub solidity was set to be the same as the HTS RI. However, since the QHF rotor has a slightly higher tip relative Mach number than the HTS RI, the tip solidity of the QHF rotor was increased slightly to ensure containment of the shock system within the blade passage. For the chosen solidity and blade number, the chord distribution which results is shown in Figure 64 along with the spanwise thickness-to-chord distribution.
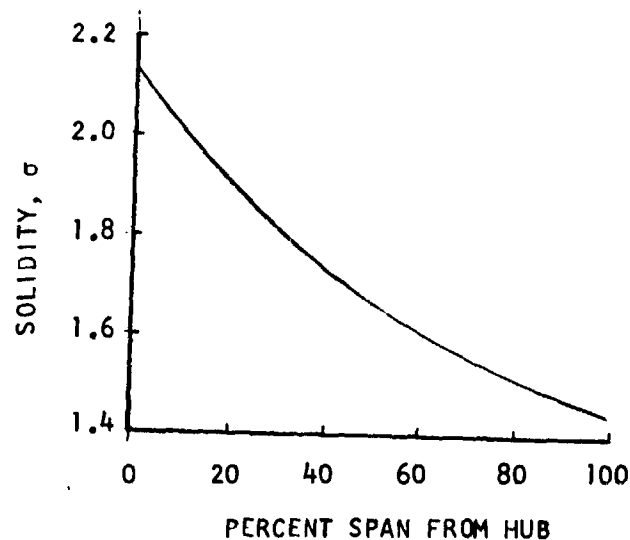


FIGURE 63. ROTOR SOLIDITY DISTRIBUTION

42
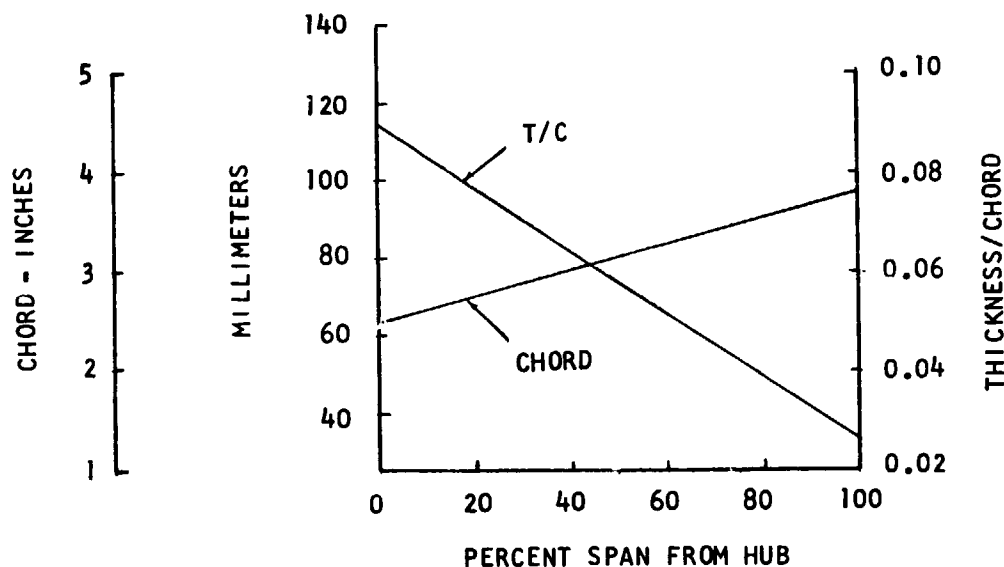
FIGURE 64. ROTOR CHORD AND THICKNESS-TO-CHORD DISTRIBUTION

Since the QHF rotor inlet value of specific flow is high by conventional
standards, the degree of assurance with which the fan can be expected to
achieve the design airflow is of particular interest. Two conditions act
as constraints on rotor airflow capacity under relative supersonic inlet
conditions; 1) average suction surface incidence angle, and 2) airfoil
passage starting margin. Experience at DDA with other fan designs has shown
that the desired incidence angle is 1.5 degrees at a point halfway between
the blade leading edge and the first captured Mach wave for supersonic blade
sections. The starting margin constraint is equivalent to the Kantrowitz
starting criterion; i.e., rotor blade sections in supersonic flow are
designed with a starting margin (minimum blade passage A/A*) of not less
than 1.03. All DDA compressors designed and tested within the past four
years have been designed using these criteria and have achieved the design
flow rate within + 1% at the design speed. These results provide confidence
that the design flow rate for the QHF fan can be achieved.

Results of the flow path analysis indicate that the QHF stator aerodynamic
design conditions are conventional. The vanes selected for the preliminary
design had double circular arc sections. Due to the desirable acoustic
characteristics of long chord vanes, a low number of vanes was selected which
would satisfy the chord requirement and still give a reasonable solidity
distribution. With the number of vanes set at 10, the chord was set at the
maximum allowable value of 229 mm (9 inches).

In order to avoid choking the vanes at the approach condition, tandem vanes
were incorporated in the stator row with the first vane resetable. As
incidence becomes increasingly negative near the low pressure ratio end of
the operating line, the first vane is reset to keep the incidence angle near
zero and to open the vane throat. The vane throat occurs at the inlet to the
passage formed by an airfoil and its adjacent airfoil.

43

# MECHANICAL DESIGN

The preliminary mechanical design had two primary objectives:

- Design a QHF test rig within an envelope which will fit the NASA-LeRC Engine Fan and Jet Noise Facility (W-2) with either the fan inlet or exhaust facing the open room. The test rig will also fit the Single-Stage Aerodynamic Test Facility (W-8) with the fan exhausting into the collector.

- Provide a continuing interaction with the acoustic and aerodynamic designs to ensure that the concepts are mechanically feasible.

## FACILITY-QHF RIG INTERFACE

A number of drawings along with verbal descriptions were furnished by NASA to define the Engine Fan and Jet Noise Facility (W-2) and the Single-Stage Aerodynamic Test Facility (W-8). This information was used to establish the interface between the QHF rig parts and the existing facility. Attention was also given to ease of installation and NASA installation practice. The results of this work are shown in DDA QHF Rig Installation drawing SK16358, which has been delivered to NASA. Reduced copies of the drawing are included in this report. Figure 65 shows the QHF fan installed in the W-2 noise facility in both the inlet and exit noise positions. Figure 66 shows the QHF fan installed in W-8, aerodynamic facility. The rig-facility interface has been defined by the drawing numbers of the NASA facility parts comprising the mating surfaces.

The assembly sequence is to install the hub support, fairing, and rotor components first. The case exit adapter spool is installed next. The split case with vanes installed will then be placed around the hub and rotor components and bolted in place along both the circumferential and longitudinal split lines. At this point the installation is complete except in the noise facility. In the inlet position a bell mouth will be required. In the exit noise position this installation will require an inner flow path fairing followed by an inner exit cone. The exit noise installation will be completed by bolting on the discharge loading spool to form the outer exit flow path.

It is anticipated that the configurations shown in Figures 65 and 66 may be subject to minor change during final design. For example, circumferential surveys may be needed at the vane exit. This can be accomplished by minor configuration changes in the area of the case aft face and exit adapter spool to avoid interference with the CC 848389-25 loading valve. Although this detail design is not part of the current task, it is intended that the preliminary design can accommodate such changes.

## MECHANICAL FEASIBILITY

DDA has successfully completed the design, fabrication, assembly, instrumentation, and test of several high tip speed compressor and fan rigs. These include 406 mm (16 in.) diameter XC9 and XC16 single-stage rigs and the XF26 which was a two-stage 365 mm (38 in.) diameter fan. All of these rigs have operated successfully at the same mechanical tip speed as required by this program. The preliminary mechanical design is based upon using components that are similar to those which were used in these rigs. The

FAN INLET NOISE POSITION

Airflow →

CF503455
CF503456

CR504043 →

← Airflow

CF503457-12

FAN EXIT NOISE POSITION
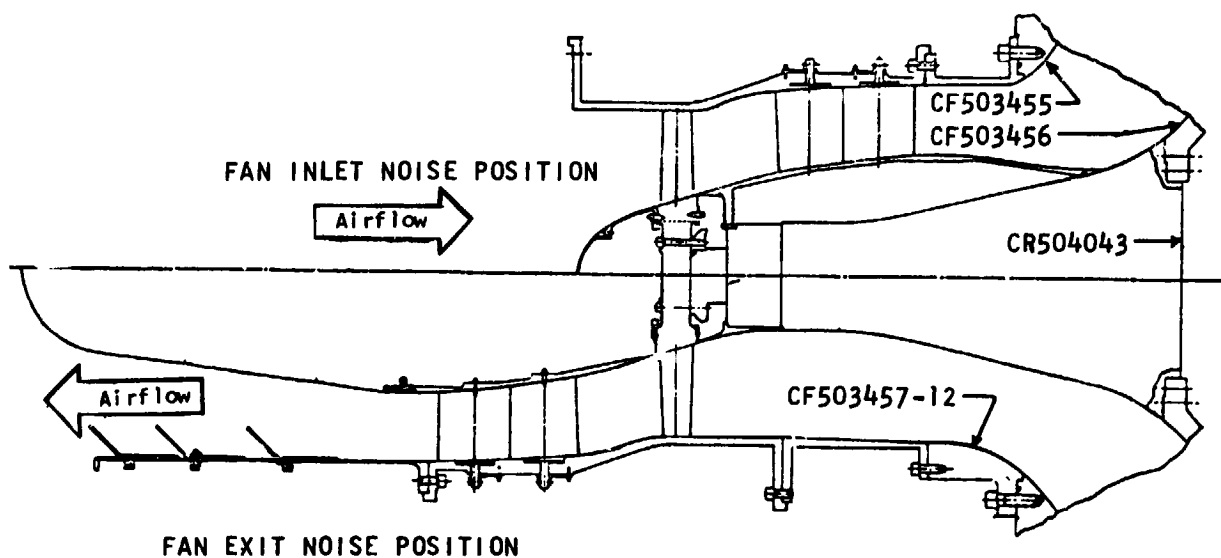
FIGURE 65. QHF FAN INSTALLED IN W-2, NOISE FACILITY



CD848402-39
CC848414

CR847430-1 →

CC848389-25

Airflow →

CF851509 →

CF848384-14
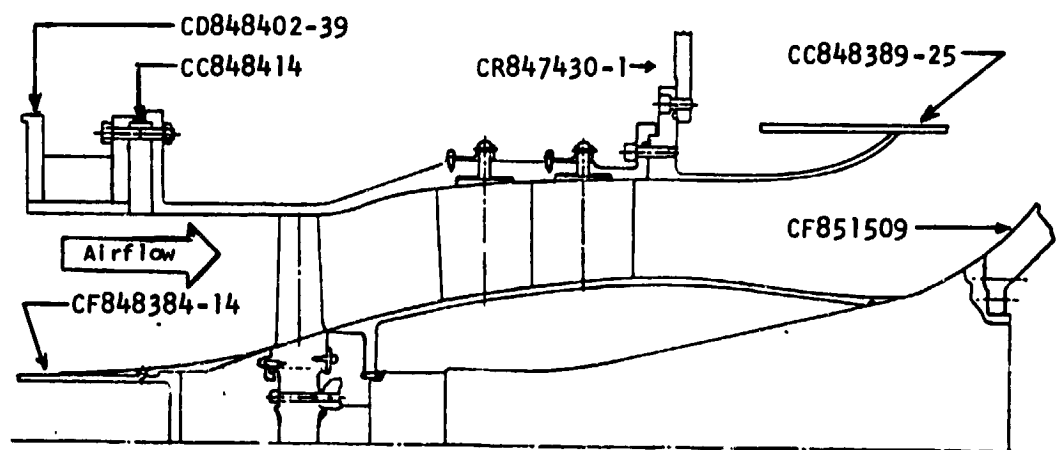
FIGURE 66. QHF FAN INSTALLED IN W-8, AERODYNAMIC PERFORMANCE FACILITY

45

area requiring the maximum attention is the rotor blade airfoil and re-
tention. The blade is frequently subject to problems of vibration, flutter,
stress, and configuration change caused by aerodynamic and mechanical load-
ing. The preliminary aerodynamic design is based upon using a scaled
version of the first stage XF26 blade. It is anticipated that little or
no fine tuning will be required as the result of complete mechanical analysis
during final design. Blade retention can utilize either a stalked or non-
stalked blade. Both have been used successfully in high speed rigs and
there is sufficient material in the wheel rim for 24 slots. In the event
a non-stalked blade is selected for the final design, care must be taken to
ensure proper fore-aft restraint of the ramp forces. Also, care must be
taken to make certain that any base change from the scaled version does not
have an adverse affect on the overall blade vibratory characteristics. The
preliminary design anticipates the use of a non-stalked blade fabricated
from annealed 6-4 Ti (AMS 4967) bar stock. It is planned to use a steel
wheel of rig type design. D6AC steel (AMS 6431) is a likely choice since
it combines high strength with reliable fracture toughness. This will
provide good strength margin, allow modification for instrumentation,
provide shear lips for attachment of rotor balance weights, allow for
fasteners to react blade ramp loads (fore-aft), and provide a stable surface
for attachment to the NASA rotor parts.

An important consideration during final design will be the analysis of the
wheel to adapter pilot. The exact size and material of the NASA adapter
must be furnished so that the wheel can be sized to make certain that the
pilot interface does not separate at high speed. This pilot must have
contact to keep the wheel centered and thus avoid rotor unbalance.

The length of the case assembly has been sized so that one part can be used
in the three applications. This is accomplished through the use of adapter
spools which fit the various NASA facility mounting structure. It is
planned that the case be a thick wall, rig type structure with a longitudinal
split line. The split line will allow the case with vanes in place to be
installed around the assembled rotor and hub. Whether the split line is
horizontal or otherwise will be set by NASA preference for ease of installa-
tion. The two rows of ten vanes will be positioned by a vane stem extending
through the case and individual lever arms on the outside of the case. The
lever arms will provide a means of individual vane reset when the rig is
installed for test. Both the features of positioning and use of a cantilevered
vane have been demonstrated on previous high tip speed rigs. The number,
size, position, attachment, and reset of the vanes is compatible with the
case split lines. One area which will require attention during final design
will be the gap between the vane airfoil and flowpath. Reset of large
vanes through large angles involves significant arc drop. The basic plan
is to favor the high power settings so that maximum gap occurs at low power
position. In the configuration for the noise facility fan exit noise
position, a portion of the inner flowpath fairing is supported by the vanes.
This design approach is similar to the inner seal bands used on the XF 26
fan rig. In the other two arrangements the inner hub fairing is attached
to the NASA hub support near the rotor wheel. The aft end of the fairing
is positioned and supported by the same hub support. It is planned to use
an "O" ring for the actual contact between the two parts. This will allow
for part and assembly tolerance stack.

There are three other components which will be described briefly. The
case-to-facility adapter spools are lathe turned parts with pilots to match
the case and facility. The fan exit noise configuration requires an inner
exit cone. This will also be a formed and welded sheet metal assembly
bolted onto the case. An adjustable three-location nozzle will be bolted
to the inside to provide a method of loading the fan.

46

# ACOUSTIC ANALYSIS OF CONCEPT

The purpose of the acoustic analysis was to determine quantitative noise
reduction benefits of the QHF fan compared with a conventional fan for CTOL
aircraft. This analysis was performed using DDA empirical and theoretical
noise prediction programs. The empirical noise prediction program is
extensively detailed in Reference 6 and is capable of describing EPNdB con-
tours for typical flight operations. The empirical computer program was
derived from data for conventional fan engines, therefore, application to
include the effects of the QHF's near-sonic inlet and long-chord exit vanes
requires inputs from the DDAD theoretical noise prediction program. The
effects of these two advanced technology aspects of the QHF fan were cal-
culated (relative to conventional fans) using the theoretical program and
factored into the empirical program. The results of the noise analysis for
both the QHF fan rig and a QHF fan engine are presented in this section.

## COMPARISONS WITH CONVENTIONAL ENGINE

Conventional high-speed fans currently used in CTOL aircraft produce highly
annoying noise levels in the vicinities of airports. Projected noise levels
of the QHF fan, scaled to full size and utilized in a CTOL application,
indicate that much of the annoyance problem will be alleviated by this ad-
vanced technology fan. Comparisons have been made of the projected noise
levels of the QHF fan and a conventional high-speed fan, the GMA 100/1,
operating on typical CTOL takeoff and approach flight paths, as shown in
Figure 67.
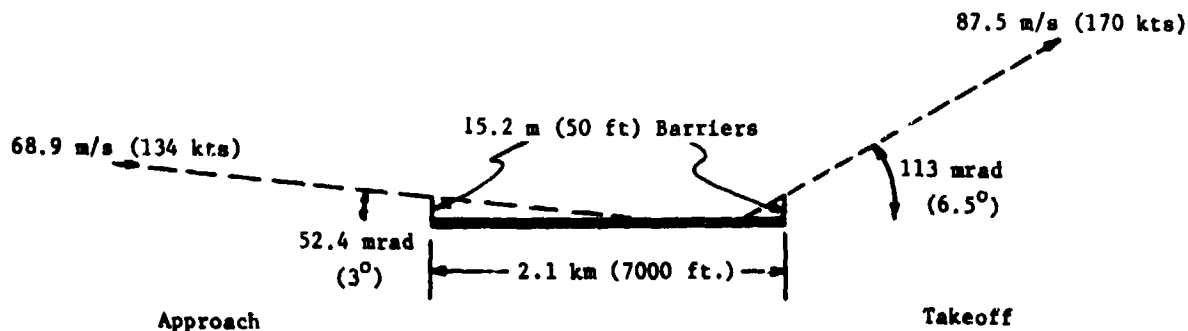


FIGURE 67. TYPICAL CTOL FLIGHT PATH

Figure 68 is a plot of the distributed perceived noise level (PNL) for a
straight and level flyover of the QHF fan scaled to GMA 100/1 fan size,
mated to the GMA 100/1 gas generator, and operating in a two engine, 9072 kg
(20,000 lbm) thrust class, 6:1 bypass ratio, 79379 kg (175,000 lbm) M.T.G.W.
airplane at takeoff conditions. The flyover altitude of 509 m (1670 ft)
corresponds to the altitude at 6.48 KM (3.5 NM) from brake release of an
airplane flying the takeoff path detailed in Figure 67. The observer is
located directly beneath the flightpath. Also shown on the figure is the
effect of core noise (no core noise implies fan alone). The peak level of
93 PNdB occurs in the rear arc since the QHF fan engine will be jet exhaust
dominated at takeoff. Eliminating core noise from the source levels reduces
the peak level approximately 3 dB.
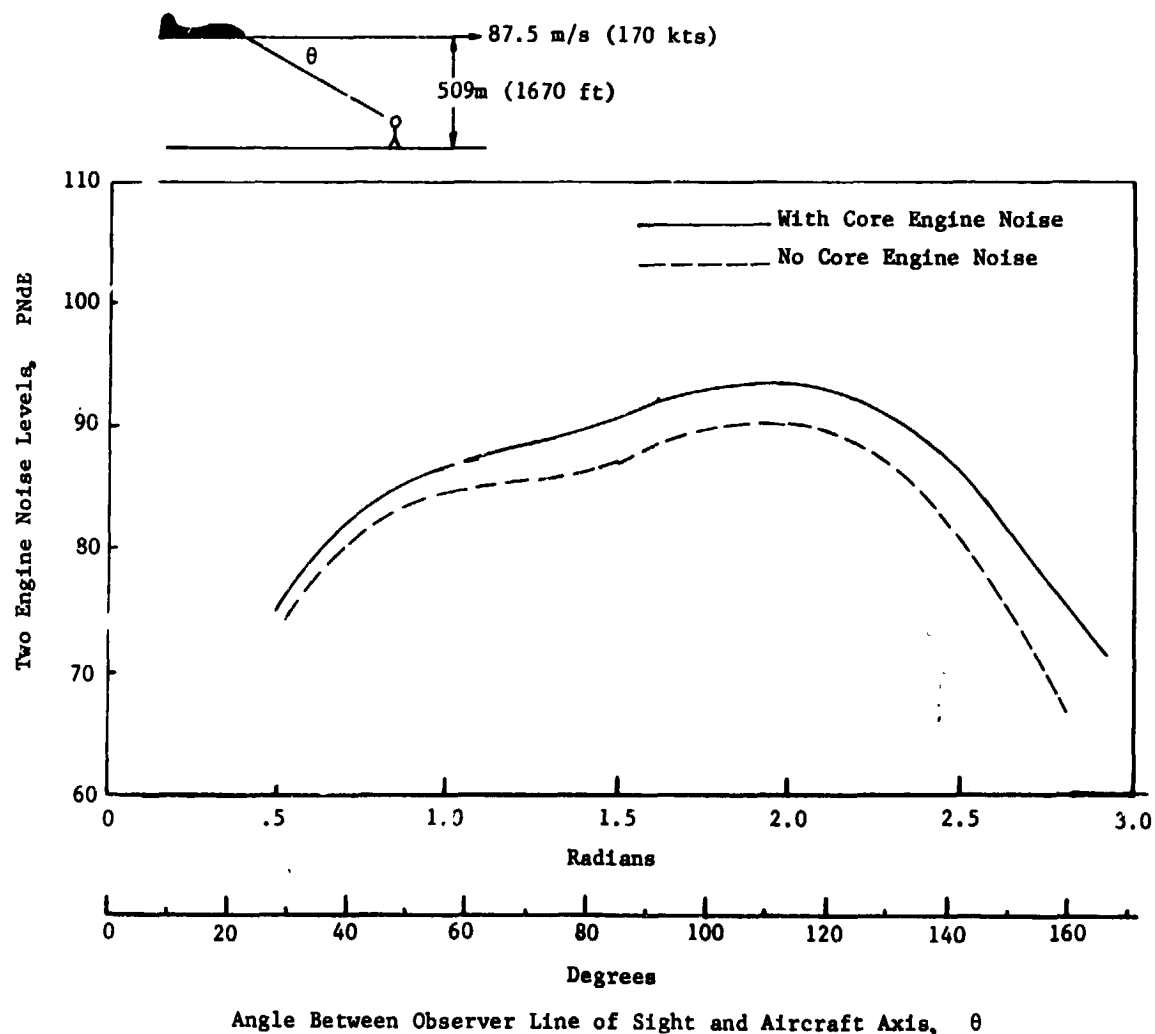


FIGURE 68. QHF FAN ENGINE DISTRIBUTED TAKEOFF NOISE LEVELS

48

Figure 69 is a similar curve for the same two engine airplane during
approach at 30% of takeoff thrust. The flyover altitude of 113 m (370 ft)
corresponds to the altitude at 1.85 km (1 naut. mile) from the end of the
runway for an airplane flying the approach path detailed in Figure 67.
Again, the observer is located directly beneath the flight path. The peak
PNL of 99 dB occurs in both the front and rear quadrants. The approach
levels are higher than the takeoff levels due to the nearness of the air-
plane to the observer. With no core noise, the approach distribution
becomes forward arc dominated and the peak level is reduced only approxi-
mately 1 dB since the core engine has little effect on the front arc noise
levels.
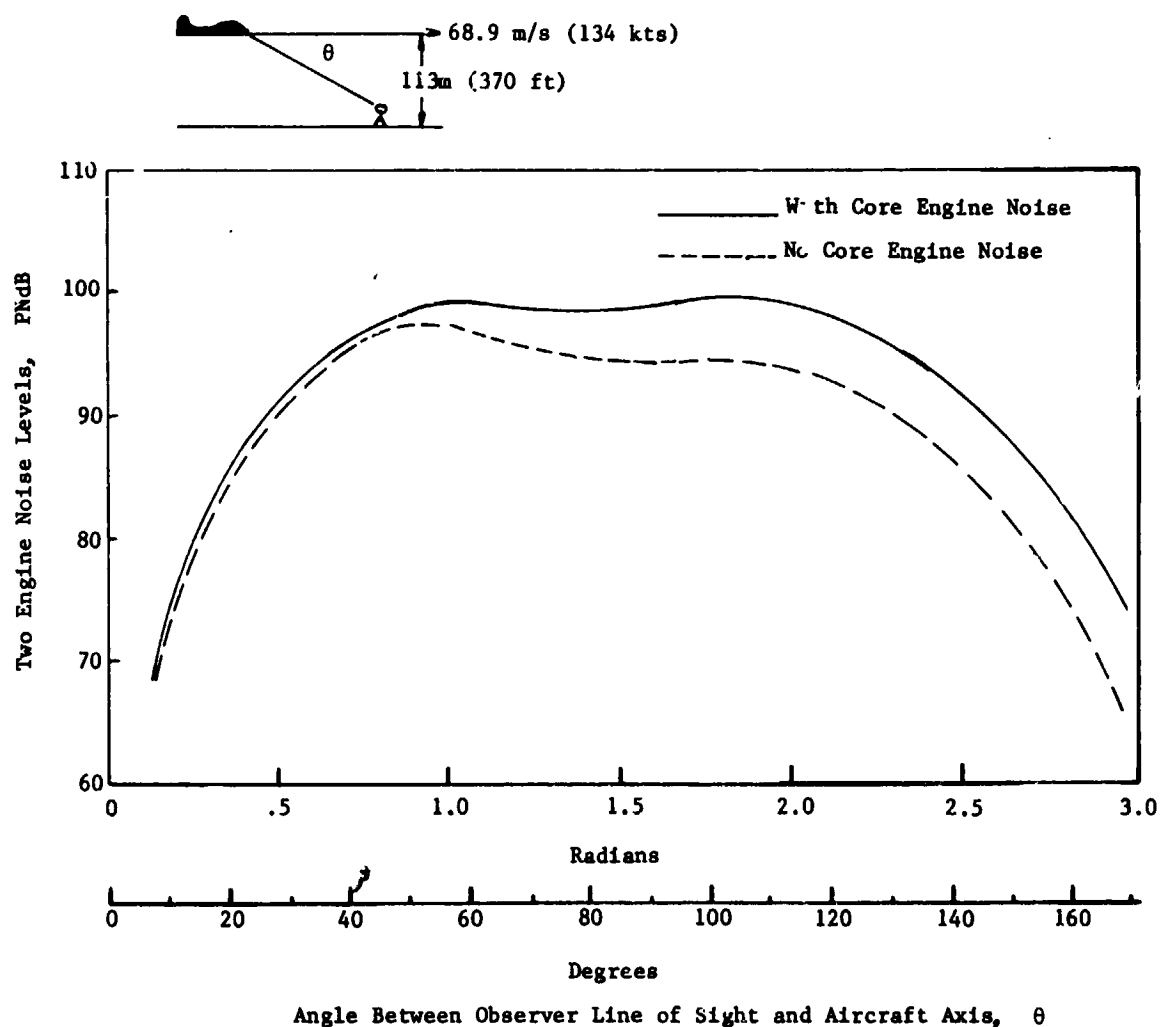


FIGURE 69. QHF FAN ENGINE DISTRIBUTED APPROACH NOISE LEVELS

Noise contours provide a method of describing the area of annoyance in the vicinities of airports. Contours for a 79379 kg (175,000 lbm) M.T.G.W. airplane with two QHF fan engines operating on the flight path of Figure 67 are presented in Figure 70 with and without core noise for a level of 100 EPNdB. As will be seen later, the exposure areas are much smaller than the areas for conventional fans, and in many cases the QHF fan engine 100 EPNdB contours would be contained within the airport boundary.

| | Enclosed Area — km$^2$ (Acres) | | | |
|---|---|---|---|---|
| QHF Fan Engine: | Takeoff | | Approach | |
| ———— With Core Noise | 1.1 | (272) | .12 | (29) |
| — — — — Without Core Noise | .68 | (169) | .03 | (7) |
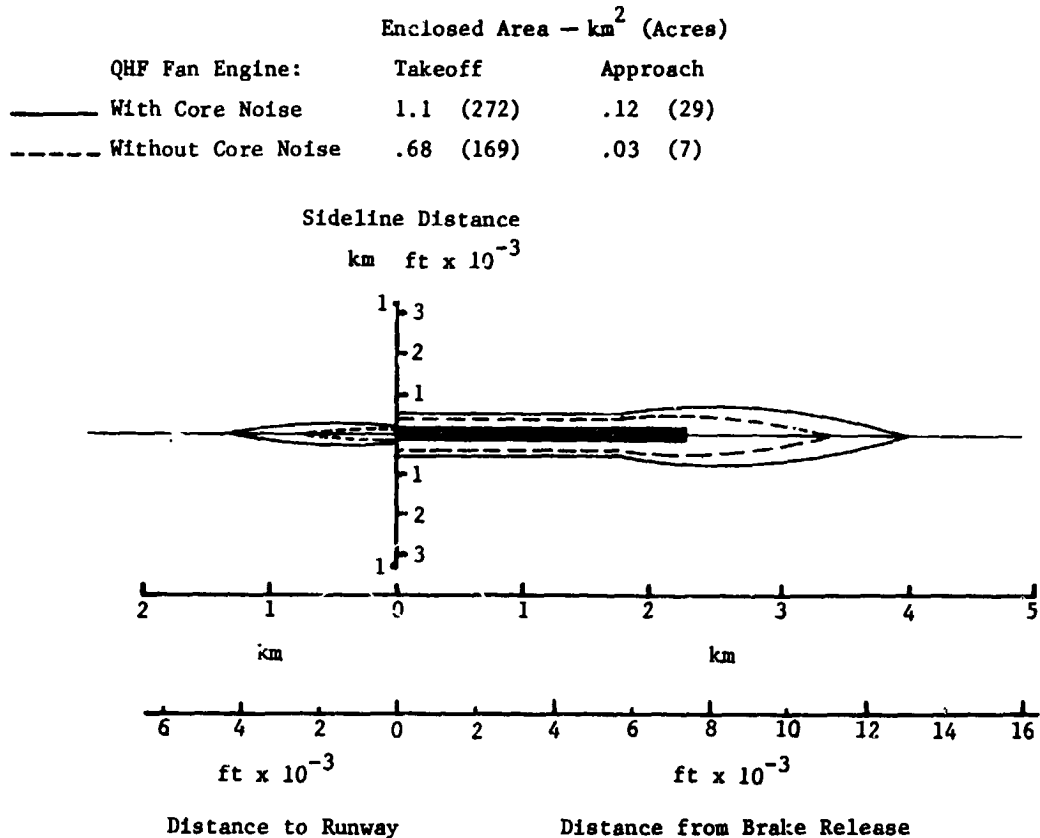


FIGURE 70. COMPARISON OF THE 100 EPNL NOISE CONTOURS FOR THE QHF FAN ENGINE WITH AND WITHOUT CORE ENGINE NOISE

Comparisons of the distributed PNL's for the QHF fan engine versus the GMA 100/1 fan engine (including core engine noise) are made in Figures 71 and 72 for takeoff and approach. The effect of the near-sonic inlet at takeoff is apparent in Figure 72 due to the difference in front arc level. Since the gas generator is the same for both engines, the jet and core noise levels are equal and the rear arc difference is attributable to the long-chord vanes. The increased difference in noise levels at approach (Figure 72) is due to the fact that the QHF fan operates at a lower pressure ratio and with less blade loading while maintaining the near-sonic inlet condition.

50
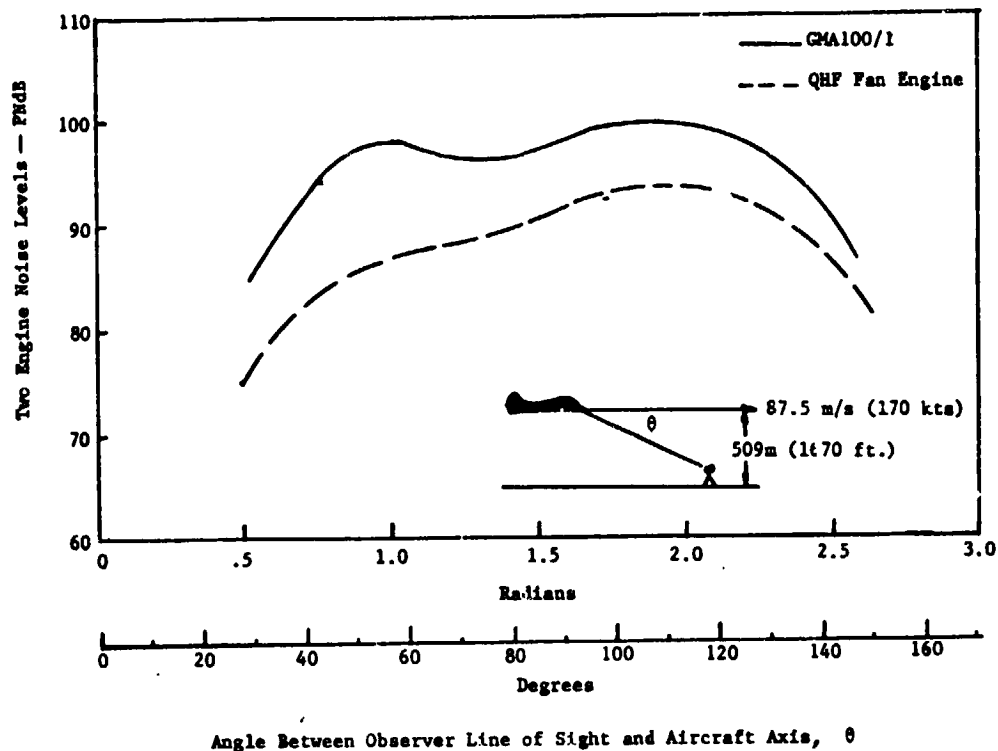
FIGURE 71.    COMPARISON OF DISTRIBUTED TAKEOFF NOISE
LEVELS WITH CORE ENGINE NOISE
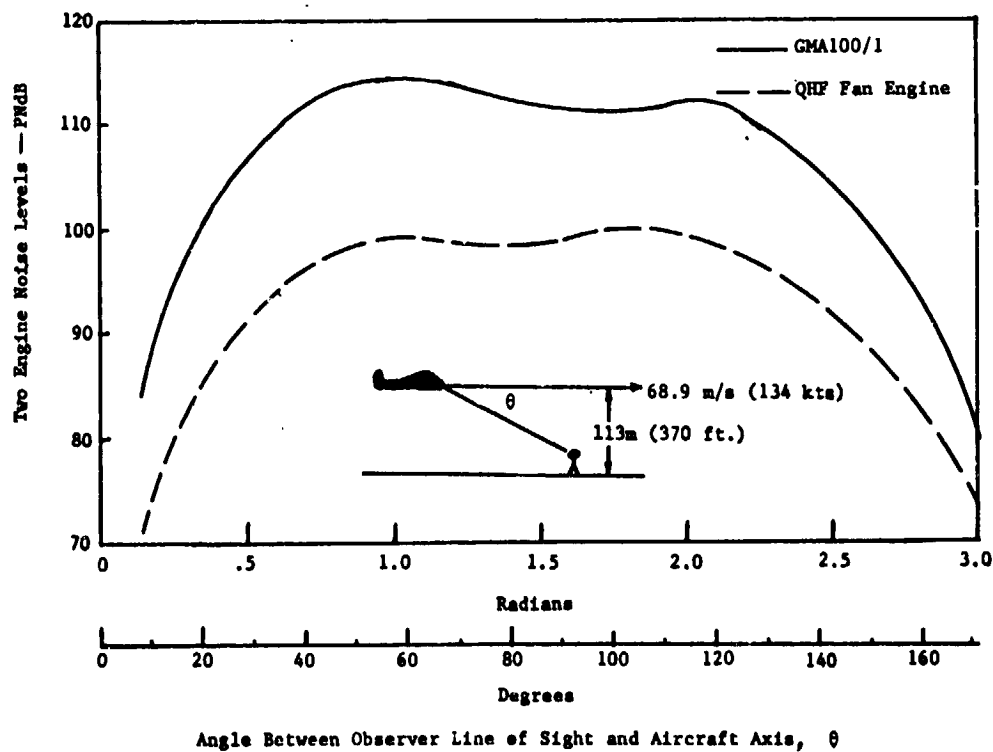


FIGURE 72.    COMPARISON OF DISTRIBUTED APPROACH NOISE
LEVELS WITH CORE ENGINE NOISE

51

The enclosed 100 EPNdB contour areas of the QHF fan engine are 82% smaller than the conventional GMA 100/1 fan engine at takeoff, and 97% smaller at approach. The contour comparison is shown in Figure 73. The QHF fan engine is also projected to meet FAR Part 36 noise levels without the need for acoustic treatment. Estimated noise levels (EPNdB) for the QHF and GMA 100/1 fan engines and corresponding Part 36 goals are:

| MEASURING STATION | GMA 100/1 | QHF FAN ENGINE | PART 36 GOALS |
|---|---|---|---|
| Takeoff | 99.5 | 92.5 | 97.0 |
| Approach | 110.2 | 95.9 | 104.0 |

These values of effective perceived noise levels are for two engine aircraft on CTOL flight path. The aircraft have maximum takeoff weights of 79,379 kg (175,000 lb). There is no acoustic treatment and no ground attenuation.

Enclosed Area, $km^2$ (Acres)

| | Takeoff | Approach |
|---|---|---|
| GMA100/1 | 6.04 (1493) | 4.09 (1011) |
| QHF Fan Engine | 1.1 (272) | .12 (29) |
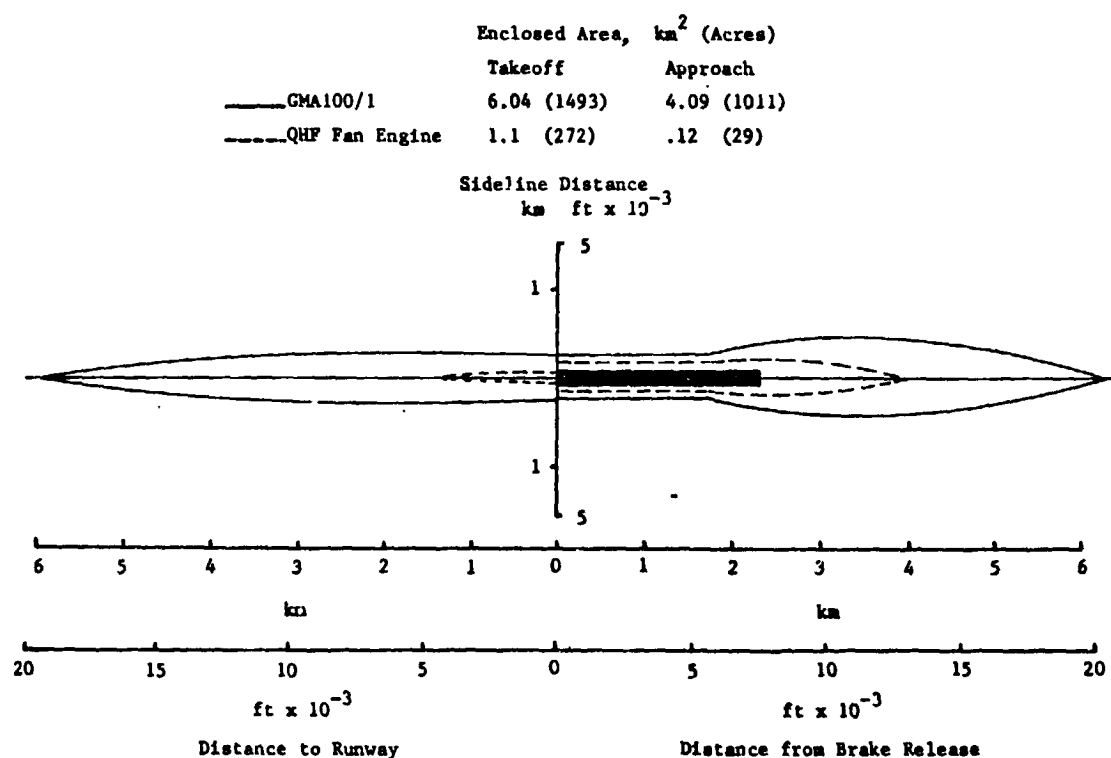


FIGURE 73. COMPARISON OF 100 EPNL NOISE CONTOURS INCLUDING CORE ENGINE NOISE

RIG NOISE PREDICTION

The expected QHF 508 mm (20 in.) rig noise levels on a 5 m (16.4 ft.) radius are shown in Figure 74 on an OASPL versus angle basis for takeoff thrust. Forward arc noise levels are for fan inlet noise only, while rear arc levels are for the fan exhaust plus fan jet. The effect of jet noise on the rear arc levels is to make the rear arc peak OASPL approximately 10 dB greater than the front arc peak level. The predicted front and rear arc fan peak spectra for takeoff thrust are shown in Figure 75. The computer program

52
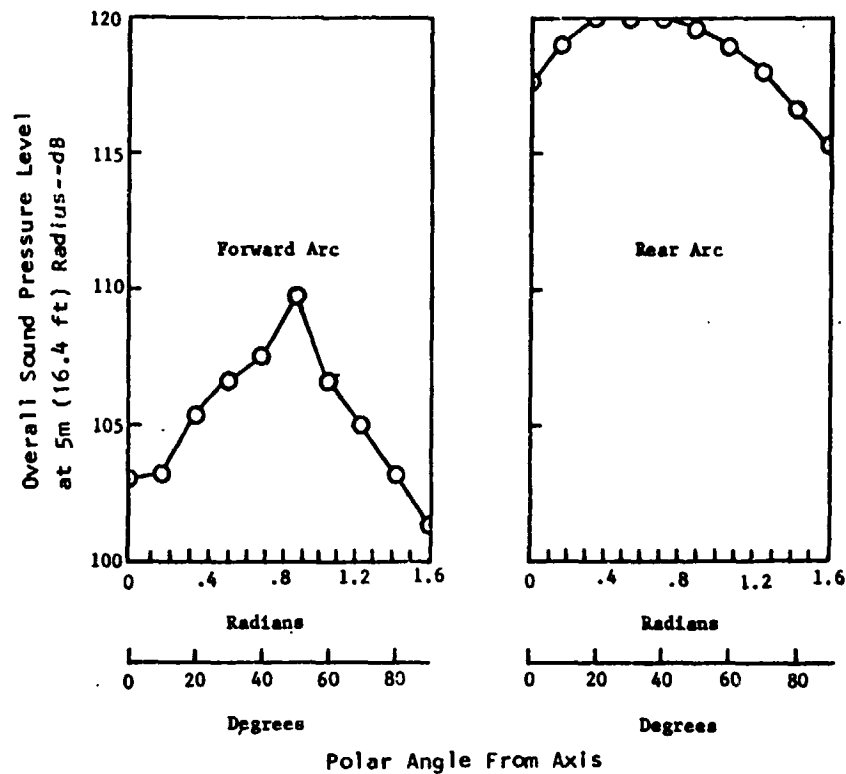
FIGURE 74. ESTIMATED TAKEOFF NOISE LEVELS
FOR THE QHF FAN RIG
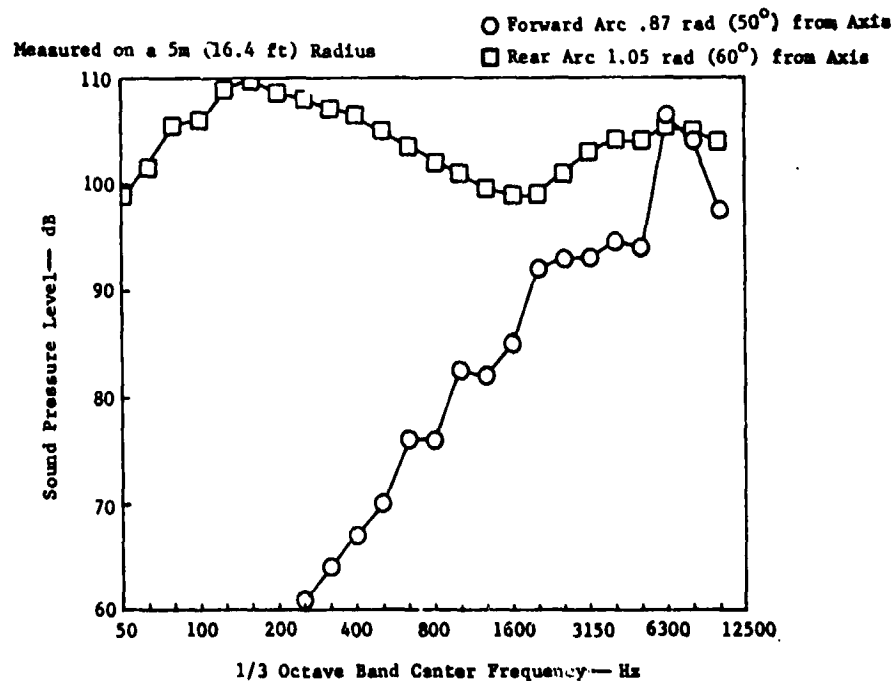


FIGURE 75. PEAK TAKEOFF SPECTRA FOR THE QHF RIG TEST

53

used for noise prediction covers the frequency range from 50 to 10,000 Hz which includes only the QHF fan rig's fundamental tone. The low frequency jet noise and the disappearance of a strong fundamental tone is noteworthy in the rear arc.

Estimated OASPL's at approach thrust (30% of takeoff thrust) are shown in Figure 76. The combination of lower fan pressure ratio, reduced blade ' loading, and lower jet exhaust velocity make the resulting OASPL's 8 dB less in the front arc and 17 dB less in the rear arc than at takeoff thrust. Estimated approach thrust fan peak spectra (Figure 77) show front and rear fan noise levels essentially the same with the exception of forward propagated multiple pure tones and fundamental tone. Low frequency jet noise is again apparent at approach.
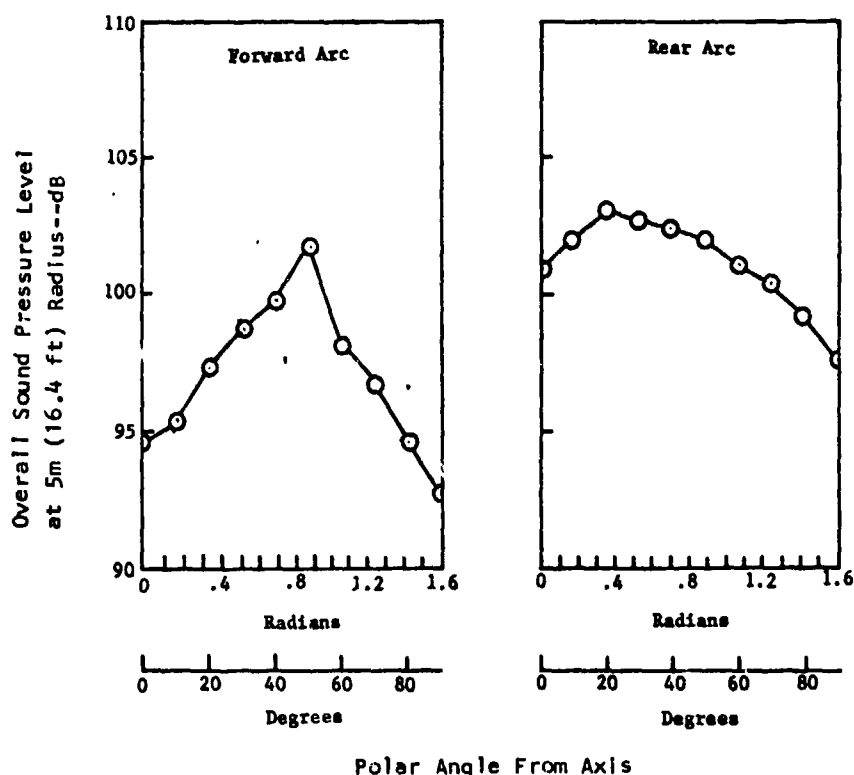
FIGURE 76. ESTIMATED APPROACH NOISE LEVELS
FOR THE QHF FAN RIG

Measured on a 5m (16.4 ft) Radius

O Forward Arc .87 rad (50°) from Axis
□ Rear Arc 1.05 rad (60°) from Axis
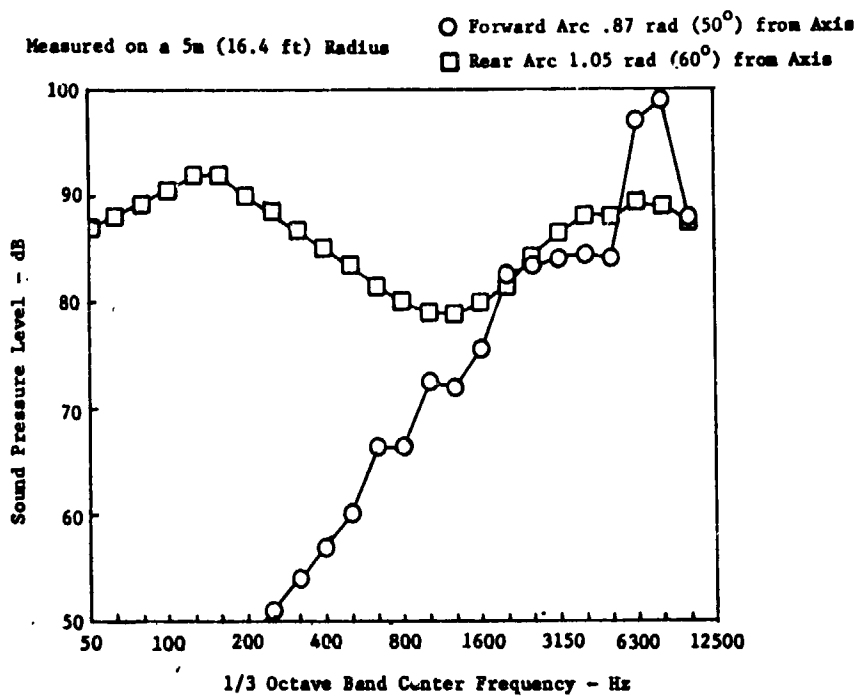
FIGURE 77.   PEAK APPROACH SPECTRA
FOR THE QHF RIG TEST

## SUMMARY OF RESULTS

The results of the acoustic design studies can be summarized in terms of a series of guidelines for the aerodynamicist to follow for the development of a quiet, high speed fan:

- Maintain high specific flow through fan
- Increase rotor relative exit angle
- Minimize the number of stator vanes
- Increase stator chord
- Reduce stator camber

Changes in other geometric and aerodynamic parameters produced insignificant changes in noise generation and radiation.

Results of the flow path analysis indicate that the QHF stator aerodynamic design conditions are conventional. The vanes selected for the preliminary design had double circular arc sections. Due to the desirable acoustic characteristics of long chord vanes, a low number of vanes was selected which would satisfy the chord requirement and still give a reasonable solidity distribution. With ten vanes, the chord was set at 229 mm (9 inches).

In order to avoid choking the vanes at the approach condition (low pressure ratio), tandem vanes were incorporated in the stator row with the first vane resetable. As incidence becomes increasingly negative near the low pressure ratio end of the operating line, the first vane is reset to keep the incidence angle near zero and to open the vane throat. The vane throat occurs at the inlet to the passage formed by an airfoil and its adjacent airfoil.

Enclosed 100 EPNdB contour areas of the QHF fan engine are 82% smaller than the conventional fan engine at takeoff, and 97% smaller at approach. The QHF fan engine is also projected to meet FAR Part 36 noise levels without the need for acoustic treatment.

# APPENDIX

<u>PREDICTED BLADE ELEMENT PERFORMANCE</u>

Blade element performance data at the design point are contained in this section. Data are given in both metric and customary English units with each data set prefaced by a units definition table. Interblade row computing stations are shown in Figure 78.
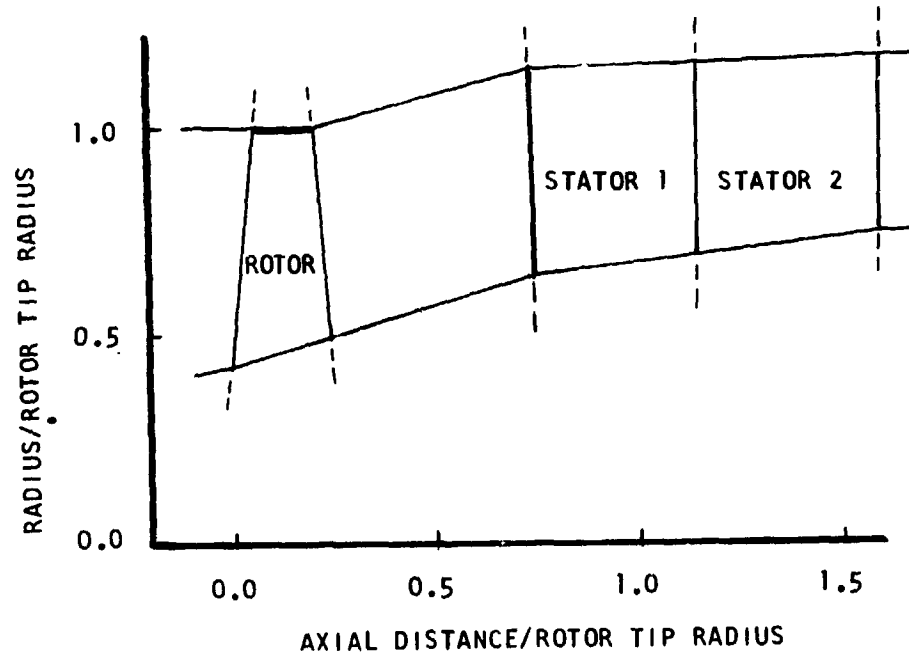


FIGURE 78. COMPUTING STATIONS FOR CONFIGURATION 3
RIG FLOW PATH

| TABLE 4 | | |
|---|---|---|
| UNITS DEFINITION FOR TABLE 5 | | |
| METRIC OUTPUT | | |
| <u>QUANTITY</u> | | <u>DIMENSIONS</u> |
| Length | | Centimeters |
| Velocity | | Meters/second |
| Pressure | | Kilopascals |
| Temperature | | Degrees Kelvin |
| Flow Angle | | Degrees |

## TABLE 5. BLADE ELEMENT PERFORMANCE

## DESIGN POINT (SI UNITS)

## STATION 1-1, ROTOR INLET

| RADIUS | AXIAL VELOCITY | WHIRL VELOCITY | RADIAL VELOCITY | TOTAL PRESSURE | STATIC PRESSURE | TEMPERATURES TOTAL | STATIC | ABSOLUTE VELOCITY | ABSOLUTE MACH NO. | MER. VELOCITY | PERCENT SPAN | S.L. NO. |
|---|---|---|---|---|---|---|---|---|---|---|---|---|
| 10.881 | 222.2 | 0.0 | 70.12 | 101.33 | 71.79 | 288.2 | 261.1 | 233.0 | 0.719 | 233. | 0.4 | 1 |
| 11.135 | 222.4 | 0.0 | 67.88 | 101.33 | 71.90 | 288.2 | 261.2 | 232.5 | 0.717 | 232. | 2.2 | 3 |
| 11.853 | 222.9 | 0.0 | 62.11 | 101.33 | 72.14 | 288.2 | 261.4 | 231.4 | 0.714 | 231. | 7.1 | 5 |
| 12.952 | 223.9 | 0.0 | 54.62 | 101.33 | 72.35 | 288.2 | 261.6 | 230.5 | 0.710 | 230. | 14.6 | 7 |
| 14.339 | 225.4 | 0.0 | 46.84 | 101.33 | 72.41 | 288.2 | 261.7 | 230.2 | 0.709 | 230. | 24.1 | 9 |
| 15.932 | 227.4 | 0.0 | 39.41 | 101.33 | 72.28 | 288.2 | 261.6 | 230.8 | 0.711 | 231. | 35.1 | 11 |
| 17.670 | 230.0 | 0.0 | 32.35 | 101.33 | 71.95 | 288.2 | 261.2 | 232.3 | 0.716 | 232. | 47.0 | 13 |
| 19.510 | 233.1 | 0.0 | 25.34 | 101.33 | 71.46 | 288.2 | 260.7 | 234.5 | 0.724 | 234. | 59.6 | 15 |
| 21.420 | 236.6 | 0.0 | 17.08 | 101.33 | 70.83 | 288.2 | 260.1 | 237.3 | 0.734 | 237. | 72.7 | 17 |
| 23.379 | 240.3 | 0.0 | 9.74 | 101.33 | 70.09 | 288.2 | 259.3 | 240.5 | 0.745 | 241. | 86.1 | 19 |
| 25.374 | 244.0 | 0.0 | 0.08 | 101.33 | 69.29 | 288.2 | 258.4 | 244.0 | 0.757 | 244. | 99.8 | 21 |

58

TABLE 5. (CONTINUED)

## STATION 2-2, ROTOR EXIT

| RADIUS | AXIAL VELOCITY | WHIRL VELOCITY | RADIAL VELOCITY | TOTAL PRESSURE | STATIC PRESSURE | TEMPERATURES TOTAL | STATIC | ABSOLUTE VELOCITY | ABSOLUTE MACH NO. | MER. VELOCITY | PERCENT SPAN | S.L. NO. |
|---|---|---|---|---|---|---|---|---|---|---|---|---|
| 12.419 | 149.8 | 168.8 | 45.31 | 163.73 | 122.69 | 333.4 | 306.9 | 230.2 | 0.655 | 157. | 0.4 | 1 |
| 12.643 | 149.7 | 166.5 | 44.57 | 163.88 | 123.44 | 333.5 | 307.5 | 228.3 | 0.649 | 156. | 2.1 | 3 |
| 13.278 | 149.5 | 160.4 | 42.58 | 154.33 | 175.40 | 334.1 | 309.2 | 223.4 | 0.633 | 155. | 7.0 | 5 |
| 14.263 | 149.3 | 152.3 | 39.76 | 165.01 | 178.03 | 335.0 | 311.5 | 216.9 | 0.613 | 154. | 14.5 | 7 |
| 15.519 | 149.9 | 143.3 | 36.69 | 165.89 | 130.78 | 336.1 | 314.0 | 210.6 | 0.593 | 154. | 24.2 | 9 |
| 16.971 | 151.5 | 134.5 | 33.65 | 166.90 | 133.29 | 337.4 | 316.3 | 205.4 | 0.576 | 155. | 35.3 | 11 |
| 18.503 | 154.6 | 126.2 | 30.80 | 168.00 | 135.32 | 338.6 | 318.3 | 201.9 | 0.564 | 158. | 47.5 | 13 |
| 20.215 | 158.9 | 119.3 | 28.09 | 167.16 | 136.76 | 340.2 | 320.1 | 200.7 | 0.559 | 161. | 60.2 | 15 |
| 21.922 | 164.6 | 114.5 | 25.50 | 170.35 | 137.49 | 342.3 | 321.9 | 202.1 | 0.562 | 167. | 73.3 | 17 |
| 23.649 | 172.1 | 111.4 | 23.08 | 171.55 | 137.38 | 345.2 | 323.9 | 206.5 | 0.572 | 174. | 86.6 | 19 |
| 25.376 | 182.2 | 111.5 | 20.85 | 172.76 | 136.20 | 349.1 | 326.2 | 214.6 | 0.593 | 183. | 99.8 | 21 |

| RELATIVE MACH NOS. INLET | MACH NOS. EXIT | TOTAL TEMP RISE | TOTAL TEMP RATIO | WHEEL SPEED IN | WHEEL SPEED OUT | ROTOR PRESSURE RATIO | ROTOR ADIABATIC EFFICIENCY | ROTOR POLYTROPIC EFFICIENCY |
|---|---|---|---|---|---|---|---|---|
| 1.021 | 0.528 | 45.20 | 1.157 | 235.0 | 268.3 | 1.616 | 94.0 | 94.4 |
| 1.032 | 0.528 | 45.38 | 1.157 | 240.5 | 273.1 | 1.617 | 93.8 | 94.2 |
| 1.064 | 0.568 | 45.93 | 1.159 | 256.0 | 296.8 | 1.622 | 93.2 | 93.7 |
| 1.117 | 0.620 | 45.85 | 1.163 | 279.8 | 308.1 | 1.628 | 92.2 | 92.8 |
| 1.189 | 0.693 | 47.05 | 1.166 | 300.7 | 335.2 | 1.637 | 91.1 | 91.8 |
| 1.277 | 0.783 | 49.23 | 1.171 | 347.1 | 366.6 | 1.647 | 90.0 | 90.7 |
| 1.378 | 0.885 | 50.47 | 1.175 | 381.7 | 400.7 | 1.658 | 89.0 | 89.8 |
| 1.478 | 0.992 | 52.00 | 1.180 | 421.4 | 436.6 | 1.669 | 87.6 | 88.5 |
| 1.608 | 1.100 | 54.09 | 1.198 | 462.7 | 473.5 | 1.681 | 85.5 | 86.5 |
| 1.732 | 1.206 | 57.01 | 1.198 | 505.0 | 510.9 | 1.693 | 82.3 | 83.6 |
| 1.861 | 1.308 | 60.99 | 1.212 | 548.1 | 548.1 | 1.705 | 78.0 | 79.7 |

| S.L. NO. | DIFFUSION FACTOR | OMEGA BAR | DELTA PS/Q | SOLIDITY | TOTAL TURNING | ABSOLUTE FLOW ANGLE INLET | ABSOLUTE FLOW ANGLE EXIT | EQUIVALENT DIFFUSION FACTOR | RELATIVE FLOW ANGLE INLET | RELATIVE FLOW ANGLE EXIT | RELATIVE VELOCITY INLET | RELATIVE VELOCITY EXIT | RELATIVE TEMPERATURE INLET | RELATIVE TEMPERATURE EXIT |
|---|---|---|---|---|---|---|---|---|---|---|---|---|---|---|
| 1 | 0.567 | 0.064 | 0.753 | 2.130 | 12.82 | 0.0 | 47.16 | 1.500 | 45.25 | 32.43 | 331. | 185. | 316. | 324. |
| 3 | 0.563 | 0.065 | 0.741 | 2.104 | 11.66 | 0.0 | 46.83 | 1.483 | 45.97 | 34.31 | 335. | 189. | 317. | 325. |
| 5 | 0.540 | 0.069 | 0.707 | 2.038 | 8.77 | 0.0 | 45.91 | 1.423 | 47.89 | 39.12 | 345. | 200. | 321. | 329. |
| 7 | 0.508 | 0.075 | 0.451 | 1.949 | 5.28 | 0.0 | 44.60 | 1.342 | 50.52 | 45.24 | 362. | 219. | 327. | 336. |
| 9 | 0.466 | 0.081 | 0.579 | 1.854 | 2.18 | 0.0 | 42.89 | 1.254 | 53.38 | 51.20 | 386. | 246. | 336. | 344. |
| 11 | 0.421 | 0.086 | 0.500 | 1.764 | -0.08 | 0.0 | 40.90 | 1.176 | 56.15 | 56.23 | 414. | 279. | 347. | 355. |
| 13 | 0.377 | 0.089 | 0.422 | 1.683 | -1.46 | 0.0 | 38.68 | 1.118 | 58.68 | 60.14 | 447. | 317. | 361. | 368. |
| 15 | 0.343 | 0.095 | 0.349 | 1.612 | -2.14 | 0.0 | 36.48 | 1.080 | 60.91 | 63.05 | 482. | 356. | 377. | 383. |
| 17 | 0.311 | 0.106 | 0.245 | 1.550 | -2.27 | 0.0 | 34.50 | 1.062 | 62.85 | 65.12 | 520. | 396. | 395. | 400. |
| 19 | 0.289 | 0.125 | 0.229 | 1.468 | -1.95 | 0.0 | 32.78 | 1.065 | 64.53 | 66.48 | 559. | 435. | 415. | 418. |
| 21 | 0.275 | 0.152 | 0.182 | 1.552 | -1.22 | 0.0 | 31.29 | 1.090 | 66.00 | 67.22 | 600. | 474. | 438. | 438. |

**TABLE 5. (CONTINUED)**

**STATION 3-3, STATOR 1 INLET**

| RADIUS | AXIAL VELOCITY | WHIRL VELOCITY | RADIAL VELOCITY | TOTAL PRESSURE | STATIC PRESSURE | TEMPERATURES TOTAL | STATIC | ABSOLUTE VELOCITY | ABSOLUTE MACH NO. | MER. VELOCITY | PERCENT SPAN | S.L. NO. |
|---|---|---|---|---|---|---|---|---|---|---|---|---|
| 16.122 | 134.1 | 130.0 | 27.12 | 153.73 | 134.81 | 333.4 | 315.3 | 190.2 | 0.534 | 139. | 0.3 | 1 |
| 16.300 | 136.0 | 129.1 | 27.10 | 153.69 | 135.15 | 333.5 | 315.6 | 189.5 | 0.532 | 139. | 1.8 | 3 |
| 16.917 | 135.6 | 126.7 | 26.09 | 164.33 | 136.11 | 334.1 | 316.5 | 187.5 | 0.526 | 138. | 5.9 | 5 |
| 17.542 | 135.1 | 123.2 | 26.71 | 165.01 | 137.52 | 335.0 | 318.0 | 184.8 | 0.517 | 138. | 12.5 | 7 |
| 18.731 | 135.0 | 118.7 | 26.31 | 165.89 | 139.19 | 336.1 | 319.6 | 181.7 | 0.507 | 138. | 21.2 | 9 |
| 20.034 | 135.2 | 113.9 | 25.95 | 166.93 | 140.97 | 337.4 | 321.4 | 178.6 | 0.497 | 138. | 31.7 | 11 |
| 21.506 | 135.7 | 108.9 | 25.36 | 168.03 | 142.77 | 338.6 | 323.2 | 175.8 | 0.488 | 138. | 43.4 | 13 |
| 23.138 | 136.0 | 104.4 | 24.72 | 169.16 | 144.57 | 340.2 | 325.2 | 173.2 | 0.479 | 138. | 56.3 | 15 |
| 24.821 | 135.6 | 101.1 | 23.75 | 170.35 | 146.37 | 342.3 | 327.7 | 170.8 | 0.470 | 138. | 70.0 | 17 |
| 26.634 | 134.2 | 99.3 | 22.07 | 171.55 | 148.23 | 345.2 | 331.0 | 168.4 | 0.462 | 136. | 84.5 | 19 |
| 28.551 | 131.6 | 99.1 | 19.89 | 172.76 | 150.19 | 349.1 | 335.4 | 165.8 | 0.451 | 133. | 99.8 | 21 |

60

## TABLE 5. (CONTINUED)

## STATION 4-4, STATOR 1 EXIT

| RADIUS | AXIAL VELOCITY | WHIRL VELOCITY | RADIAL VELOCITY | TOTAL PRESSURE | STATIC PRESSURE | TEMPERATURES TOTAL | STATIC | ABSOLUTE VELOCITY | ABSOLUTE MACH NO. | VELOCITY | PERCENT SPAN | S.L. NO. |
|---|---|---|---|---|---|---|---|---|---|---|---|---|
| 17.692 | 9?.7 | 25.9 | 13.22 | 159.17 | 150.54 | 333.4 | 328.1 | 102.9 | 0.283 | 102. | 0.3 | 1 |
| 17.900 | 100.6 | 26.3 | 13.36 | 159.55 | 150.53 | 333.5 | 329.0 | 103.1 | 0.289 | 102. | 2.1 | 3 |
| 18.476 | 107.8 | 27.6 | 14.53 | 161.05 | 150.72 | 334.1 | 327.8 | 112.7 | 0.309 | 109. | 7.0 | 5 |
| 18.336 | 114.9 | 28.5 | 15.27 | 162.71 | 150.96 | 335.0 | 327.9 | 119.4 | 0.329 | 116. | 14.3 | 7 |
| 20.614 | 121.5 | 29.1 | 15.53 | 164.35 | 151.24 | 336.1 | 328.2 | 125.9 | 0.347 | 123. | 23.5 | 9 |
| 21.657 | 127.3 | 29.0 | 15.25 | 165.89 | 151.56 | 337.4 | 328.7 | 131.4 | 0.361 | 128. | 34.1 | 11 |
| 21.029 | 132.3 | 29.5 | 14.52 | 167.29 | 151.91 | 338.6 | 329.4 | 136.0 | 0.374 | 133. | 45.8 | 13 |
| 24.501 | 136.3 | 27.3 | 13.63 | 168.55 | 152.28 | 340.2 | 330.4 | 139.7 | 0.383 | 137. | 56.4 | 15 |
| 24.057 | 144.0 | 27.6 | 12.06 | 169.73 | 152.68 | 342.3 | 332.0 | 143.0 | 0.391 | 140. | 71.6 | 17 |
| 27.491 | 143.2 | 27.2 | 13.37 | 170.77 | 153.07 | 345.2 | 334.5 | 146.1 | 0.398 | 144. | 85.5 | 19 |
| 29.364 | 146.3 | 27.0 | 7.33 | 171.77 | 153.45 | 349.1 | 338.0 | 149.1 | 0.404 | 147. | 99.8 | 21 |

| ABSOLUTE MACH NOS. INLET | EXIT | TOTAL TEMP RISE | TOTAL TEMP RATIO | WHEEL SPEED IN | OUT | STAGE PRESSURE RATIO | STAGE ADIABATIC EFFICIENCY | STAGE POLYTROPIC EFFICIENCY |
|---|---|---|---|---|---|---|---|---|
| 0.534 | 0.283 | 45.20 | 1.157 | 0.0 | 0.0 | 1.571 | 89.1 | 89.8 |
| 0.532 | 0.286 | 45.34 | 1.157 | 0.0 | 0.0 | 1.575 | 88.2 | 89.9 |
| 0.526 | 0.309 | 45.99 | 1.153 | 0.0 | 0.0 | 1.580 | 89.1 | 89.7 |
| 0.517 | 0.329 | 46.85 | 1.163 | 0.0 | 0.0 | 1.606 | 89.4 | 90.1 |
| 0.507 | 0.347 | 47.55 | 1.166 | 0.0 | 0.0 | 1.622 | 89.3 | 90.0 |
| 0.497 | 0.361 | 49.28 | 1.171 | 0.0 | 0.0 | 1.637 | 88.4 | 89.4 |
| 0.448 | 0.374 | 50.47 | 1.175 | 0.0 | 0.0 | 1.651 | 88.2 | 89.0 |
| 0.472 | 0.383 | 52.00 | 1.180 | 0.0 | 0.0 | 1.663 | 87.0 | 87.9 |
| 0.470 | 0.391 | 54.09 | 1.188 | 0.0 | 0.0 | 1.675 | 84.9 | 85.9 |
| 0.462 | 0.398 | 57.01 | 1.163 | 0.0 | 0.0 | 1.665 | 81.5 | 82.9 |
| 0.451 | 0.404 | 60.33 | 1.212 | 0.0 | 0.0 | 1.695 | 77.1 | 78.8 |

| S.L. NO. | DIFFUSION FACTOR | OMEGA BAR | DELTA PS/P | SOLIDITY | TOTAL TURNING | ABSOLUTE FLOW ANGLE INLET | EXIT | EQUIVALENT DIFFUSION FACTOR |
|---|---|---|---|---|---|---|---|---|
| 1 | 0.564 | 0.167 | 0.544 | 1.076 | 24.57 | 42.12 | 14.54 | 1.791 |
| 3 | 0.543 | 0.151 | 0.545 | 1.046 | 21.43 | 42.26 | 14.47 | 1.791 |
| 5 | 0.536 | 0.116 | 0.515 | 1.03? | 24.24 | 42.40 | 14.21 | 1.783 |
| 7 | 0.525 | 0.084 | 0.486 | 0.924 | 28.28 | 41.89 | 13.83 | 1.773 |
| 9 | 0.454 | 0.057 | 0.451 | 0.93? | 27.96 | 40.91 | 13.34 | 1.760 |
| 11 | 0.513 | 0.037 | 0.455 | 0.97? | 27.45 | 39.62 | 12.75 | 1.746 |
| 13 | 0.602 | | | 0.817 | 26.87 | 38.26 | 12.10 | 1.732 |
| 15 | 0.453 | | | 0.744 | 26.16 | 37.06 | 11.51 | 1.726 |
| 17 | 0.444 | | | 0.715 | 25.55 | 3.29 | 11.02 | 1.720 |
| 19 | 0.473 | | | 0.470 | 25.26 | 36.13 | 10.74 | 1.749 |
| 21 | 0.472 | 0.344 | | 0.628 | 25.39 | 36.69 | 10.65 | 1.767 |

# TABLE 5. (CONCLUDED)

## STATION 5-5, STATOR 2 EXIT

| RADIUS | AXIAL VELOCITY | WHIRL VELOCITY | RADIAL VELOCITY | TOTAL PRESSURE | STATIC PRESSURE | TEMPERATURES TOTAL | STATIC | ABSOLUTE VELOCITY | ABSOLUTE MACH NO. | MER. VELOCITY | PERCENT SPAN | S.L. NO. |
|---|---|---|---|---|---|---|---|---|---|---|---|---|
| 18.658 | 103.8 | 0.0 | 5.93 | 159.94 | 150.05 | 333.4 | 329.0 | 104.0 | 0.286 | 104. | 0.2 | 1 |
| 19.144 | 104.1 | 0.0 | 6.01 | 159.22 | 150.03 | 333.5 | 327.9 | 106.2 | 0.293 | 106. | 2.0 | 3 |
| 19.540 | 113.3 | 0.0 | 6.24 | 160.73 | 150.20 | 334.1 | 327.7 | 113.4 | 0.312 | 113. | 6.8 | 5 |
| 20.436 | 120.8 | 0.0 | 6.37 | 162.44 | 150.41 | 335.0 | 327.7 | 121.0 | 0.333 | 121. | 13.9 | 7 |
| 21.415 | 127.7 | 0.0 | 6.34 | 164.13 | 150.64 | 336.1 | 328.0 | 127.9 | 0.352 | 128. | 22.0 | 9 |
| 22.553 | 133.7 | 0.0 | 6.14 | 165.72 | 150.89 | 337.4 | 328.4 | 133.8 | 0.368 | 134. | 33.4 | 11 |
| 23.818 | 138.7 | 0.0 | 5.78 | 167.15 | 151.15 | 338.6 | 329.0 | 138.8 | 0.382 | 139. | 45.0 | 13 |
| 25.188 | 142.9 | 0.0 | 5.28 | 168.41 | 151.42 | 340.2 | 330.0 | 143.0 | 0.392 | 143. | 57.6 | 15 |
| 26.544 | 146.5 | 0.0 | 4.67 | 169.51 | 151.69 | 342.3 | 331.5 | 146.5 | 0.401 | 147. | 71.0 | 17 |
| 28.175 | 149.7 | 0.0 | 3.98 | 170.49 | 151.95 | 345.2 | 334.0 | 149.8 | 0.409 | 150. | 85.1 | 19 |
| 29.772 | 152.7 | 0.0 | 3.24 | 171.33 | 152.19 | 349.1 | 337.5 | 152.8 | 0.415 | 153. | 99.8 | 21 |

| ABSOLUTE MACH NO. INLET | MACH NO. EXIT | WHIRL VELOCITY | TOTAL TEMP RISE | TOTAL TEMP RATIO | WHEEL SPEED IN | OUT | STAGE PRESSURE RATIO | STAGE ADIABATIC EFFICIENCY | STAGE POLYTROPIC EFFICIENCY |
|---|---|---|---|---|---|---|---|---|---|
| 0.283 | 0.286 | 0.0 | 45.20 | 1.157 | 0.0 | 0.0 | 1.568 | 87.6 | 86.4 |
| 0.289 | 0.293 | 0.0 | 45.38 | 1.157 | 0.0 | 0.0 | 1.571 | 87.8 | 88.5 |
| 0.305 | 0.312 | 0.0 | 45.95 | 1.159 | 0.0 | 0.0 | 1.586 | 88.7 | 89.4 |
| 0.329 | 0.333 | 0.0 | 46.95 | 1.163 | 0.0 | 0.0 | 1.603 | 89.0 | 89.7 |
| 0.347 | 0.352 | 0.0 | 47.06 | 1.166 | 0.0 | 0.0 | 1.620 | 89.0 | 89.8 |
| 0.361 | 0.368 | 0.0 | 49.20 | 1.171 | 0.0 | 0.0 | 1.635 | 89.6 | 89.4 |
| 0.374 | 0.382 | 0.0 | 52.47 | 1.175 | 0.0 | 0.0 | 1.650 | 88.0 | 88.9 |
| 0.383 | 0.392 | 0.0 | 52.00 | 1.180 | 0.0 | 0.0 | 1.662 | 86.8 | 87.7 |
| 0.393 | 0.401 | 0.0 | 54.06 | 1.188 | 0.0 | 0.0 | 1.673 | 84.6 | 85.7 |
| 0.398 | 0.409 | 0.0 | 57.01 | 1.193 | 0.0 | 0.0 | 1.683 | 81.2 | 82.6 |
| 0.404 | 0.415 | 0.0 | 60.98 | 1.212 | 0.0 | 0.0 | 1.691 | 76.7 | 78.4 |

| S.L. NO. | DIFFUSION FACTOR | OMEGA BAR | DELTA PS/Q | SOLIDITY | TOTAL TURNING | ABSOLUTE FLOW ANGLE INLET | EXIT | EQUIVALENT DIFFUSION FACTOR |
|---|---|---|---|---|---|---|---|---|
| 1 | 0.112 | 0.038 | -0.056 | 0.993 | 14.56 | 14.56 | 0.0 | 1.314 |
| 3 | 0.112 | 0.035 | -0.055 | 0.982 | 14.47 | 14.47 | 0.0 | 1.314 |
| 5 | 0.114 | 0.030 | -0.050 | 0.954 | 14.21 | 14.21 | 0.0 | 1.314 |
| 7 | 0.114 | 0.023 | -0.047 | 0.915 | 13.83 | 13.83 | 0.0 | 1.315 |
| 9 | 0.114 | 0.017 | -0.044 | 0.873 | 13.34 | 13.34 | 0.0 | 1.315 |
| 11 | 0.113 | 0.012 | -0.047 | 0.823 | 12.75 | 12.75 | 0.0 | 1.313 |
| 13 | 0.113 | 0.009 | -0.040 | 0.777 | 12.10 | 12.10 | 0.0 | 1.311 |
| 15 | 0.111 | 0.009 | -0.053 | 0.732 | 11.51 | 11.51 | 0.0 | 1.310 |
| 17 | 0.112 | 0.011 | -0.058 | 0.690 | 11.03 | 11.03 | 0.0 | 1.311 |
| 19 | 0.116 | 0.016 | -0.064 | 0.651 | 10.74 | 10.74 | 0.0 | 1.315 |
| 21 | 0.125 | 0.024 | -0.069 | 0.615 | 10.65 | 10.65 | 0.0 | 1.323 |

62

## TABLE 6
### UNITS DEFINITION FOR TABLE 7 ENGLISH OUTPUT

| QUANTITY | DIMENSIONS |
|---|---|
| Length | Inches |
| Velocity | Feet/second |
| Pressure | Pounds Force/inch$^2$ |
| Temperature | Degrees Rankine |
| Flow Angle | Degrees |

## TABLE 7. BLADE ELEMENT PERFORMANCE, DESIGN POINT (ENGLISH UNITS)

### STATION 1-1, ROTOR INLET

| RADIUS | AXIAL VELOCITY | WHIRL VELOCITY | RADIAL VELOCITY | TOTAL PRESSURE | STATIC PRESSURE | TEMPERATURES TOTAL | STATIC | ABSOLUTE VELOCITY | ABSOLUTE MACH NO. | MER. VELOCITY | PERCENT SPAN | S.L. NO. |
|---|---|---|---|---|---|---|---|---|---|---|---|---|
| 4.284 | 729.2 | 0.0 | 230.13 | 14.70 | 10.41 | 518.7 | 469.9 | 764.6 | 0.719 | 765. | 0.4 | 1 |
| 4.384 | 729.8 | 0.0 | 212.76 | 14.70 | 10.43 | 518.7 | 470.2 | 763.0 | 0.719 | 743. | 2.2 | 3 |
| 4.667 | 731.5 | 0.0 | 203.92 | 14.70 | 10.46 | 518.7 | 470.6 | 759.4 | 0.714 | 759. | 7.1 | 5 |
| 5.099 | 734.1 | 0.0 | 177.24 | 14.70 | 10.49 | 518.7 | 471.0 | 756.3 | 0.711 | 756. | 14.6 | 7 |
| 5.545 | 739.6 | 0.0 | 153.71 | 14.70 | 10.50 | 518.7 | 471.1 | 755.4 | 0.710 | 755. | 24.1 | 9 |
| 6.272 | 746.3 | 0.0 | 129.33 | 14.70 | 10.48 | 518.7 | 470.9 | 757.4 | 0.712 | 757. | 35.1 | 11 |
| 6.957 | 754.8 | 0.0 | 106.16 | 14.70 | 10.43 | 518.7 | 470.3 | 762.2 | 0.717 | 762. | 47.0 | 13 |
| 7.631 | 765.0 | 0.0 | 83.17 | 14.70 | 10.36 | 518.7 | 469.3 | 769.5 | 0.724 | 749. | 59.6 | 15 |
| 8.433 | 777.4 | 0.0 | 57.32 | 14.70 | 10.27 | 518.7 | 468.1 | 778.3 | 0.734 | 779. | 72.7 | 17 |
| 9.204 | 782.7 | 0.0 | 32.04 | 14.70 | 10.16 | 518.7 | 466.7 | 789.3 | 0.745 | 789. | 86.1 | 19 |
| 9.990 | 800.8 | 0.0 | 0.27 | 14.70 | 10.05 | 518.7 | 465.2 | 800.8 | 0.757 | 801. | 99.9 | 21 |

# TABLE 7. (CONTINUED)

## STATION 2-2, ROTOR EXIT

| RADIUS | AXIAL VELOCITY | WHIRL VELOCITY | RADIAL VELOCITY | TOTAL PRESSURE | STATIC PRESSURE | TEMPERATURES TOTAL | TEMPERATURES STATIC | ABSOLUTE VELOCITY | ABSOLUTE MACH NO. | MER. VELOCITY | PERCENT SPAN | S.L. NO. |
|---|---|---|---|---|---|---|---|---|---|---|---|---|
| 4.890 | 491.5 | 553.7 | 148.63 | 23.75 | 17.90 | 599.8 | 552.4 | 755.1 | 0.655 | 513. | 0.4 | 1 |
| 4.977 | 491.1 | 546.2 | 146.20 | 23.77 | 17.90 | 600.1 | 553.5 | 748.9 | 0.649 | 512. | 2.1 | 3 |
| 5.228 | 490.3 | 526.2 | 139.67 | 23.83 | 18.19 | 601.1 | 556.5 | 732.7 | 0.634 | 510. | 7.0 | 5 |
| 5.615 | 489.5 | 499.7 | 130.44 | 23.93 | 18.57 | 602.8 | 560.6 | 711.7 | 0.613 | 507. | 14.5 | 7 |
| 6.110 | 491.6 | 470.1 | 120.37 | 24.05 | 18.97 | 604.7 | 565.1 | 690.8 | 0.593 | 506. | 24.2 | 9 |
| 6.631 | 497.0 | 441.1 | 110.35 | 24.21 | 19.33 | 607.0 | 569.3 | 673.6 | 0.576 | 507. | 35.3 | 11 |
| 7.304 | 507.1 | 413.9 | 101.03 | 24.37 | 19.63 | 609.3 | 572.8 | 662.3 | 0.565 | 517. | 47.5 | 13 |
| 7.959 | 521.2 | 351.4 | 92.12 | 24.53 | 19.84 | 612.0 | 576.0 | 658.3 | 0.560 | 529. | 60.2 | 15 |
| 8.631 | 539.8 | 375.8 | 83.65 | 24.71 | 19.94 | 615.8 | 579.2 | 662.8 | 0.562 | 544. | 73.3 | 17 |
| 9.311 | 564.4 | 366.8 | 75.71 | 24.83 | 19.93 | 621.0 | 582.8 | 677.4 | 0.577 | 569. | 86.6 | 19 |
| 9.990 | 597.5 | 365.6 | 63.37 | 25.06 | 19.76 | 628.1 | 586.9 | 703.9 | 0.593 | 602. | 96.8 | 21 |

| RELATIVE INLET MACH NOS. | MACH NOS. EXIT | TOTAL TEMP RATIO | TOTAL TEMP RISE | WHEEL SPEED IN | SPEED OUT | ROTOR PRESSURE RATIO | ROTOR ADIABATIC EFFICIENCY | ROTOR POLYTROPIC EFFICIENCY |
|---|---|---|---|---|---|---|---|---|
| 1.022 | 0.523 | 1.156 | 51.12 | 771.1 | 880.1 | 1.616 | 94.0 | 94.5 |
| 1.052 | 0.533 | 1.157 | 51.45 | 789.1 | 905.0 | 1.617 | 93.8 | 94.4 |
| 1.064 | 0.568 | 1.159 | 82.43 | 843.0 | 941.0 | 1.622 | 93.2 | 93.9 |
| 1.115 | 0.620 | 1.162 | 84.07 | 917.0 | 1010.9 | 1.629 | 92.2 | 92.9 |
| 1.190 | 0.693 | 1.166 | 96.05 | 1016.1 | 1099.8 | 1.637 | 91.1 | 91.9 |
| 1.278 | 0.783 | 1.170 | 84.23 | 1129.0 | 1202.6 | 1.647 | 90.0 | 90.9 |
| 1.378 | 0.885 | 1.175 | 90.57 | 1252.2 | 1314.9 | 1.659 | 89.0 | 89.9 |
| 1.433 | 0.993 | 1.183 | 93.32 | 1392.6 | 1432.5 | 1.669 | 87.6 | 88.7 |
| 1.608 | 1.101 | 1.187 | 97.04 | 1517.9 | 1553.6 | 1.681 | 85.5 | 86.7 |
| 1.732 | 1.207 | 1.197 | 102.28 | 1655.8 | 1675.9 | 1.693 | 82.3 | 83.8 |
| 1.961 | 1.333 | 1.211 | 109.39 | 1798.2 | 1798.3 | 1.705 | 73.0 | 79.8 |

| S.L. NO. | DIFFUSION FACTOR | OMEGA BAR | DELTA PS/Q | SOLIDITY | TOTAL TURNING | ABSOLUTE FLOW ANGLE INLET | ABSOLUTE FLOW ANGLE EXIT | EQUIVALENT DIFFUSION FACTOR | RELATIVE FLOW ANGLE INLET | RELATIVE FLOW ANGLE EXIT | RELATIVE VELOCITY INLET | RELATIVE VELOCITY EXIT | RELATIVE TEMPERATURE INLET | RELATIVE TEMPERATURE EXIT | S.L. NO. |
|---|---|---|---|---|---|---|---|---|---|---|---|---|---|---|---|
| 1 | 0.567 | 0.064 | 0.753 | 2.130 | 12.80 | 0.0 | 47.16 | 1.500 | 45.24 | 32.44 | 1086. | 608. | 568. | 583. | 1 |
| 3 | 0.561 | 0.065 | 0.741 | 2.104 | 11.64 | 0.0 | 46.83 | 1.480 | 45.96 | 34.32 | 1058. | 620. | 571. | 586. | 3 |
| 5 | 0.540 | 0.066 | 0.707 | 2.038 | 8.75 | 0.0 | 45.91 | 1.423 | 47.88 | 39.13 | 1132. | 657. | 577. | 592. | 5 |
| 7 | 0.508 | 0.075 | 0.651 | 1.949 | 5.27 | 0.0 | 44.60 | 1.341 | 50.51 | 45.24 | 1199. | 720. | 588. | 604. | 7 |
| 9 | 0.466 | 0.081 | 0.579 | 1.854 | 2.16 | 0.0 | 42.99 | 1.253 | 53.37 | 51.71 | 1246. | 808. | 605. | 619. | 9 |
| 11 | 0.421 | 0.086 | 0.500 | 1.744 | -0.09 | 0.0 | 40.91 | 1.176 | 56.15 | 56.24 | 1360. | 916. | 625. | 639. | 11 |
| 13 | 0.377 | 0.089 | 0.422 | 1.683 | -1.47 | 0.0 | 39.68 | 1.117 | 58.67 | 60.15 | 1446. | 1037. | 645. | 662. | 13 |
| 15 | 0.340 | 0.095 | 0.349 | 1.612 | -2.15 | 0.0 | 36.48 | 1.079 | 60.90 | 63.05 | 1582. | 1168. | 678. | 680. | 15 |
| 17 | 0.311 | 0.105 | 0.285 | 1.550 | -2.28 | 0.0 | 34.50 | 1.061 | 62.84 | 65.13 | 1706. | 1299. | 712. | 710. | 17 |
| 19 | 0.289 | 0.125 | 0.229 | 1.458 | -1.97 | 0.0 | 32.79 | 1.064 | 64.53 | 66.49 | 1835. | 1428. | 745. | 752. | 19 |
| 21 | 0.275 | 0.152 | 0.182 | 1.452 | -1.73 | 0.0 | 31.29 | 1.090 | 65.99 | 67.22 | 1868. | 1554. | 787. | 787. | 21 |

## TABLE 7. (CONTINUED)

### STATION 3-3, STATOR 1 INLET

| RADIUS | AXIAL VELOCITY | WHIRL VELOCITY | RADIAL VELOCITY | TOTAL PRESSURE | STATIC PRESSURE | TEMPERATURES TOTAL | TEMPERATURES STATIC | ABSOLUTE VELOCITY | ABSOLUTE MACH NO. | MER. VELOCITY | PERCENT SPAN | S.L. NO. |
|---|---|---|---|---|---|---|---|---|---|---|---|---|
| 6.347 | 446.5 | 42.5 | 88.94 | 23.75 | 19.55 | 599.8 | 567.4 | 623.9 | 0.534 | 455. | 0.3 | 1 |
| 6.417 | 446.0 | 423.6 | 86.88 | 23.77 | 19.60 | 600.1 | 568.0 | 621.5 | 0.537 | 455. | 1.8 | 3 |
| 6.621 | 446.8 | 415.5 | 88.52 | 23.83 | 19.74 | 601.1 | 569.7 | 615.1 | 0.526 | 454. | 5.0 | 5 |
| 6.945 | 443.3 | 404.0 | 87.59 | 23.93 | 19.95 | 602.8 | 572.2 | 606.1 | 0.517 | 452. | 12.5 | 7 |
| 7.374 | 442.8 | 389.5 | 86.30 | 24.05 | 20.19 | 604.7 | 575.2 | 596.0 | 0.507 | 451. | 21.2 | 9 |
| 7.867 | 445.3 | 373.7 | 84.78 | 24.21 | 20.45 | 607.0 | 578.4 | 585.9 | 0.497 | 451. | 31.7 | 11 |
| 8.467 | 445.0 | 357.1 | 83.16 | 24.37 | 20.71 | 609.3 | 581.6 | 576.6 | 0.488 | 453. | 43.4 | 13 |
| 9.058 | 446.0 | 342.4 | 81.08 | 24.53 | 20.97 | 612.0 | 585.2 | 568.1 | 0.479 | 453. | 56.3 | 15 |
| 9.772 | 446.7 | 331.6 | 77.88 | 24.71 | 21.23 | 615.8 | 589.7 | 560.2 | 0.471 | 451. | 70.0 | 17 |
| 10.489 | 440.2 | 325.7 | 72.37 | 24.89 | 21.50 | 621.0 | 595.6 | 552.4 | 0.462 | 446. | 84.5 | 19 |
| 11.240 | 431.7 | 325.0 | 61.94 | 25.06 | 21.78 | 628.1 | 603.5 | 543.9 | 0.452 | 436. | 99.8 | 21 |

## TABLE 7. (CONTINUED)
## STATION 4-4, STATOR 1 EXIT

| RADIUS | AXIAL VELOCITY | WHIRL VELOCITY | RADIAL VELOCITY | TOTAL PRESSURE | STATIC PPRESSURE | TEMPERATURES TOTAL | STATIC | ABSOLUTE VELOCITY | ABSOLUTE MACH NO. | MER. VELOCITY | PERCENT SPAN | S.L. NO. |
|---|---|---|---|---|---|---|---|---|---|---|---|---|
| 6.965 | 323.7 | 44.4 | 43.35 | 23.09 | 21.83 | 599.8 | 590.3 | 337.4 | 0.283 | 327. | 0.3 | 1 |
| 7.047 | 330.6 | 84.1 | 44.48 | 23.14 | 21.83 | 600.1 | 590.3 | 344.7 | 0.290 | 334. | 2.1 | 3 |
| 7.274 | 353.4 | 90.3 | 47.64 | 23.36 | 21.86 | 601.1 | 589.9 | 367.9 | 0.309 | 357. | 7.0 | 5 |
| 7.613 | 377.0 | 93.6 | 51.08 | 23.63 | 21.93 | 602.8 | 590.0 | 391.6 | 0.329 | 380. | 14.3 | 7 |
| 8.037 | 398.5 | 95.3 | 50.92 | 23.84 | 21.94 | 604.7 | 590.6 | 412.9 | 0.347 | 402. | 23.5 | 9 |
| 8.527 | 417.3 | 95.1 | 50.03 | 24.06 | 21.08 | 607.0 | 591.5 | 431.0 | 0.362 | 420. | 34.1 | 11 |
| 9.066 | 432.4 | 93.5 | 47.64 | 24.26 | 22.03 | 609.3 | 592.7 | 446.0 | 0.374 | 435. | 45.8 | 13 |
| 9.646 | 444.9 | 91.4 | 44.05 | 24.45 | 22.09 | 612.0 | 594.6 | 458.3 | 0.384 | 449. | 56.4 | 15 |
| 10.259 | 458.7 | 89.9 | 49.51 | 24.61 | 22.14 | 615.8 | 597.5 | 469.1 | 0.392 | 460. | 71.6 | 17 |
| 10.818 | 469.5 | 89.3 | 34.01 | 24.77 | 22.20 | 621.0 | 601.9 | 479.1 | 0.399 | 471. | 95.5 | 19 |
| 11.501 | 474.9 | 90.4 | 27.33 | 24.91 | 22.26 | 626.1 | 608.2 | 489.1 | 0.405 | 481. | 99.8 | 21 |

| ABSOLUTE MACH NOS. INLET | EXIT | TOTAL TEMP RISE | TOTAL TEMP RATIO | TOTAL PRESSURE RATIO | WHEEL SPEED IN | OUT | STAGE PRESSURE RATIO | STAGE ADIABATIC EFFICIENCY | STAGE POLYTROPIC EFFICIENCY | S.L. NO. |
|---|---|---|---|---|---|---|---|---|---|---|
| 0.554 | 0.283 | 81.12 | 1.156 | 1.156 | 0.0 | 0.0 | 1.571 | 88.1 | 86.8 | 1 |
| 0.532 | 0.290 | 81.45 | 1.157 | 1.157 | 0.0 | 0.0 | 1.575 | 88.2 | 86.9 | 3 |
| 0.526 | 0.305 | 82.43 | 1.159 | 1.159 | 0.0 | 0.0 | 1.589 | 89.1 | 89.7 | 5 |
| 0.517 | 0.329 | 84.07 | 1.162 | 1.162 | 0.0 | 0.0 | 1.606 | 89.4 | 90.0 | 7 |
| 0.507 | 0.347 | 86.05 | 1.165 | 1.165 | 0.0 | 0.0 | 1.622 | 89.3 | 90.0 | 9 |
| 0.497 | 0.362 | 88.29 | 1.173 | 1.173 | 0.0 | 0.0 | 1.637 | 88.8 | 89.5 | 11 |
| 0.498 | 0.374 | 90.57 | 1.175 | 1.175 | 0.0 | 0.0 | 1.651 | 88.2 | 88.9 | 13 |
| 0.479 | 0.384 | 53.32 | 1.180 | 1.180 | 0.0 | 0.0 | 1.663 | 87.0 | 87.8 | 15 |
| 0.471 | 0.392 | 97.06 | 1.187 | 1.187 | 0.0 | 0.0 | 1.675 | 84.8 | 85.8 | 17 |
| 0.462 | 0.399 | 102.28 | 1.197 | 1.197 | 0.0 | 0.0 | 1.685 | 81.5 | 82.7 | 19 |
| 0.452 | 0.405 | 109.39 | 1.211 | 1.211 | 0.0 | 0.0 | 1.695 | 77.1 | 78.7 | 21 |

| S.L. NO. | DIFFUSION FACTOR | OMEGA BAR | DELTA PS/P | SOLIDITY | TOTAL TURNING | ABSOLUTE FLOW ANGLE INLET | EXIT | EQUIVALENT DIFFUSION FACTOR |
|---|---|---|---|---|---|---|---|---|
| 1 | 0.656 | 0.157 | 0.544 | 1.076 | 28.57 | 43.14 | 14.56 | 1.794 |
| 3 | 0.683 | 0.151 | 0.535 | 1.064 | 28.50 | 42.97 | 14.47 | 1.792 |
| 5 | 0.640 | 0.116 | 0.518 | 1.031 | 28.29 | 42.49 | 14.21 | 1.783 |
| 7 | 0.595 | 0.094 | 0.486 | 0.984 | 27.97 | 41.80 | 13.83 | 1.773 |
| 9 | 0.554 | 0.057 | 0.451 | 0.929 | 27.47 | 40.81 | 13.34 | 1.760 |
| 11 | 0.519 | 0.039 | 0.408 | 0.873 | 26.87 | 39.62 | 12.75 | 1.747 |
| 13 | 0.490 | 0.028 | 0.362 | 0.817 | 26.16 | 38.27 | 12.10 | 1.732 |
| 15 | 0.448 | 0.025 | 0.314 | 0.767 | 25.55 | 37.07 | 11.51 | 1.725 |
| 17 | 0.457 | 0.027 | 0.263 | 0.715 | 25.26 | 36.30 | 11.03 | 1.720 |
| 19 | 0.441 | 0.035 | 0.208 | 0.670 | 25.39 | 36.13 | 10.74 | 1.749 |
| 21 | 0.436 | 0.044 | 0.145 | 0.628 | 26.04 | 36.69 | 10.65 | 1.787 |

## TABLE 7. (CONCLUDED)

## STATION 5-5, STATOR 2 EXIT

| RADIUS | AXIAL VELOCITY | WHIRL VELOCITY | RADIAL VELOCITY | TOTAL PRESSURE | STATIC PRESSURE | TEMPERATURES TOTAL | TEMPERATURES STATIC | ABSOLUTE VELOCITY | ABSOLUTE MACH NO. | MER. VELOCITY | PERCENT SPAN | S.L. NO. |
|---|---|---|---|---|---|---|---|---|---|---|---|---|
| 7.464 | 340.3 | 0.0 | 19.45 | 23.04 | 21.75 | 599.8 | 590.1 | 340.9 | 0.286 | 341. | 0.3 | 1 |
| 7.527 | 347.9 | 0.0 | 19.69 | 23.09 | 21.76 | 600.1 | 590.0 | 348.4 | 0.293 | 348. | 2.0 | 3 |
| 7.740 | 371.4 | 0.0 | 20.47 | 23.31 | 21.79 | 601.1 | 549.6 | 371.9 | 0.313 | 372. | 6.6 | 5 |
| 8.04 | 396.2 | 0.0 | 20.70 | 23.55 | 21.82 | 602.8 | 589.7 | 396.7 | 0.333 | 397. | 12.9 | 7 |
| 8.431 | 418.9 | 0.0 | 22.80 | 23.81 | 21.85 | 604.7 | 590.1 | 419.4 | 0.352 | 419. | 22.0 | 9 |
| 8.679 | 432.5 | 0.0 | 20.14 | 24.04 | 21.87 | 607.0 | 591.0 | 434.9 | 0.368 | 439. | 33.4 | 11 |
| 9.577 | 454.0 | 0.0 | 19.66 | 24.24 | 21.92 | 609.3 | 592.0 | 455.3 | 0.382 | 455. | 45.0 | 13 |
| 9.916 | 468.6 | 0.0 | 17.32 | 24.43 | 21.95 | 612.0 | 593.7 | 468.9 | 0.393 | 469. | 57.6 | 15 |
| 10.480 | 480.4 | 0.0 | 15.31 | 24.53 | 22.00 | 615.8 | 596.4 | 480.7 | 0.402 | 491. | 71.0 | 17 |
| 11.093 | 491.1 | 0.0 | 13.04 | 24.73 | 22.04 | 621.0 | 630.9 | 491.3 | 0.409 | 491. | 85.1 | 19 |
| 11.721 | 500.7 | 0.0 | 13.63 | 24.85 | 22.07 | 628.1 | 607.2 | 501.0 | 0.415 | 501. | 99.8 | 21 |

| ABSOLUTE MACH NO. INLET | MACH NO. EXIT | TOTAL TEMP RISE | TOTAL TEMP RATIO | WHEEL SPEED IN | WHEEL SPEED OUT | STAGE PRESSURE RATIO | STAGE ADIABATIC EFFICIENCY | STAGE POLYTROPIC EFFICIENCY |
|---|---|---|---|---|---|---|---|---|
| 0.283 | 0.286 | 81.12 | 1.156 | 0.0 | 0.0 | 1.568 | 87.6 | 88.3 |
| 0.290 | 0.293 | 81.45 | 1.157 | 0.0 | 0.0 | 1.571 | 87.8 | 88.4 |
| 0.309 | 0.313 | 82.43 | 1.159 | 0.0 | 0.0 | 1.536 | 88.7 | 89.3 |
| 0.329 | 0.333 | 84.37 | 1.162 | 0.0 | 0.0 | 1.620 | 88.0 | 89.7 |
| 0.347 | 0.352 | 86.05 | 1.166 | 0.0 | 0.0 | 1.620 | 89.0 | 89.7 |
| 0.362 | 0.363 | 88.29 | 1.170 | 0.0 | 0.0 | 1.635 | 88.6 | 89.5 |
| 0.374 | 0.382 | 91.57 | 1.175 | 0.0 | 0.0 | 1.652 | 88.0 | 88.7 |
| 0.384 | 0.393 | 93.32 | 1.180 | 0.0 | 0.0 | 1.662 | 86.8 | 87.6 |
| 0.392 | 0.402 | 97.06 | 1.187 | 0.0 | 0.0 | 1.673 | 84.4 | 85.6 |
| 0.399 | 0.409 | 102.28 | 1.197 | 0.0 | 0.0 | 1.693 | 81.2 | 82.5 |
| 0.405 | 0.415 | 109.39 | 1.211 | 0.0 | 0.0 | 1.651 | 76.7 | 78.3 |

| S.L. NO. | DIFFUSION FACTOR | OMEGA BAR | DELTA DS/Q | SOLIDITY | TOTAL TURNING | ABSOLUTE FLOW ANGLE INLET | ABSOLUTE FLOW ANGLE EXIT | EQUIVALENT DIFFUSION FACTOR |
|---|---|---|---|---|---|---|---|---|
| 1 | 0.112 | 0.038 | -0.056 | 0.693 | 14.56 | 14.56 | 0.0 | 1.314 |
| 3 | 0.112 | 0.026 | -0.055 | 0.992 | 14.47 | 14.47 | 0.0 | 1.314 |
| 5 | 0.114 | 0.030 | -0.060 | 0.994 | 14.21 | 14.21 | 0.0 | 1.314 |
| 7 | 0.114 | 0.023 | -0.047 | 0.915 | 13.83 | 13.83 | 0.0 | 1.315 |
| 9 | 0.114 | 0.017 | -0.046 | 0.870 | 13.34 | 13.34 | 0.0 | 1.315 |
| 11 | 0.113 | 0.012 | -0.047 | 0.823 | 12.75 | 12.75 | 0.0 | 1.313 |
| 13 | 0.112 | 0.009 | -0.046 | 0.777 | 12.10 | 12.10 | 0.0 | 1.311 |
| 15 | 0.113 | 0.009 | -0.053 | 0.732 | 11.51 | 11.51 | 0.0 | 1.310 |
| 17 | 0.112 | 0.011 | -0.058 | 0.690 | 11.03 | 11.03 | 0.0 | 1.311 |
| 19 | 0.116 | 0.016 | -0.064 | 0.651 | 10.74 | 10.74 | 0.0 | 1.315 |
| 21 | 0.116 | 0.024 | -0.069 | 0.615 | 10.65 | 10.65 | 0.0 | 1.323 |

67

# REFERENCES

1.  Kemp, N. H. and Sears, W. R., "The Unsteady Forces Due to Viscous Wakes in Turbomachines", J. Aero Sci. 22, p. 478 (1955).

2.  Osborne, C., "Compressibility Effects in the Unsteady Interactions Between Blade Rows", Ph.D. Thesis, Cornell University, 1971.

3.  Horlock, J. H., "Fluctuating Lift Forces on Airfoils Moving Through Transverse and Chordwise Gusts", Journal of Basic Engineering, Series D., Vol. 90, No. 4, Dec. 1968, pp. 494-500.

4.  Naumann, H. and Yeh, H., "Lift and Pressure Fluctuations of a Cambered Airfoil Under Periodic Gusts and Applications in Turbomachinery", ASME Paper No. 72-GT-30, 1972.

5.  Mani, R., "Noise Due to Interaction of Inlet Turbulence With Isolated Stators and Rotors", Journal of Sound and Vibration, 17, 251-260 (1971).

6.  Helms, H. E.: Quiet Clean STOL Experimental Engine Study Program. Task II-Preliminary Design Studies, Part B. EDR 7610, November 1972.

7.  Koch, R. L., Ciskowski, T. M. and Garzon, J. R., Turbofan Noise Reduction Using a Near Sonic Inlet, AIAA Paper No. 74-1098, 21 October 1974.

8.  Miller, B. A. and Abbott, J. M., Low Speed Wind Tunnel Investigation of the Aerodynamic and Acoustic Performance of a Translating Center-body Choked Flow Inlet, NASA TMX-2773, June 1973.

9.  Groth, H. W., Sonic Inlet Noise Attenuation and Performance with a J-85 Turbojet Engine as a Noise Source, AIAA Paper No. 74-91, 30 January 1974.

10. Rice, E. J., Attenuation of Sound in Soft-Walled Circular Ducts. NASA TMX 52442, May 1968.

11. Renshaw, J. H.: Quiet Turbofan STOL Aircraft for Short Haul Transportation. Volume I, Final Report. NASA CR-114612, 14 June 1973.

12. Brent, J. A., and Clemmons, D. R., Single-Stage Experimental Evaluation of Tandem-Airfoil Rotor and Stator Blading for Compressors, NASA CR-134713, Part IV: Final Report, November 1974.